SELF-REGULATING MATERIALS WITH TRANSIENT LIFETIMES VIA INTERNAL FEEDBACK IN PH

Von der Fakultät für Mathematik, Informatik und Naturwissenschaften der RWTH Aachen University zur Erlangung des akademischen Grades eines Doktors der Naturwissenschaften genehmigte Dissertation

vorgelegt von

M. Sc. Thomas Heuser

aus

Lübeck

Berichter*:* *Prof. Dr. Martin Möller*

Prof. Dr. Andreas Walther

Tag der mündlichen Prüfung*:* *16.10.2017*

Inside Back Cover: T. Heuser, *Angew. Chem. Int. Ed.*, **2015**, 54 “Tempus edax rerum” (Ovid)

The work presented in this thesis was carried out at DWI - Leibniz-Institut für Interaktive Materialien at RWTH Aachen University from July 2013 until December 2016 under the supervision of Prof. Dr. Andreas Walther. Formal director of the thesis is Prof. Dr. Martin Möller.

Parts of this work have been published in the following articles:

Chapter 2:

1. Generic Concept to Program the Time Domain of Self-Assemblies with a Self-Regulation Mechanism
   Thomas Heuser, Ann-Kathrin Steppert, Catalina Molano Lopez, Baolei Zhu, Andreas Walther
   Nano Letters, **2015,** 15, 2213-2219.

Chapter 3:

2. Biocatalytic Feedback-Driven Temporal Programming of Self-Regulating Peptide Hydrogels
   Thomas Heuser, Elisabeth Weyandt, Andreas Walther
   Angewandte Chemie International Edition, **2015**, 54, 13258-13262

Chapter 4:

3. Photonic Devices out of Equilibrium: Transient Memory, Signal Propagation and Sensing
   Thomas Heuser, Rémi Merindol, Aileen Klaus, Sebastian Löscher, Andreas Walther
   Advanced Materials, **2017**, DOI: 10.1002/adma.201606842

Chapter 5:

4. Antagonistic Enzymes in a Biocatalytic pH Feedback System Program Autonomous DNA Hydrogel Life Cycles
   Laura Heinen, Thomas Heuser and Andreas Walther
   submitted

EIDESSTATTLICHE ERKLÄRUNG

Hiermit erkläre ich, Thomas Heuser, an Eides statt, dass ich die vorliegende Dissertation selbstständig verfasst und keine anderen als die angegebenen Quellen und Hilfsmittel benutzt habe.

Aachen, 19.04.2017 _____

Author's contributions

Publication 1

Together with Andreas Walther (AW), I conceived the experimental procedure and established the internal feedback system in pH. Catalina Molano Lopez synthesized the block copolymer BCP-2 under supervision of Baolei Zhu and conducted the experiments for time-programmed vesicles under my supervision. During her master thesis, Ann-Kathrin Steppert synthesized the phenol-ligand for the gold nanoparticle functionalization, and conducted the experiments for temporally programmed Au-NP clusters under my supervision. I performed the experimental work on self-regulating block copolymer micelles (BCP-1) and peptide hydrogels. I performed all TEM and UV-Vis measurements. I and AW analyzed all results, wrote the manuscript and finalized the article together with the co-authors.

Publication 2

Together with AW, I conceived the experimental procedure and established the biocatalytic feedback system in pH. Figure 1a was achieved in course of the bachelor thesis of E. Weyandt, conducted under my supervision. I performed all experimental work and analysis on the self-regulating peptide hydrogels. I and AW analyzed all results, wrote the manuscript and finalized the article together.

Publication 3

Together with AW, I conceived the experimental procedure and I conducted the experiments for self-regulating photonic memories. Sebastian Löscher and Dr. Rémi Merindol (RM) conceived the experimental procedure, planned and conducted the experiments relating to the propagation of pH waves and remote control via photo acid release. Aileen Klaus prepared the photonic films and in parts performed experimental work during her internship under my supervision and during her bachelor thesis under supervision of RM. I, RM and AW analyzed the results, wrote the manuscript and finalized the article together.

Publication 4

Together with AW, I conceived the pH feedback. I performed all experiments and analysis establishing the biocatalytic feedback system preceded by an initial lag time. Laura Heinen (LH) and AW conceived the DNA hydrogel and LH performed all experiments for the characterization of the DNA hydrogel. I and LH together performed all pH and rheological measurements on the transient DNA hydrogel. Alexander Steinschulte supported the rheological measurements. I, LH and AW analyzed the results, wrote the manuscript and finalized the article together.

1 INHALTSVERZEICHNIS

ABSTRACT

The forthcoming generation of soft materials will be designed to autonomously adapt to their environment, in a way similar to living systems, in an active and self-regulating manner. While molecular engineering allows to program the spatial superstructures arising from soft matter building motifs, control over the time domain remains a major challenge. Within my thesis, I focus on the integration of preorchestrated temporal signatures into responsive self-assembling systems, to create adaptable and self-regulating materials. Within the last decade scientists widely mastered the spatial organization of complex and hierarchically ordered structures. In the simplest case, recognition between complementary building motifs, such as DNA base pairing, encodes the formation of the emerging super-structure. Classical responsiveness enables switching between separated equilibrium states upon external triggering and allows to induce assembly/disassembly processes on demand. The decisive step to conceive the next generation of bioinspired materials requires structuring under out-of-equilibrium conditions, to integrate lifelike characteristics, such as adaption, predefined lifetimes and autonomous self-regulation. In this work I present kinetic and biocatalytic strategies to program transient, preconfigured pH-profiles encoding the lifetimes of various pH-responsive self-assemblies. First I will showcase a general kinetic concept wherein temporal control is realized by combining a rapid promoter (base) and a slow hydrolyzing deactivator (acid) creating a transient alkaline pH-profile that controls the self-assembly response. Further, we refined this approach to include the feedback-driven biocatalytic conversion of urea into ammonia, which, concerted with an acidic buffer, results in time-controlled acidic pH-profiles. The system coupled to a peptide gelator enables temporal programming of hydrogel lifetimes depending on the concentration of the biocatalyst. Integration of our biocatalytic feedback system with a photonic gel based on a pH-sensitive block copolymer further facilitates self-regulating displays and pH-signal propagation. In the last part, both the promoting and deactivating pathway are substituted by biocatalytic feedback-controlled reactions, and I will present the transient formation of DNA-hydrogels preceded by an initial lag time. Though the fundamental objective of temporal control is similar for all approaches presented, they demonstrate different levels of complexity, from simple ester hydrolysis, towards feedback-regulated biocatalytic control, and finally comprising two antagonistic biocatalytic switches in the end.

ZUSAMMENFASSUNG

Die Fähigkeit lebender Organismen, sich aktiv an ihre Umgebung anzupassen, wird von einer Vielzahl selbst-regulierender Prozesse gesteuert und dient damit als Vorbild für eine neue Generation autonomer, weicher Materialien. Die räumliche Domäne einer entstehenden Überstruktur lässt sich bereits durch gezieltes molekulares Design der zugrunde liegenden Bausteine steuern, wohingegen die Kontrolle der zeitlichen Domäne als eine große Herausforderung verbleibt. In meiner Arbeit befasse ich mich mit der Integration zeitlicher Signaturen in responsive, selbst-assemblierende Systeme, um so adaptionsfähige und selbst-regulierende Materialien zu erzeugen. Im vergangenen Jahrzehnt ist es Wissenschaftlern generell gelungen, die räumliche Organisation komplexer und hierarchisch aufgebauter Strukturen zu kontrollieren. Im einfachsten Fall steuert die gegenseitige Erkennung komplementärer Bausteinen, wie zum Beispiel DNA Basenpaarung, den Aufbau der entstehenden Überstruktur. Die Implementierung responsiver Komponenten erlaubt eine Schaltung zwischen getrennten Gleichgewichtszuständen durch äußere Reize und ermöglicht es so, Assemblierungs-/Disassemblierungsprozesse gezielt zu steuern. Um lebensähnliche Eigenschaften wie zum Beispiel Anpassung, vorgegebene Lebenszeiten und Selbstregulierung in der nächsten Generation bioinspirierter Materialien zu verwirklichen, ist der Strukturaufbau unter Nichtgleichgewichtsbedingungen ein wichtiges Kriterium. In meiner Arbeit programmiere ich transiente, kinetisch und biokatalytisch kontrollierte pH-Profile, welche die Lebenszeit verschiedener pH-responsiver, selbst-assemblierender Systeme steuern. Als erstes präsentiere ich ein kinetisches Konzept, welches die zeitliche Kontrolle eines selbst-assemblierenden Systems ermöglicht, indem dieses direkt an ein transientes, alkalisches pH-Profil gekoppelt wird. Durch die Kombination eines schnellen Promotors (Base) und eines langsam hydrolysierenden Deaktivators (Säure) lässt sich dieses pH-Profil realisieren. Diesen kinetischen Ansatz haben wir weiterentwickelt und den Feedback-gesteuerten biokatalysierten Umsatz von Urea in Ammonium-Ionen mit einem sauren Puffer gekoppelt, was uns die zeitliche Kontrolle von sauren pH-Profilen ermöglicht. Koppelt man diese an einen Peptid-Gelator, ermöglicht die Veränderung der Konzentration des Biokatalysators die zeitliche Steuerung der Lebenszeit der Hydrogele. Integriert man dieses biokatalytische Feedback System in ein photonisches Gel, welches auf einem pH-responsiven Blockcopolymer basiert, lassen sich so selbst-regulierende Bildschirme sowie fernsteuerbare Signalverbreitung realisieren. Abschließend ersetze ich sowohl den aktivierenden als auch den deaktivierenden Schritt durch Feedback-kontrollierte biokatalytische Reaktionen, wodurch ich sowohl einen vorgebebenen Startzeitpunkt, als auch die Lebenszeit transienter DNA-Hydrogele orthogonal steuern kann. Obwohl die Zielsetzung zeitlicher Kontrolle in allen präsentierten Konzepten grundlegend ist, zeichnen sie sich durch unterschiedliche Komplexität und Kontrollierbarkeit aus. Während das erste System auf einfacher Esterhydrolyse basiert, beruht das letzte auf zwei entgegengesetzt wirkenden, orthogonal steuerbaren Biokatalysatoren.

1 INTRODUCTION

1.1 Motivation

In biological systems, complex reaction networks control the formation of transient structures with high spatiotemporal precision. In fact, smooth progress of vital functions relies on a myriad of self-regulating processes, perfectly synchronized in time and operated under non-equilibrium conditions. Such autonomous systems are orchestrated by positive or negative feedback loops, precisely timed via kinetic or catalytic control and maintained under constant dissipation of energy. However, the challenge is to transfer these principles of self-regulation into present-day soft matter systems.

The integration of fully autonomous control mechanisms would bring about the design of interactive and intelligent soft materials far beyond the simple stimuli-responsiveness of present materials. Rational control over synthetic feedback-controlled reaction networks combined with advanced responsive soft matter offers a potential way to preorchestrate switching mechanisms of material systems in time, creating artificial, self-regulating systems. Present strategies to address the time domain of self-assembled structures, described in the following chapter, distinguish themselves by different levels of autonomy and programmability. However, an approach of broader applicability to target the lifetime of diverse responsive building motifs is still needed. The temporal modulation of environmental conditions, such as the pH value of an aqueous solution, appears to be advantageous as non-equilibrium dynamics are integrated into the surroundings and not necessarily into the responsive self-assembling entity, which allows unbiased and individual configuration. Hence, the motivation of my study is to develop a platform concept for the integration of preorchestrated temporal signatures into pH-responsive self-assemblies.

1.2 Temporal Control in Natural Systems

Biological systems are subjected to continuous adaption and reorganization. The concentration of proteins, messenger molecules and also the activity of enzymes fluctuate permanently. Biological structures form with high spatial precision and decay once they reach the predefined end of their lifespan. How does nature coordinate a myriad of diverse processes, simultaneously, precisely and independently on different levels of a living organism?

Natural complexity relies on the autonomous regulation of individual processes and provides feasible inspiration how to integrate mechanisms of self-regulation and temporal control into soft materials. Here, cascades of individual reactions, so-called reaction networks, regulate the spatiotemporal occurrence of for instance oscillating protein concentrations or the formation of transient biological structures. The preorchestration of activation/formation and delayed deactivation/degradation implies kinetic control, feedback and continuous dissipation of energy, thus complex non-linear behavior far from the thermodynamic equilibrium.

One of the most promising approaches to realize artificial non-equilibrium systems, is the integration of feedback mechanisms into soft materials, as they are prominent in biocatalytic processes. Here, a system is regulated by its own product, either amplifying (positive, autocatalytic) or attenuating (negative) its own production.[1] This introduction will start with two distinct examples of regulatory networks in natural systems, to demonstrate the tremendous potential of feedback control in temporal self-regulation. While the first network modulates the circadian rhythm (sleep-wake cycle) with a period of 24 hours, the second controls the calcium metabolism presenting rapid adaption and signal propagation. Besides these feedback-controlled oscillations, energy-dissipating systems facilitate self-regulating structure formation. With the focus set on programmable lifetimes, I will discuss the archetypal example of dynamic microtubule growth in presence of a chemical fuel.

The day and night cycle on earth sets the rhythm of a biological master clock located in the suprachiasmatic nucleus (SCN), a small region in the brain, of most higher organisms. Here, the orchestration of a transcriptional reaction network by positive and delayed negative feedback results in the oscillating expression of clock-genes with a period of 24 hours.[2] In mammals, the two regulatory proteins CLOCK and BMAL1 are the central pacemakers of this circadian oscillation, as they promote the expression of further genes by binding to a specific nucleotide sequence (E-box, Figure 1a). Once bound, transcription of Period (*mPer1* and

mPer2) and Cryptochrome (*mCry1* and *mCry2*) genes drives the negative feedback mechanism (Figure 1a; red arrow, left). At the beginning of the circadian cycle, PER and CRY proteins accumulate in the cytoplasm, where they encounter dimerization and post-translational phosphorylation by a set of Casein kinases (CK1ε and CK1δ).[3] This modification reaction is a critical factor in the regulatory network as it implements a significant delay into the negative feedback-loop, maintaining the 24 hour period of the circadian oscillation (Figure 1a, dashed red arrow).[4] Upon translocation into the nucleus, the PER:CRY dimers interact with the CLOCK:BMAL1 complexes to inhibit the transcription of their own genetic sequence (*mPer* and *mCry*).

Concurrent to the negative regulatory loop, the CLOCK:BMAL1 dimer also activates the transcription of the receptors *Rev-erbα* and *Rorα*. The resulting proteins bind to corresponding response elements (ROREs) in the *Bmal1* promoter sequence to either promote (ROR) or repress (REV-ERB) *Bmal1* gene transcription (Figure 1a, green/red arrow, right).[5] Both, positive and negative regulation of the *Bmal1* expression were shown to stabilize the overall oscillatory behavior.

Emanating from the central pacemaker, interconnected circadian oscillators can be found throughout the body in peripheral organs/tissue as lung, liver and skeletal muscles. Yamazaki et al. developed a transgenic rat model, where the *mPer1* gene promoter is coupled to a luciferase reporter sequence.[5] The animals were subjected to a day/night cycle of precisely 12 hours each, killed and extracts of the brain/periphery organs were cultured and analyzed in constant darkness. As shown in Figure 1b, rhythmic peaks of bioluminescence prove the periodic transcription of the *Per1:Luc* gene in course of the SCN core oscillation with a persistence of up to 32 days.[2] In response, light emission in cultured liver cells expresses similar damped oscillatory behavior with a rhythmical delay of 7 to 11 hours.

The hierarchical organization of interconnected oscillatory reaction networks is an impressive example of natural spatiotemporal control, which regulates numerous physiological processes. In the long term, circadian oscillations adapt to minor variations of the day/night cycle (seasons change) as well as severe perturbations caused by time shifts due to intercontinental travelling, nonetheless restoring the overall period of 24 hours (adaptation).

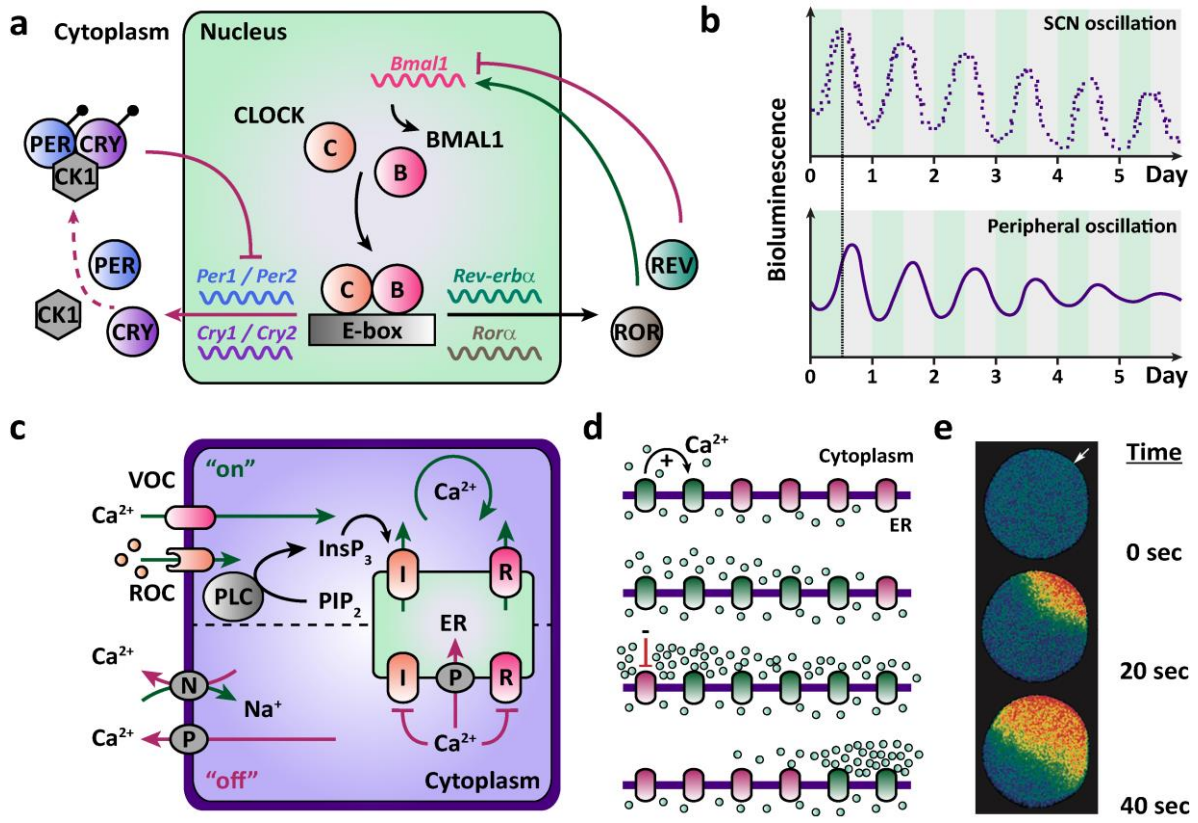

Figure 1: Regulatory reaction networks in natural systems. a) Scheme of the interconnected transcriptional feedback mechanisms in mammal circadian oscillation. (Adapted with permission from Ref.[6, 7]) b) Light emission during the periodic transcription of the *Per1:Luc* gene in transgenic rat. The core oscillation in the suprachiasmatic nucleus (SCN) sets the rhythm for a network of coupled oscillators in peripheral tissue and organs. (Adapted with permission from Ref.[5]) c) Schematic representation of calcium homeostasis. (Adapted with permission from Ref.[8, 9]) d) Scheme of the spatiotemporal occurrence of calcium waves due to Ca^{2+}-induced positive and negative feedback. e) Cytosolic calcium waves of a starfish egg upon fertilization by a single sperm (white arrow). The wave is indicated with a Ca^{2+}-sensitive fluorescent dye. (d, e: Reprinted with permission from Ref.[10])

In contrast, a signaling network of feedback-controlled membrane channels, pumps and exchangers modulates the cellular Ca^{2+} concentration. With exceptionally rapid spatiotemporal precision the network regulates singular transient signals, such as highly localized [Ca^{2+}]-sparks responsible for cardiac muscle contraction, or sustained oscillatory calcium waves during fertilization or proliferation.[11] Despite the tremendous diversity of such local or global events, with periods ranging from microseconds to minutes, all signals are generated through the delicate balance of calcium influx from the extracellular environment or internal stores, such as the endoplasmic reticulum (ER), and subsequent removal as schematically illustrated in Figure 1c.[12]

In the initial phase of calcium signaling, membrane depolarization and different receptor molecules initiate rapid Ca^{2+}-entry through either voltage-operated- (VOCs) or receptor-regulated ion channels (ROCs) located in the plasma membrane.[8] The increasing concentration of cytosolic Ca^{2+} then induces the depletion of internal calcium stores in the ER, driven by a positive feedback mechanism termed "calcium-induced calcium release" (CICR).[13] Primarily, external ligand molecules must activate phospholipase-C (PLC) to initiate the enzymatic conversion of phosphatidylinositol 4,5-biphosphat (PIP_2) to inositol-1,4,5-trisphosphate ($InsP_3$).[14] During the CICR process, Ca^{2+} and $InsP_3$ bind to the endoplasmic receptor $InsP_3R$ (I), to induce channel opening of the intracellular calcium stores. In cardiac cells and neurons the ryanodine receptor family (R) controls several signaling pathways in a similar cooperative sensitivity towards calcium itself and cyclic ADP ribose.[15]

In order to prevent cytotoxication by elevated calcium concentration, a negative feedback mechanism restricts further Ca^{2+} release, once a critical concentration is reached (signaling). Both, $InsP_3Rs$ and RYRs show a bell-shaped activity profile dependent on the surrounding calcium concentration with maximum probability of channel opening for moderate calcium concentrations and nearly inactive behavior for low and high concentrations. Consequently, excess calcium inhibits the endoplasmic ion channels and subsequently the concerted mobilization of various pumps such as Ca^{2+}-ATPase (P) and ion-exchangers (N) restores the cellular Ca^{2+}-resting level. In fact, bell-shaped activity profiles are also encountered for biocatalytic reactions, which are ideally suited to integrate feedback-controlled self-regulating mechanisms into soft materials as discussed in Chapter 3.

The feedback-controlled character of localized Ca^{2+} release is the fundamental mechanism of calcium signaling. As schematically illustrated in Figure 1d, active $InsP_3$/RYR receptors release signal-Ca^{2+}, which diffuses into the cytosol. Positive feedback (CICR) excites nearby receptor molecules generating a regenerative calcium wave, which propagates across the cell. Once the local Ca^{2+} concentration restricts further release, pumps restore the resting level. Such calcium waves and oscillations can be visualized utilizing Ca^{2+}-sensitive fluorescent dyes as shown in Figure 1e. For instance during the fertilization of an egg, the sperm cell injects PLC to promote the enzymatic production of $InsP_3$ activating the described calcium-signaling network. Localized activation of an enzyme to promote the conversion of a diffusing species, on his part activating nearby biocatalysts, is utilized in a similar way to create propagating pH-waves as described in Chapter 4.

Giving a short summary, diverse physiological processes are precisely coordinated in space and time by regulatory reaction-networks. The emergence of oscillatory behavior relies on the complex balance of positive and temporally delayed negative feedback, facilitating singular transient, sustained or oscillatory Ca^{2+} signals and waves, exemplarily. The latter allow signal propagation within the cell and transduction beyond, mediating processes such as muscle contraction, chemotaxis, motility and proliferation.[12]

On the cellular level, processing of such internal/external information induces morphogenesis and migration, which postulates a dynamic rearrangement of the cell structure and its content.[16] This spatiotemporal organization relies on the cytoskeleton, which consists of three different types of filaments. Among these, microtubules are responsible for the position of the organelles, morphogenesis and the formation of the mitotic spindle during cell division.[10] The highly dynamic and adaptive character of microtubules, which is mandatory for their function within the cell, stems from the continuous alternation between slowly growing and rapid shrinking of the microtubule filaments. This behavior is termed "dynamic instability"[17] and is the archetypal example of a chemically fueled energy-dissipating system driven by the tubulin-catalyzed hydrolysis of guanosine triphosphate (GTP).

The underlying structural unit of microtubule formation is the heterodimer αβ-tubulin. The asymmetric protein polymerizes in a head-to-tail fashion into linear protofilaments. Lateral association of thirteen filaments results in the overall hollow tubular structure as depicted in Figure 2a. In the nucleation stage, tubulin subunits assemble into small oligomers. The weak non-covalent interactions between the tubulin molecules result in a kinetic barrier, which sets a critical number of subunits required forming a stable, growing filament.

During microtubule growth, free GTP-containing tubulin molecules add to the filament as depicted in Figure 2b. Once incorporated, GTP is hydrolyzed to guanosine diphosphate (GDP), which is the energy-dissipating step. The cleaved phosphate group is released and GDP remains in the growing microtubule. In fact, hydrolysis is structurally coupled to the polymerization of tubulin. The growing plus-end presents the β-subunit of the heterodimer, which binds GTP effectively, but is unable to promote hydrolysis. The catalytic activity is provided by the α-subunit of the next tubulin monomer to be incorporated.[18] The catalytic interplay of neighboring tubulin molecules also explains the significant difference in the rate of hydrolysis for slowly hydrolyzing free GTP-containing tubulin molecules and rapidly hydrolyzing polymerized

ones.[19] Consequently, the growing filament mostly consists of GDP-tubulin molecules except of a small GTP-containing cap, which has not yet been hydrolyzed. Loss of the protecting cap results in rapid depolymerization ("catastrophe" see Figure 2b). The fast depolymerization is caused by a structural transition of the tubulin molecules upon hydrolysis. GTP-containing tubulin forms straight protofilaments as indicated for the growing microtubule in Figure 2b. Upon hydrolysis the tubulin dimer bends, which implements significant strain into the protofilaments, promoting the disassembly.[18, 20] In vivo, a myriad of accessory proteins and enzymes as plus-end-tracking proteins (+TIPs), microtubule polymerases and various kinesins add further control mechanisms and dynamics to the assembly/disassembly cycle of microtubules.[21] The dynamic assembly of tubulin in vitro, originating from a central centrosome is illustrated in Figure 2c.

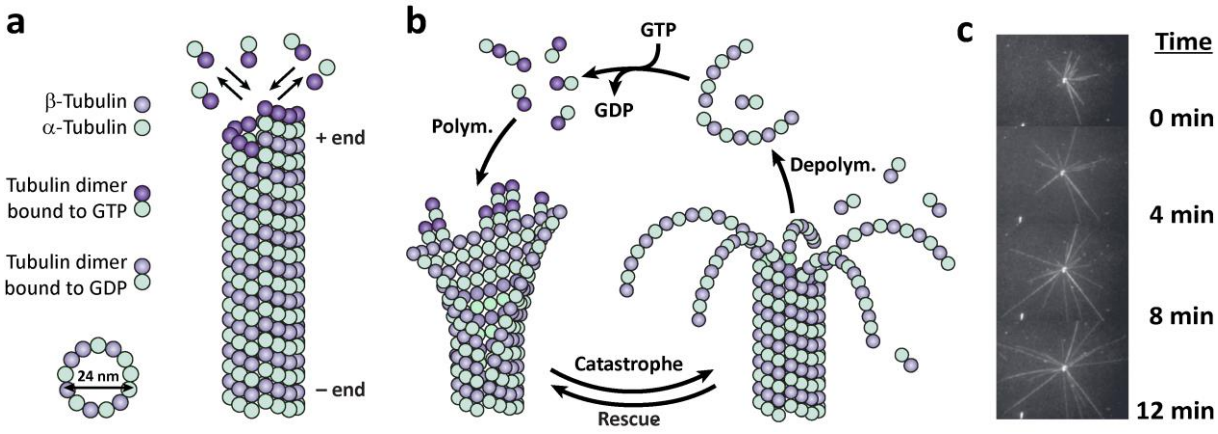

Figure 2: Dynamic assembly of microtubules. a) Structure of a growing microtubule filament and the respective GTP/GDP-containing tubulin subunits. b) Illustration of the dynamic instability of microtubules: The hydrolysis of GTP fuels the out-of-equilibrium self-assembly of microtubules. (a-b: Reprinted and adapted with permission from Ref.[22]) c) Dynamic assembly of tubulin around the centrosome. (Reprinted with permission from Ref.[23])

In summary, natural strategies of self-regulation and temporal control inspire to create artificial fully autonomous systems with programmable lifetimes. Fundamental, to realize such transiently formed soft materials, is to comply with the mandatory kinetic balance of rapid activation and delayed deactivation. Among potential approaches, reaction networks are highly suitable to orchestrate transient behavior, regulated by positive/negative feedback mechanisms as described for circadian oscillations and Ca^{2+} signaling. Within synthetic systems, autocatalytic (self-accelerating) inorganic reactions enable the integration of feedback mechanisms, often encountered in classical oscillators, as described in section 1.3. Further,

biocatalytic reactions provide enhanced means of feedback-controlled catalytic programmability to realize transient self-assemblies and will be discussed within section 1.3.3 and 1.4.

Structuring under continuous energy dissipation, explained for the dynamic instability of microtubules is yet another route towards self-regulating materials. Starving the availability of a chemical fuel presents a promising approach to realize highly autonomous structure formation (see section 1.4). The strategies presented distinguish themselves by different levels of autonomy, field and spectrum of applicability, accessible material lifetimes and precision. I will start with classical redox and pH oscillators as the origin of synthetic out-of-equilibrium systems, proceed towards transient structure formation via biocatalytic control and finally conclude with artificial energy-dissipating systems.

1.3 Synthetic Reaction Networks

Vital functions within the cell and living systems in general are encoded in biochemical reaction networks as described in the previous section. On the molecular level, precise orchestration of individual reactions in space and time enables singular non-equilibrium events, sustained transient states and chaotic or oscillating behavior. In fact, the existence of non-linear phenomena in nature is already known since the beginning of the last century and furnished important theoretical models long before synthetic reaction networks became conceivable. First, Lotka designed a simplistic model of an oscillating system comprising two sequential autocatalytic reactions assuming constant feed of the reactants.[24] Prigogine *et al.* later published a thermodynamic approach comprising four hypothetical, individual reactions one of them being autocatalytic, giving rise to stable oscillations.[25] This *Brusselator* is one of the most important models describing autocatalytic, oscillating chemical reactions and moreover introduced the concept of dissipating systems.[26]

Pertaining to these early reports on the structure of simple reaction networks and our contemporary knowledge of complex biological systems (section 1.2), we are able to identify basic principles of synthetic reaction networks. In the simplest case the interaction of one positive and one negative feedback loop is sufficient to create periodic bistability.[27] While the activation of the system primarily consists of an autocatalytic production (positive feedback) of a substrate or product, consecutive negative feedback controls the removal of the activating species. Stable oscillations in the concentration of the respective substrate/product arise, if the

negative feedback is delayed pertaining to the activation step and continuous supply of reactants is maintained. Temporal separation may result from the overall reaction kinetics or complex regulatory feedback loops interposed between activation and deactivation.[27] Despite the pioneering work of Lotka, Voltera and Prigogine (among others) unraveling these fundamental principles of non-linear chemical systems, designing synthetic reaction networks remained a major challenge. In recent years researchers increasingly addressed the question, how to integrate mechanisms of self-regulation and temporal control into soft matter systems to furnish autonomous and adaptive materials, as reviewed recently.[27-30] Within the next chapter I will introduce different strategies to translate the temporal signature of oscillating chemical reaction networks into a material response. Conceptually, I will distinguish the self-assembling system being implicated in the core oscillation, as in the case of redox oscillators (Belousov-Zhabotinsky) or being passively immersed in a non-linear aqueous environment driven by an individual oscillator creating periodic variations for instance in pH.

1.3.1 The Belousov-Zhabotinsky Reaction

Among the field of synthetic non-linear chemical systems, the Belousov-Zhabotinsky (BZ) reaction is the archetypal example and presumably the origin of man-made feedback-controlled oscillators. Inspired by the Krebs cycle, B. Belousov noticed a solution of cerium sulfate, potassium bromate and malonic acid, under strong acidic conditions to periodically change its color from colorless to yellow.[31] Attempts to publish his findings were rejected by various journals, as such non-equilibrium behavior, at that time, was sentenced to violate the Second Law of Thermodynamics.[32] A. Zhabotinsky later on improved the reaction mixture and published a first draft of the mechanism.[33] In fact, the BZ reaction evolves from a complex network of various individual reactions, giving rise to oscillating oxidation and reduction of a metal catalyst, being responsible for visible color-patterns. Field and Noyes published the first detailed mechanism,[34, 35] which was later on simplified to comprise three central reaction steps.[36, 37] During the initial "Bray period", bromide ions are consumed by bromate forming bromous acid. Once the concentration of bromide falls to a critical value, autocatalytic production of bromous acid (positive feedback) initiates the second phase of the reaction, which involves oxidation of the present metal catalyst. Closing the autocatalytic cycle, the last process regenerates the inhibitory bromide (negative feedback), involving the reduction of the catalyst.[37] Depending on the introduced redox catalyst (ferroin, cerium, ruthenium, etc.), the redox cycle is visible by rhythmic color changes.

The central metal catalyst provides a suitable working point towards the integration of autonomous behavior and temporal signatures into soft polymer-based materials. As the core-oscillation does not result in pronounced global chemical/physical rhythmicity, such as periodic changes in pH or temperature, it is essential to connect the material response directly to the redox cycle of the catalyst. Yoshida and coworkers first managed to convert the autonomous BZ-oscillation into mechanical changes of a polymer gel.[38] Key of the strategy is to covalently incorporate the BZ-catalyst ruthenium(II) tris(2,2´-bipyridine) ($Ru(bpy)_3^{2+}$) into a copolymer gel, as illustrated in Figure 3a. Translation of the chemical into a mechanical oscillation requires a second monomer, sensitive to changes in the redox state of the BZ catalyst such as poly-N-isopropylacrylamide (pNIPAAm). pNIPAAm is an extensively studied thermoresponsive polymer, which undergoes a reversible volume phase transition (swollen state to collapsed state) upon heating above its lower critical solution temperature (LCST) around 32 °C.[38-40] In close vicinity to the BZ-catalyst, the position of the LCST is directly connected to the ruthenium redox state, located at higher temperatures for the oxidized Ru(III) and lower temperatures for the reduced Ru(II) state, compared to the LCST of the NIPAAm homopolymer.[41] If the surrounding temperature is kept constant and the gel is immersed in a catalyst-free solution containing the BZ-substrates, the core redox oscillation translates into hydrophilic/hydrophobic changes of the pNIPAAm segment, which consequently renders a swelling/deswelling oscillation of the entire polymer gel. Within this section I describe different strategies to integrate self-regulating lifelike properties such as actuation, mass transport and autonomous locomotion into soft polymer gels. Further, the BZ-oscillation facilitates self-regulating structures of polymer-based self-assemblies.

To approach self-regulating actuators, Maeda and coworkers modified the gel preparation by adding 2-acrylamido-2-methylpropane-sulfonic acid (AMPS) and conduction of the polymerization above the LCST of pNIPAAm.[42] Thereby, the polymer forms a microphase-separated porous gel, with ruthenium-rich domains aggregated due to hydrophobic interactions. The modified structure allows a fast response to redox changes of the metal catalyst and results in an amplification of the original volume oscillation. In fact, the amplitude of the oscillation increased significantly and peristaltic motion within the gel becomes visible if the gel size exceeds the wavelength of the chemical wave, as illustrated in Figure 3b. The major fraction of the gel shows an orange color representative for the reduced state of the ruthenium catalyst. Following a reaction/diffusion mechanism, confined areas of locally swollen gel, corresponding to the oxidized ruthenium state (green), propagate within the gel coupled to the chemical wave

front.[42, 43] The peristaltic motion shows an amplitude of around 100 µm, which allows active transport of a poly(acrylamide) cylinder along the gel surface as depicted in Figure 3c.[44]

Besides actuation and transport, the out-of-equilibrium oscillation is further exploited to drive the autonomous motion of a self-walking gel as reported by the same workgroup.[45] Unidirectional movement of the poly(NIPAAm-*co*-Ru(bpy)$_3$-*co*-AMPS) gel is achieved by an asymmetric volume oscillation. The gel is polymerized in a mold facing a hydrophilic side at the top and a hydrophobic side at the bottom, which results in a nonuniform distribution of the different monomers. The resulting gel has a high concentration of hydrophilic AMPS on the surface and hydrophobic Ru(bpy)$_3$ at the opposite side. Immersed in an aqueous solution, the high swelling ratio of AMPS implements an asymmetric bending towards the hydrophobic side of the gel. Consequently, while the chemical wave propagates along the gel, the curvature increases as localized swelling, respective to the oxidized state of the catalyst, forces the gel into a stretching motion (1-4, Figure 3d). Afterwards, the gel bends to restore the initial conformation, which can be easily followed by the oscillating displacement (Δl) between the two edges. Translation of the bending/stretching oscillating into unidirectional movement is realized by an asymmetrical ratchet-like surface placed below the gel to prevent backsliding during the stretching process.

Much in contrast to propagating chemical waves, revealed by pulsatile motion in polymer gels of macroscopic size, redox changes of the ruthenium catalyst occur homogenously without pattern formation if the gel size falls below the length of the chemical wave (several millimeters).[46] Microgels formed by precipitation polymerization of the p(NIPAAm-*co*-Ru(bpy)$_3$) polymer, show the same dependence of the volume phase transition temperature (VPTT) as the respective macro-gels. If the ionic strength of the surrounding BZ solution is modulated correctly, the redox oscillation results in rhythmic flocculation (reduced state) and redispersion (oxidized state) of the microgels as a consequence of colloidal bistability depending on the redox state of the ruthenium catalyst.[47]

However, targeting dynamic structures comprising higher levels of hierarchy requires more complex building blocks. Tamate and coworkers achieved autonomous formation/fragmentation cycles of polymer vesicles.[48] Appropriate block ratio of hydrophobic to hydrophilic segments facilitates a unimer-to-micelle transition of the amphiphilic PEO-*b*-p(NIPAAm-*r*-Ru(bpy)$_3$) diblock copolymer as illustrated in Figure 3e.

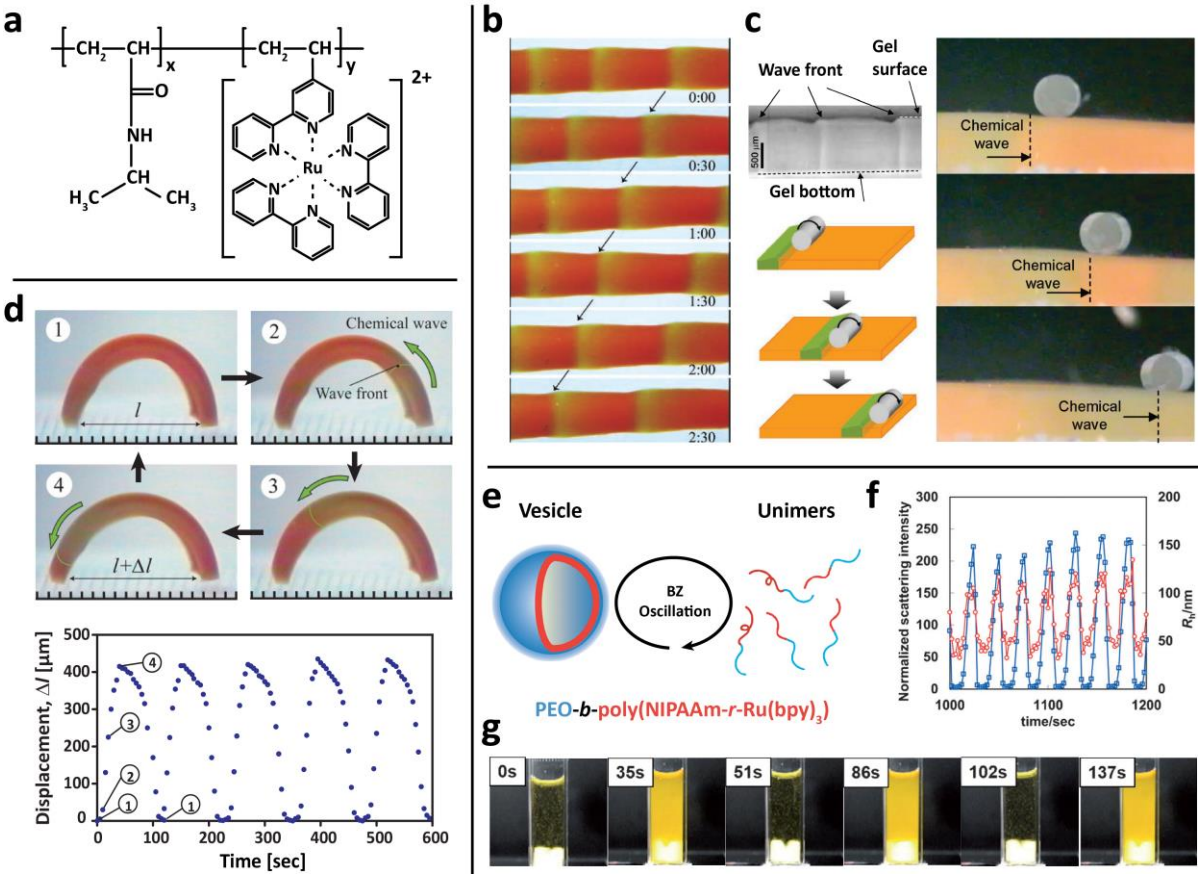

Figure 3: Self-regulating volume oscillation in polymer gels driven by the BZ-reaction. a) Chemical structure of the poly(NIPAAm-*co*-Ru(bpy)$_3^{2+}$) block copolymer. (Adapted with permission from Ref.[46]) b) Peristaltic motion within a NIPAAm-*co*-Ru(bpy)$_3$ gel copolymerized with 2-acrylamido-2-methylpropane-sulfonic acid (AMPS). Chemical waves propagate throughout the gel in a reaction-diffusion mechanism, visible by the green color of the ruthenium catalyst in the oxidized state. (Reprinted with permission from Ref.[42]) c) The peristaltic motion is utilized to move a poly(acrylamide) cylinder on the gel surface. (Adapted and reprinted with permission from Ref.[44]) d) Autonomous motion of a self-walking p(NIPAAM-*co*-Ru(bpy)$_3$-*co*-AMPS) gel. The anisotropic contraction is realized creating a hydrophilic/hydrophobic gradient within the gel. A ratchet below the gel prevents backsliding and results in autonomous unidirectional motion. (Adapted and reprinted with permission from Ref.[45]) e) Assembly/disassembly oscillation of PEO-*b*-p(NIPAAm-*r*-Ru(bpy)$_3$) vesicles, visualized in terms of periodic variation of the scattering intensity/hydrodynamic radius during DLS-measurements (f) and macroscopically by rhythmic color-changes (g). (e-g: Adapted and reprinted with permission from Ref.[48])

Self-assembly is induced passing the aggregation temperature, which differs by 3°C between the oxidized and reduced state of the ruthenium catalyst as a consequence of changing hydrophilicity. Hence, within this temperature range, the polymer becomes bistable and resides

in the self-assembled (reduced) or disassembled (oxidized) state, which is one prerequisite for non-linear phenomena. In course of the BZ-reaction conducted in the bistable regime, dynamic light scattering (DLS) measurements reveal the unimer-to-micelle oscillation as periodic changes of the light scattering intensity and the hydrodynamic radius as depicted in Figure 3f. Furthermore, the self-oscillating behavior is directly visible in terms of turbidity (Figure 3g). In presence of vesicles the solution appears turbid with a tinge of orange (reduced state), as the disassembled state results in an opaque solution.

In summary, incorporation of the BZ-catalyst into soft polymer materials allows to translate periodic oxidation/reduction cycles into autonomous mechanical oscillations. The preparation of soft-actuators, autonomous locomotion and dynamic structuring proves the potential of chemical reaction networks to target self-assembled out-of-equilibrium materials. Among various synthetic oscillators, the BZ-reaction occupies a prominent position due to a high level of autonomy. Stable and long lasting oscillations are feasible over hundreds of cycles without replenishment of the respective substrates.[27, 37] Nonetheless, addressing the time domain (oscillations frequency) is profoundly difficult. Variation of the substrate concentration or the temperature are both tolerable in a narrow range while operating beyond results in the collapse of the oscillation. Further, tunability is given by illumination with light, which liberates bromide ions, the inhibitory species of the BZ-reaction (negative feedback).[49] Besides harsh and toxic reactants, the necessity to covalently attach the BZ catalyst into the polymer structure restricts the range of conceivable materials such as peptides or DNA and respective future applications.

1.3.2 pH-Oscillations

Selective variation of the hydrogen ion concentration (H^+) and the respective local/global pH value is a key control mechanism in biological processes.[50] The integration of a self-regulating system, singularly or periodically modulating the pH of the aqueous environment, would be a highly advantageous way to control the lifetime of pH-responsive materials. First, pH-responsiveness is easily implemented into chemical/biochemical building blocks (e.g. -COOH, $-NH_2$)[51-57] and second, the pH-oscillation integrates non-equilibrium dynamics into the surrounding aqueous solution, without molecular modification of the responsive material. In contrast to the BZ-reaction, reagents of the core oscillation are not required to be covalently attached to the chemical building block of the respective self-assembly, which allows independent engineering of the oscillator or the pH-responsive material. In this section

I describe the potential of feedback-driven pH-oscillations, translating into autonomous complexation/precipitation cycles of metal ions or self-regulating rhythmic transitions between self-assembled structures. First, I present an example for classical inorganic pH-oscillators, driven by a cascade of redox reactions. Further I proceed with an organic approach, utilizing the base-catalyzed conversion of a hydrolytically instable compound to conclude with mostly challenging biocatalytically controlled pH-oscillations.

Synthetic chemical oscillators operated under non-buffered conditions are always accompanied by periodic changes in pH.[58] In terms of classification, these small-amplitude variations, also reported for the Bray and the BZ reaction,[59] are not the kinetic driving force or the redox oscillation, but rather a consequence of the periodic behavior. As most pH-oscillators similarly rely on redox reactions, I will hereby follow the classical definition by Orbán and Epstein, proving the variation of the H^+ concentration and the corresponding pH-change as the mandatory kinetic driving force of the oscillation.[58]

In the mid-1980s De Kepper and Epstein conceived an algorithm, based on a mathematical model,[60] to systematically design synthetic pH-oscillators.[61] Assuming a closed system, most individual reactions will asymptotically approach a stable equilibrium state. Thus, non-linear phenomena, such as sustained oscillations in pH, are only feasible in an open system under constant exchange of reactants, as in the case of a continuous-flow stirred tank reactor (CSTR).[62] In dependence of the flow rate and concentration of the reactant-feed, the system can now reach two distinct stable states. Hence, the combination of a CSTR, an autocatalytic reaction providing a bistable region depending on the flow rate and a negative-feedback species that reacts slowly with the autocatalyst led to the discovery of a multitude of different pH-oscillators as summarized in Figure 4a.[50]

In a classical pH-oscillator, the key component is the central oxidant, which allows to classify groups of oscillating reactions, like the bromate, hydrogen peroxide, chlorite or iodate family. Besides the oxidant, each system consists of either one or two reducing agents. Their conjoint acting gives rise to positive feedback, autocatalytic production of H^+, and a delayed negative switch, responsible for H^+ consumption.[63] Here, I will briefly discuss the Landolt-reaction representative for the group of inorganic redox pH-oscillators and demonstrate two examples how rhythmic variation in pH translates into periodic precipitation/complexation of metal ions and volume oscillation of a pH-responsive hydrogel.

Landolt-type oscillators typically comprise iodate (IO_3^{2-}) or bromate (BrO_2^-) as the central oxidant and sulfite (SO_3^{2-}) or ferrocyanide ($Fe(CN)_6^{4-}$) as reducing agents. A simplified scheme of the reaction mechanism is depicted in Figure 4b. In the initial stage of the reaction, at neutral conditions, iodate (Ox.) promotes the oxidation of sulfite (S_1), which serves as the positive feedback, autocatalytically producing H^+. The resulting decrease in pH and the depletion of sulfite induce the oxidation of ferrocyanide (S_2) by iodate, consuming protons and thereby acting as negative switch in the oscillatory cycle.[63] Translation of the periodic variation in pH into a potential material response now only requires the target system to operate within the amplitude of the pH-oscillation.

Epstein and Orbán reported the integration of the Landolt oscillation with two simple equilibrium reactions yielding periodic complexation/precipitation of calcium and aluminum ions.[64] The chelating-agent ethylenediaminetetraacetic acid (EDTA), well known for its ability to sequester multivalent metal ions, shows a highly pH-dependent complex-formation constant. Close to neutral conditions (pH ≈ 6) and in presence of Ca^{2+}, EDTA forms the Ca-EDTA complex, which rapidly dissociates when the pH is strongly decreased (pH ≈ 3). Hence, in course of the Landolt-reaction periodic Ca^{2+}-pulses can be monitored with selective electrodes and dyes. The same principle also accounts for the oscillating precipitation of aluminum hydroxide as illustrated in Figure 4c. Highly soluble around pH = 6, $Al(OH)_3$ precipitates once the surrounding pH is decreased towards acidic conditions. The periodic precipitation can be easily monitored with the naked eye in terms of varying turbidity.

Similar as reported by Yoshida utilizing the BZ-reaction,[42, 44, 46] Ryan *et al.* prepared a pH-responsive hydrogel, which undergoes periodic volume oscillations in course of the Landolt-reaction.[65] Within the collapsed pMAA gel, polymer chains form dense hydrophobic clusters under strongly acidic conditions, which disintegrate upon deprotonation of the acid groups, promoting volume expansion. The gel dimensions closely follow the pH-lead of the oscillating reaction as depicted in Figure 4d. Optical micrographs further illustrate the deswelling transition of the respective pMAA gel during the autocatalytic H^+-production within the pH-cycle (Figure 4e).

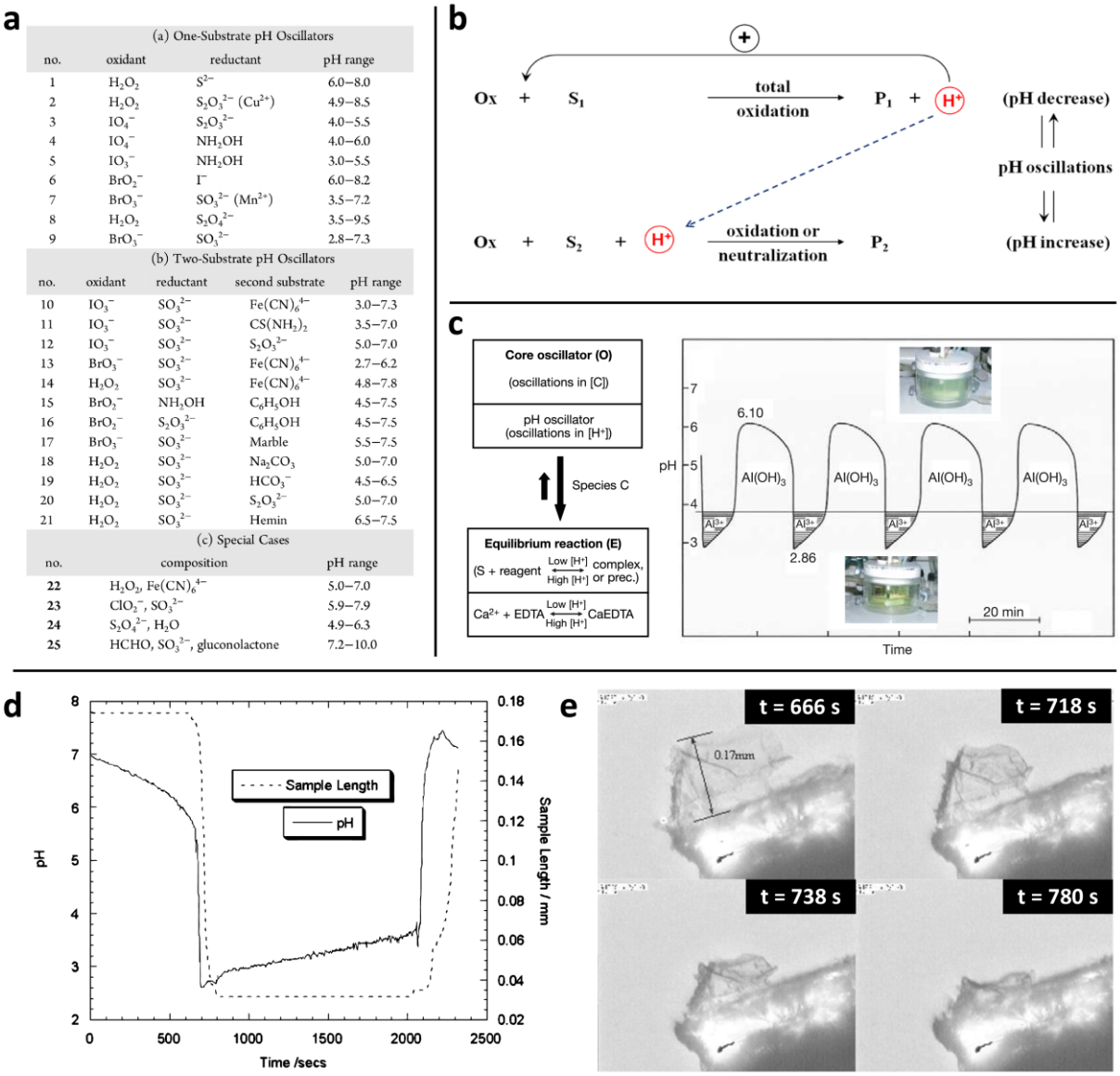

Figure 4: Translation of pH-oscillations into a material response: The Landolt-oscillator. a) Table with established pH-oscillators classified by the number of components required in addition to the central oxidant. (Reprinted with permission from Ref.[63]) b) Schematic representation of the feedback-cycle of H^+ production/consumption for a two-substrate oscillator, such as the Landolt-system. (Reprinted with permission from Ref.[63]) c) Complexation/precipitation oscillation of aluminum hydroxide driven by the Landolt-reaction. (Reprinted and adapted with permission from Ref.[64]) d) Volume oscillation of a pH-responsive poly methacrylic acid (pMAA) gel in response to the Landolt oscillator. e) Optical micrographs of the respective pMAA gel piece in course of the pH-cycle. (d, e: Reprinted and adapted with permission from Ref.[65])

In fact, the Landolt-reaction is ubiquitously utilized to implement temporal signatures into responsive materials, which further lead to volume oscillations in polymer multilayers or polyelectrolyte brushes and rhythmic actuation of synthetic muscles.[66-68] However, sustained oscillations still require continuous feeding of fresh reactants to maintain the non-linear character, which severely restricts self-regulating applications in closed systems. Poros *et al.* developed a simple method to operate various pH-oscillators, which all involve sulfite as reductant, in a closed configuration.[69] Equipping the reaction vessel with a silica bed, which was loaded with sodium sulfite before, allows to maintain the reactant-feed by diffusion from the layer under batch conditions. Still, the majority of pH-oscillators relies on redox chemistry comprising harsh reactants as peroxides, halogen species, sulfur and transition metals, which restricts applications demanding biocompatible components.

To overcome the obstacle of insufficient biocompatibility, Kovacs *et al.* developed the first organic pH-oscillator operating in a CSTR.[70] The methylene glycol – sulfite reaction, in which methylene glycol undergoes dehydration, was studied primarily.[71] In course of the reaction, the production of OH^- proceeds in an autocatalytic fashion and thereby serves as the positive feedback.[72] Simulations revealed periodic oscillations in pH, if the reaction is coupled with a base-consuming step.[73] The base-catalyzed hydrolysis of gluconic acid δ-lactone (GDL), furnishing gluconic acid, provides such a negative switch (Figure 5a). While a single pH-peak appears from batch-conditions, large-amplitude oscillations in pH are observed under continuous feeding of fresh GDL in a CSTR (Figure 5b).[70] As described for the Landolt-reaction, the methylene glycol – sulfite – gluconolactone (MGSG) oscillator can be utilized to translate rhythmic pH-changes into a material´s response.

Lagzi *et al.* described the periodic vesicle-to-micelle transition of oleic-acid molecules, driven by the MGSG oscillator (Figure 5c).[74] In the protonated state, close to the pK_a value of oleic acid (pH ≈ 8), the molecules assemble into bilayer membrane vesicles with a hydrodynamic radius of around 100 nm, proven by dynamic light scattering (DLS) measurements. The presence of vesicular structures is also visible with the naked eye, as the solution turns turbid. Increasing the pH beyond pH = 8 results in rapid deprotonation of the acid groups causing the formation of unilamellar micelles with a hydrodynamic radius less than 10 nm. Coupled to the MGSG oscillator, the fatty acid molecules rhythmically switch back and forth between the self-assembled vesicular and micellar state, as depicted in Figure 5d.

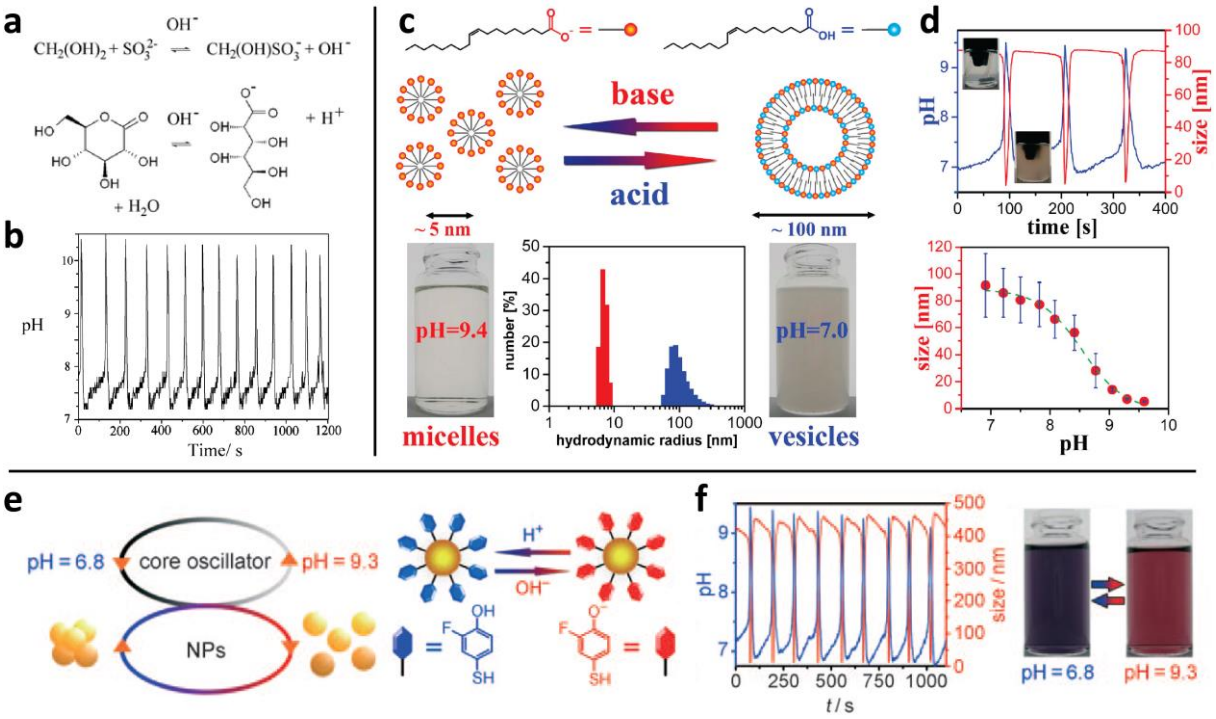

Figure 5: The organic methylene glycol - sulfite - gluconolactone oscillator: a) Base-catalyzed dehydration of methylene glycol and hydrolysis of gluconic acid δ-lactone providing positive and negative feedback to the oscillatory cycle. b) Sustained oscillations in pH under continuous feeding of GDL in a CSTR. (a, b: Reprinted with permission from Ref.[70]) c) Vesicle-to-Micelle transition of oleic acid molecules driven by the MGSG oscillator. The size distribution measured by dynamic light scattering allows to distinguish between the micelle/vesicle states. d) In course of the pH-oscillation, the fatty acid molecules commute between the micelle and vesicle structure. (c, d: Reprinted and adapted with permission from Ref.[74]) e) Rhythmic gold nanoparticle aggregation/dispersion proceeding in-phase with the MGSG pH-oscillation. The nanoparticles are functionalized with a 2-fluoro *p*-mercaptophenol ligand to implement pH-responsiveness. f) DLS measurements and periodic color changes reveal switching between particle aggregation and subsequent redispersion. (e, f: Reprinted and adapted with permission from Ref.[75])

Engineering electrostatic forces between surface-functionalized gold nanoparticles (AuNPs) allows to translate the MGSG-oscillation into rhythmic Au-NP aggregation/dispersion, as reported by the same group (Figure 5e).[75] The nanoparticles are coated with a pH-responsive ligand bearing a phenol group. If the pH of the surrounding solution is above the pK_a (pH ≈ 9), the majority of acid groups are deprotonated, which results in electrostatic interparticle repulsion and homogenous dispersion of the AuNPs. Below pH ≈ 7, the ligand becomes protonated, which shields the electrostatic charges and fosters aggregation. With respect to the MGSG-reaction, the AuNPs oscillate between both states, which can be monitored by DLS as

the hydrodynamic size varies significantly among individual NPs and larger aggregates (Figure 5f). Macroscopically, the oscillation can be monitored by visible color-changes, as the solution turns purple upon aggregation and remains red in the dispersed state. The respective color corresponds to the position of the surface plasmon resonance band, which shows a pronounced red shift upon particle redispersion.

In summary, the MGSG-oscillator provides large-amplitude pH-oscillations as a consequence of positive feedback and a delayed negative switch. Omitting redox species commonly utilized in previous pH-oscillators facilitates applications in a biocompatible environment. Here, base-catalyzed hydrolysis of GDL serves as the negative switch within the oscillatory cycle. In my thesis, I do not target rhythmic pH-changes, though I will demonstrate a preorchestrated transient alkaline pH-state in a closed configuration, following from the kinetic balance of GDL hydrolysis and rapid alkaline activation (Chapter 2). Furthermore the presence of GDL is a potential starting point to implement biocatalytic reaction pathways and substitute the negative switch with the glucose-oxidase catalyzed conversion of glucose into GDL. In fact, the typical bell-shaped pH-dependent enzyme activity implies autocatalytic feedback-controlled behavior, which, depending on the direction of the enzyme-switch, may result in sustained pH-oscillations in combination with the positive/negative feedback-correspondent. Nonetheless, examples of enzyme-driven pH-oscillators are restricted by the availability of suitable enzymes operating large-amplitude pH-switches, such as glucose oxidase (GOx) and urease, which I will discuss within the next section.

The enzyme glucose oxidase (E) catalyzes the oxidation of glucose (G) into GDL (P), which in aqueous environment undergoes base-catalyzed hydrolysis to furnish gluconic acid (GA). The central mechanism is depicted in Figure 6a.[76] Throughout the reaction the redox cofactor flavin adenine dinucleotide (FAD), initially present in the oxidized state (E_{ox}), becomes reduced (E_r), accepting the electrons originating from the glucose oxidation step. To restart the catalytic cycle, a second electron accepting substrate such as molecular oxygen (O_2) regenerates FAD. In the present approach, oxygen is substituted by ferricyanide ($[Fe(CN)_6]^{3-}$) to oxidize the FAD cofactor, as the reaction is autocatalytic in pH (positive feedback). In a typical batch-experiment, GOx rapidly converts glucose into GDL, which instantaneously undergoes base-catalyzed hydrolysis, steadily decreasing the pH (Figure 6b). Operated under continuous-flow conditions bistability is found for different flow-rates of ferricyanide and hydroxide. Computer-controlled inflow of hydroxide serves as the negative switch resulting in sustained oscillations

in pH (Figure 6c).

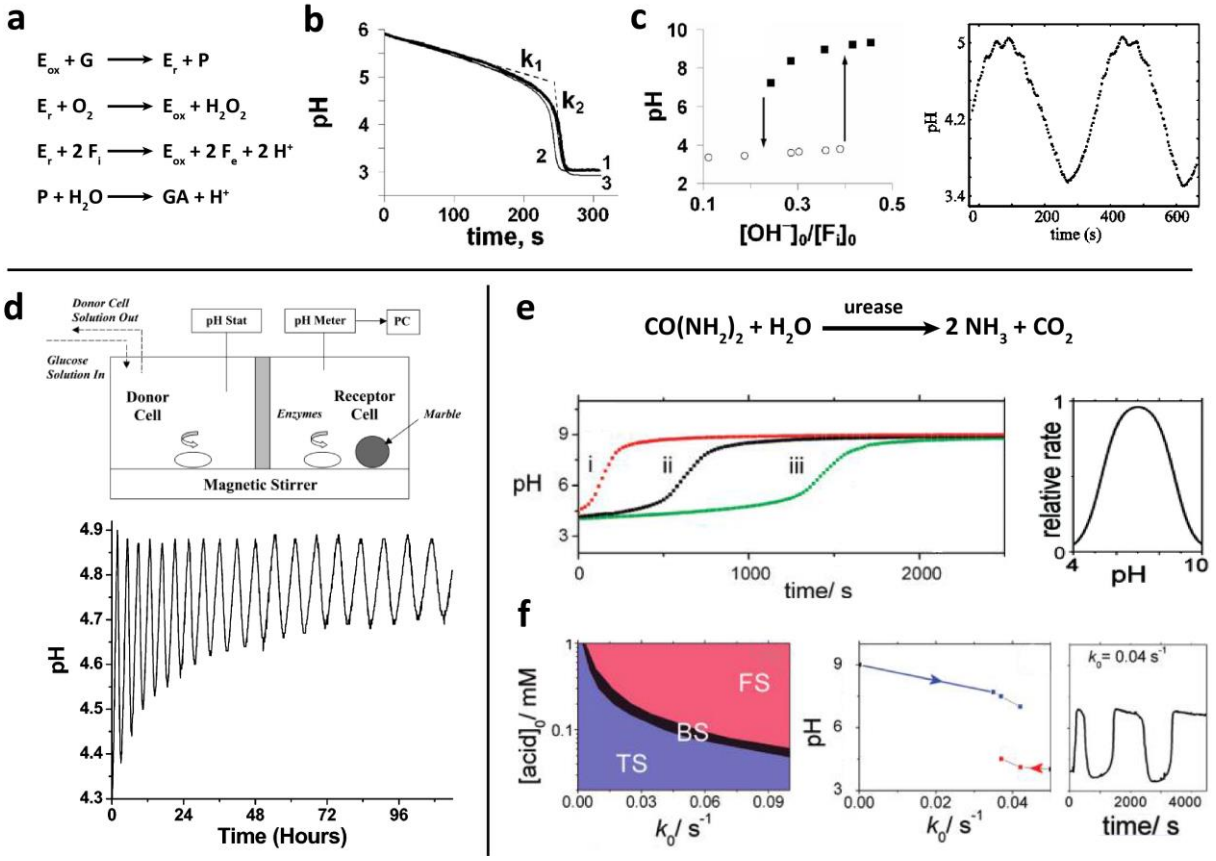

Figure 6: Biocatalytic feedback-controlled oscillations in pH: a) The central reaction mechanism includes positive feedback in the reaction of glucose and ferricyanide with GOx. b) The feedback-driven biocatalytic conversion of glucose into GDL results in a continuous pH-decrease. c) Depending on the flow rate of ferricyanide and hydroxide, the system shows a region of bistability. Operated in a CSTR, sustained oscillations in pH can be observed. Computer-controlled inflow of hydroxide provides the negative switch. (a-c: Reprinted and adapted with permission from Ref.[76]) d) Chemomechanical oscillation in the glucose – glucose oxidase system. A bistable pH-hysteretic p(NIPAAm-*co*-MAA) hydrogel regulates the glucose permeability towards the receptor cell. Glucose oxidation liberates hydrogen ions to control the membrane permeability in a negative feedback loop. The resulting volume/permeability oscillations translate into stable oscillations in pH. (Reprinted and adapted with permission from Ref.[77]) e) Feedback-driven alkaline pH-switch in the urea-urease system. The bell-shaped pH-dependency of the urease activity provides an autocatalytic production of base. f) Operated in a CSTR, the reaction shows regions of bistability for a small range of flow rates (urease, urea and acetic acid). (e, f: Reprinted and adapted with permission from Ref.[1])

In a different approach, Dhanarajan *et al.* utilized a pH-hysteretic poly(NIPAAm-*co*-MAA) hydrogel membrane to integrate a chemomechanical feedback into the glucose – glucose oxidase reaction (Figure 6d).[77] The membrane separates the donor/receptor sub-units and integrates a bistable switch into the system. The donor cell maintains a stable pH (pH = 7) and provides a constant concentration of glucose, which permeates the swollen hydrogel membrane towards the receptor cell, containing GOx. The biocatalytic conversion of glucose liberates hydrogen ions, which diffuse towards the membrane. Protonation of the charged MAA groups initiates the collapse of the outer membrane layer, which subsequently restricts the flow into the membrane for further glucose molecules (negative feedback). The pH within the receptor cell gradually increases and the membrane returns to the original high permeability state again.

The GOx-catalyzed oxidation of glucose provides an acidic switch, which, in combination with an appropriate negative feedback, facilitates periodic pH-changes. In the opposite direction, the urea – urease system operates an alkaline pH-switch upon the autocatalytic production of ammonia in a highly pH-dependent fashion (Figure 6e).[1, 78, 79]

The bell-shaped activity profile displays two separated regions of low enzymatic activity under acidic (pH < 4) and alkaline (pH > 9) conditions, which encompass an area of high conversion-rate with the maximum located at pH = 7.[80, 81] Starting from acidic conditions (pH ≈ 4), the production of base is initially slow. As the pH gradually increases, the reaction self-accelerates (pH ≈ 7) displaying a steep pH-jump until the curve levels off at around pH = 9 due to the formation of an ammonium buffer. Providing the system with increasing amounts of acetic acid to adjust the initial pH, clearly shifts the onset of the pH-jump towards longer time scales as a consequence of the higher concentration of acid groups to be neutralized and slight differences in the initial pH (Figure 6e; i, ii and iii). Operated under non-equilibrium conditions in a CSTR, bistability can be observed for different flow rates (k_0) of urea, urease and acetic acid. Increasing the flow rate starting from the reacted low-flow state (blue curve) and conversely decreasing the flow rate from the unreacted high-flow state (red curve), span an area of high and low pH values coexisting for identical flow rates. Only for a narrow range of flow rates aperiodic oscillations can be observed (Figure 6f).

Though, periodic oscillations have not yet been reported for the urea-urease system, the autocatalytic base-producing switch has been utilized to support propagating pH-waves. Under batch-conditions in the absence of stirring, the positive feedback promotes the diffusion-driven propagation of an alkaline pH-front, which converts acidic environment surrounding the wave front into base left behind.[82] Based on the very same principle, the urease feedback was utilized (during the course of this thesis by others) to control propagating fronts of base-catalyzed Michael addition of thiol and acrylate reactants in an aqueous solution.[83] Depending on the initial concentration of substrate and enzyme an induction period prior to the gelation can be controlled with high confidence. Independent from the enzymatic switch, varying the degree of crosslinking within the hydrogel further allows controlling the lifetime, as the gel is prone to ester-hydrolysis. In contrast, within my thesis I will utilize the urease-catalyzed feedback-driven generation of base to demonstrate pH-responsive hydrogels with predefined lifetimes via active catalytic control. In combination with an acidic buffer, the concentration of urease ultimately controls the temporal fate of transient preorchestrated pH-profiles encoding the lifetime of the respective self-assembly (Chapter 3, 4).

In the end, there is a plethora of established pH-oscillators, which compare with a multitude of available pH-responsive self-assembling systems to be coupled with. Nonetheless, the level of autonomy clearly obstructs the way towards self-regulating materials in closed systems, as constant feeding of reactants is required to maintain the non-equilibrium character. Increasing interest and understanding of biocatalytic reactions may notably forward the field as simple enzymatic switches and advanced reaction networks facilitate preorchestrated self-regulating materials, as I will present in the course of this work.

1.3.3 Biocatalytic Reaction Networks

Within the previous section, I described the principle of self-accelerating biocatalytic reactions, to serve as a positive feedback. In combination with a simple negative switch, such as the computer controlled inflow of acid or base, the overall system gives rise to oscillations in pH. In nature, complex non-equilibrium behavior originates from interconnected biocatalytic reaction networks (see also section 1.2).[84] Hence, substituting both, negative and positive feedback within a synthetic regulatory cycle by biocatalytic reactions opens pathways towards adaptive and autonomous behavior far from equilibrium.

Semenov *et al.* designed an enzymatic reaction network based on hydrolysis of the precursor-molecule trypsinogen (*Tg*) into trypsin (*Tr*) in an autocatalytic fashion (positive feedback).[85] The detailed regulatory cycle is depicted in Figure 7a. In the next step, trypsin cleaves the lysine group of the protoinhibitor (Ac-Lys(Me)-Gln-Inh), before aminopeptidase M converts the resulting intermediate (H-Gln-Inh) into the active inhibitory species (negative feedback). The N-terminal cleavage of glutamine (Gln) by aminopeptidase thereby integrates the required delay, to temporally separate the positive and negative feedback loop. Carefully balancing the concentrations and flow rates within a CSTR results in stable oscillations in the trypsin concentration as illustrated in Figure 7b.

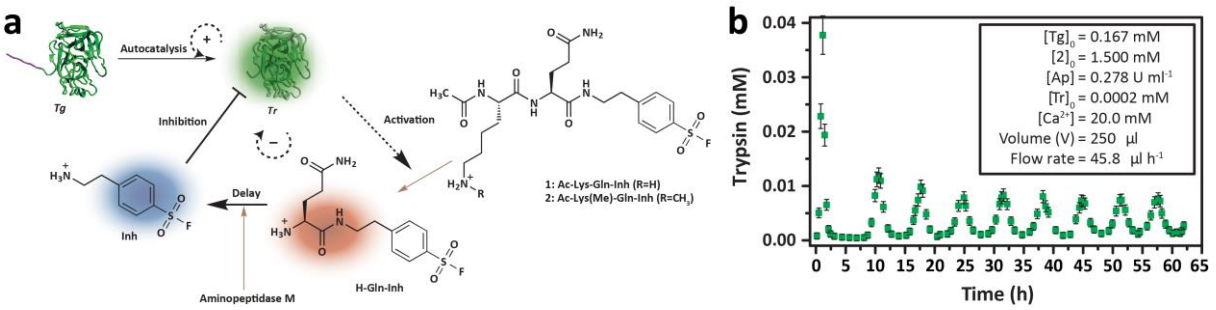

Figure 7: Enzymatic reaction networks: a) Detailed reaction profile with inherent feedback mechanisms in the trypsin oscillator. b) Sustained oscillations in trypsin concentration in a CSTR. (a, b: Adapted and reprinted with permission from Ref.[85])

Besides the integration of temporal signatures, biocatalytic reaction networks are capable of programming Boolean logic gates (AND/OR) into hydrogel materials.[86] Here, the presence of hydrogen peroxide promotes the gel-sol transition of a tripeptide hydrogel. Encapsulation of different enzymes allows encoding the logic operation upon addition of the respective substrates. Exemplarily, the incorporation of acetylcholine esterase (AChE) and choline oxidase (COx) allows to program the OR-gate. Since AChE regulates the hydrolysis of acetylcholine into choline, which subsequently becomes oxidized by COx into hydrogen peroxide, both acetylcholine OR choline induce gel-sol transition. Such enzyme-based logic gates can be coupled to promote pH-sensitive biofuel cells and nanoparticles.[87, 88]

1.4 Transient Hydrogels under Catalytic Control and Energy Dissipation in Closed Systems

Within the section above I described an enzymatic reaction network with stable oscillations in the trypsin concentration, driven by the biocatalytic activation of an inhibitory species. Moreover, enzymes can be utilized to directly manipulate the self-assembly process, for instance by the biocatalytic formation of a hydrogelator originating from distinct precursor molecules.

Debnath *et al*. described the transient self-assembly of a peptide hydrogelator with the biocatalyst *a*-chymotrypsin as the central pacemaker.[89] The protease kinetically controls the formation and disintegration of the transient hydrogel within a sol-gel-sol reaction pathway.[90] To furnish the active hydrogelator (2), naphthalene-tyrosine methyl ester (1) reacts with amide-functionalized tyrosine (4) in a α-chymotrypsin-catalyzed transacetylation reaction (Figure 8a). Competing with the activating step, the biocatalyst also controls the hydrolysis of the dipeptide amide (2) and the disintegration of the hydrogel into the monopeptide acid (3) and the original amino acid (4). In presence of α-chymotrypsin, the transacetylation reaction proceeds rapidly and the maximum conversion into Nap-YY-NH_2 is reached within minutes, as illustrated in Figure 8b. Over time, the hydrolytic deactivation predominates, which, depending on the critical gelation concentration, results in a transient hydrogel-state. The lifetime of the hydrogel is directly controlled by the α-chymotrypsin concentration. While the transacetylation showed limited sensitivity on the amount of biocatalyst, the hydrolytic deactivation indicates a strong dependence, which allows tuning the lifetime within the range of 16 – 3 hours (Figure 8c).

The presented approach was further extended to realize α-chymotrypsin-catalyzed formation of self-assembling tripeptides.[91] Operated under conditions, where self-assembly is thermodynamically disfavored, the transacetylation reaction of aspartam (1*) with an amino acid (3) results in the transient formation of the hydrogelator (2) as illustrated in Figure 8d. Again, hydrolysis of the tripeptide controls the disassembly of the supramolecular structure. Within a range of different amino acids (3), only amide-functionalized tyrosine and phenylalanine produced self-supporting hydrogels.

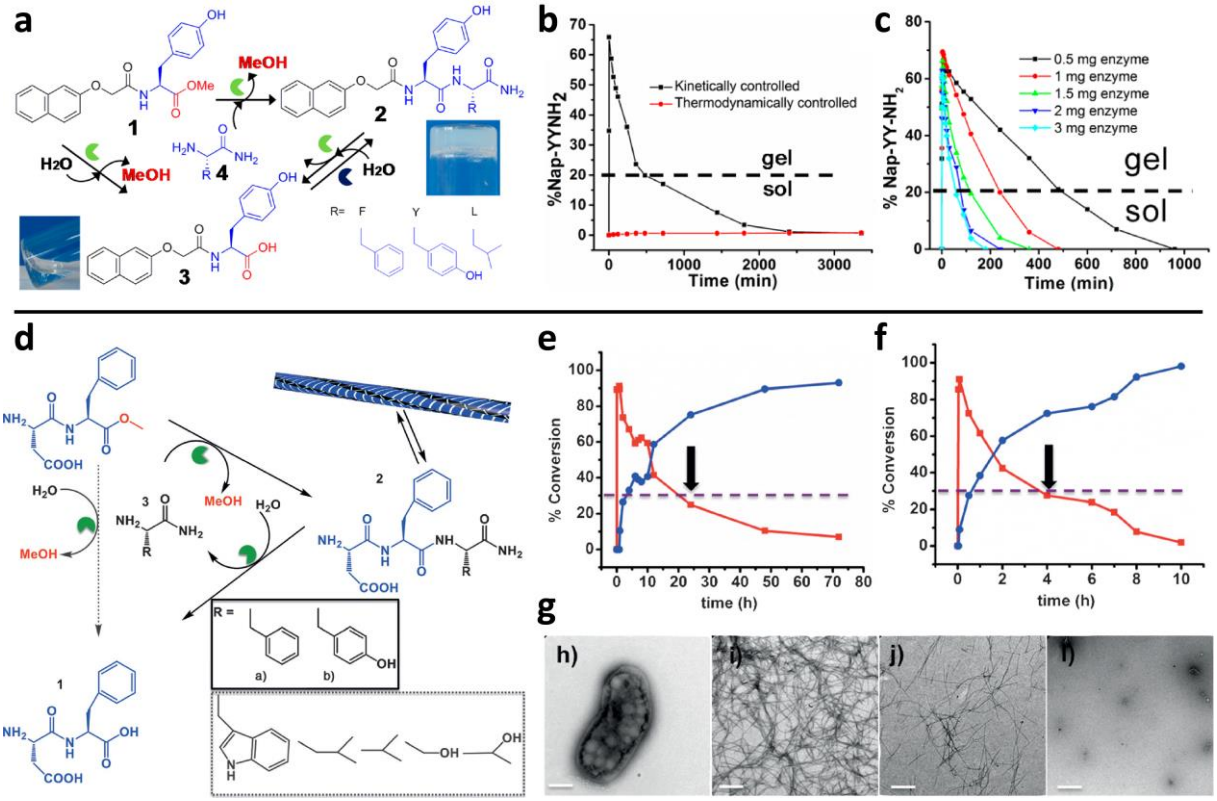

Figure 8: The kinetic balance of transacetylation and hydrolysis provides transient hydrogels: a) Scheme of the self-regulating biocatalytic self-assembly of a peptide hydrogelator. b) Kinetically controlled, transient hydrogelation of Nap-Y-NH_2 (black line). To find the final equilibrium position, the thermolysine-catalyzed direct condensation of Nap-YY-OH and Y-NH_2 is utilized (red curve). c) The enzyme concentration controls the lifetime of the transient hydrogel state. (a-c: Reprinted with permission from Ref.[89]) d) Biocatalytic self-assembly of a transient tripeptide hydrogelator. e-f) Conversion of aspartam-phenylalanine-NH_2 (red curve, e) and aspartam-tyrosine-NH_2 (red curve, f) and the corresponding hydrolysis products (blue curve, e and f) analyzed by high pressure liquid chromatography (HPLC). g) TEM images of aspartam (h) and the resulting tyrosine tripeptide after 0.08, 4 and 24 hours. (d-g: Reprinted with permission from Ref.[91])

The α-chymotrypsin-catalyzed formation of the hydrogelator was found to be independent of the tripeptide sequence, as the reaction with each, tyrosine and phenylalanine reached a conversion of around 90% after 30 minutes (Figure 8e, f). In contrast, substitution of phenylalanine with tyrosine dramatically shortens the lifetime of the transient hydrogel state from 24 to 4 hours. Thus, engineering the peptide sequence allows to control the kinetic pathway within biocatalytic, transient self-assembled hydrogels.

In fact, self-regulating structures can be realized following enzymatic reaction pathways. The lifetime of the self-assembled structure is directly coupled to the amount of available biocatalyst, which implies active, catalytic control. The presented approach facilitates fully autonomous, temporally predefined structure formation as the system contains all required information, as soon as the respective concentrations of substrates and the enzyme are combined. Different lifetimes can be realized varying the biocatalyst concentration or the peptide hydrogelator sequence, which demonstrates temporal programming with a high level of precision only met by chemically fueled, energy-dissipating systems presented in the following section. While α-chymotrypsin significantly restricts the range of conceivable building motifs for the formation of autonomous self-assemblies, the biocatalytic feedback system described in Chapter 3, 4 and 5 can be programmed with even higher accuracy and enables temporal programming of any pH-responsive assembly operating in the targeted pH-regime.

An alternative way to tune the lifetime of supramolecular hydrogels is to couple the activation of a non-assembling precursor building block to the consumption of a chemical fuel as schematically shown in Figure 9a. During the formation of the metastable self-assembly, the energy is dissipated, which induces the structure to collapse once the fuel is depleted, as described similarly for the dynamic instabilities of microtubules in Section 1.2.

The presented approach by Boekhoven *et al.* is based on the building block dibenzoyl cystein (DBC), which is a pH-responsive low molecular weight gelator (LMWG).[92] The reaction cycle is depicted in Figure 9b.[93] Above pH ≈ 4.5, electrostatic repulsion between the anionic carboxylate groups prevents the self-assembly into nanofibers (Figure 9b, 2a). Here, activation of the precursor molecule is coupled to the presence of a chemical fuel, dimethyl sulfate (DMS), to furnish the active hydrogelator via esterification (Figure 9b, 2b). The formed ester molecule is prone to hydrolysis in an aqueous environment, which provides the deactivating pathway to restore the DBC-carboxylate. Kinetic prerequisite for the formation of the transient hydrogel state is the rate of energy dissipation (ester hydrolysis) to fall below the rate of fuel uptake (carboxylate alkylation).

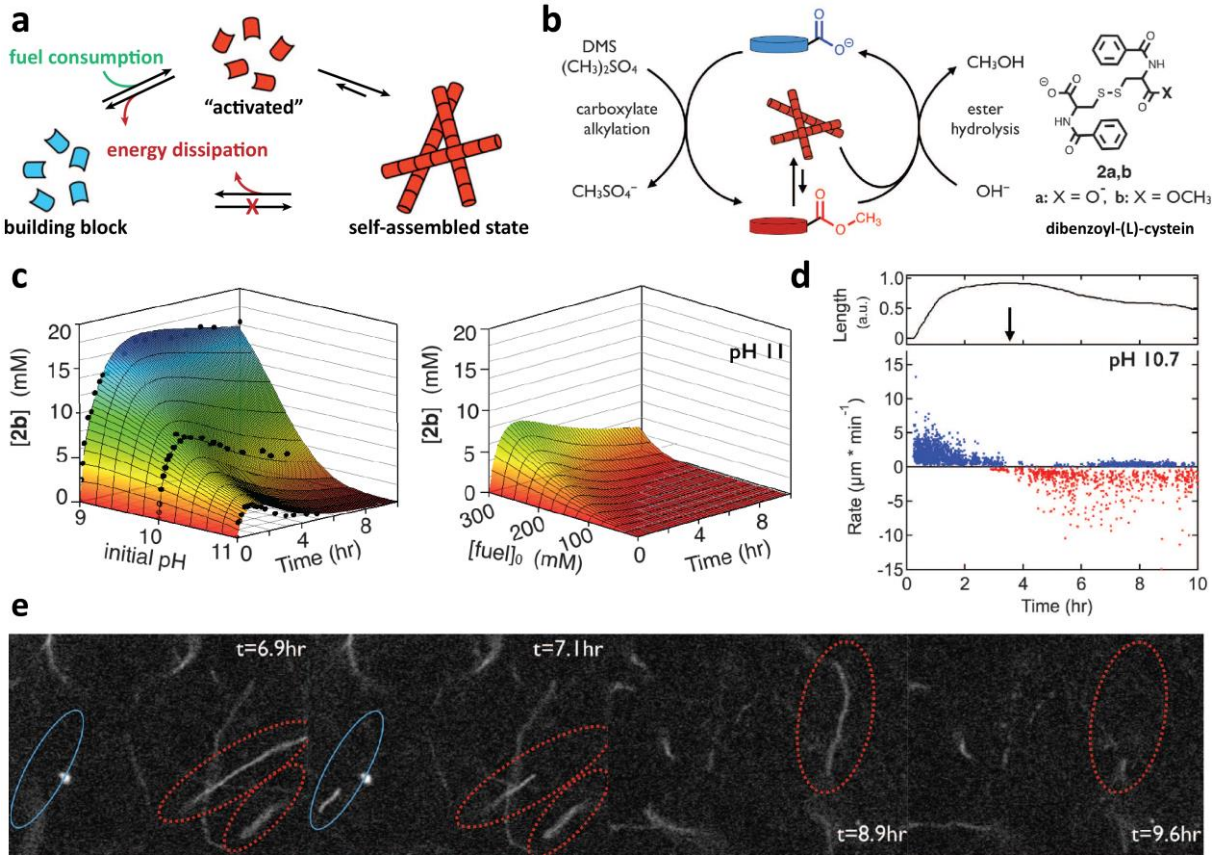

Figure 9: Dissipative self-assembly of nanofibers in presence of a chemical fuel: a) Kinetic balance of fuel consumption and energy dissipation controls the lifetime of the transient self-assembled hydrogel state. (Adapted and reprinted with permission from Ref.[92]) b) The alkylating agent DMS activates the precursor DBC via esterification (fuel consumption). Hydrolysis of the formed methyl ester reverts the inactive DBC carboxylate (energy dissipation). c) Controlling the kinetics of hydrogelator formation. While the pH value controls the rate of hydrolysis, the DMS concentration regulates the rate of alkylation. d) Analyzing the rate of assembly and disassembly and the respective fiber length for a given pH. e) Simultaneous assembly (blue circles) and disassembly (red circles) of fibers visualized by confocal microscopy. (b-e: Reprinted with permission from Ref.[93])

Balancing the kinetics of both reactions can be realized by selective variation of the fuel concentration (DMS) and the pH-value of the aqueous environment, as illustrated in Figure 9c. For a given concentration of the alkylating agent, the formation of the active hydrogelator is highly pH-dependent. As ester hydrolysis is base-catalyzed, a steady state in the concentration of the hydrogelator is realized upon addition of DMS, for moderately alkaline conditions (pH = 9). For higher pH values, the rate of hydrolysis increases, which significantly reduces the concentration of available gelator molecules, therefore reducing the hydrogel lifetime to a few hours. Extending the lifetime can be realized raising the concentration of the alkylating agent.

Upon addition of DMS, the system first shows a period of fiber growth as illustrated in Figure 9d. Reminiscent of the dynamic instability of microtubules, for a certain period the fibers simultaneously assemble and disassemble, as illustrated in Figure 9d and e. For a constant pH value, the concentration of DMS provided, preorchestrates the lifetime of the dissipative self-assembly and feeds the information required for autonomous behavior into the system, representing a landmark approach towards self-regulating soft materials.

1.5 Self-Assembly via Energy Dissipation using External Fields

In contrast, external energy sources such as the application of magnetic fields or illumination with light allow the formation of non-equilibrium structures with high spatiotemporal precision on request, but lack the high degree of autonomy provided by chemically fueled systems. Present examples in literature comprise the formation of dynamic ferrofluid droplet patterns in a time-varying magnetic field and non-equilibrium assembly of Au-NPs to form metastable inks upon exposure to UV-light, as I will briefly describe in the following.

Exposed to a magnetic field of adjustable strength, ferrofluid droplets assemble into patterned structures on a superhydrophobic surface as depicted in Figure 10a.[94] Upon increasing field strength, parental droplets divide into daughter droplets, which are kinetically trapped as a consequence of magnetic repulsion and the hydrophobic surface underneath, though they coalesce once the field is switched off. Non-equilibrium structures are formed under continuous energy supply, which in the present approach is realized by an oscillating horizontal movement of the magnetic field as schematically illustrated in Figure 10b. Above a critical frequency, reduced distance between the ferrofluid droplets allows to overcome the kinetic trapping, which results in the formation of dynamic patterns. In a different approach, the balance of energy-driven rotation and hydrodynamic repulsion of small objects on the water surface led to the emergence of similar patterns.[95] In both examples, dynamic structures are only stable under continuous energy input, which equates the lifetime of the self-assembled state with the duration of rotation or oscillation of the surrounding magnetic field. Once switched off, the system reverts to the equilibrium state. In fact, both systems constantly dissipate energy, but do not involve self-regulating behavior where, if at all, the relaxation towards the thermodynamic minimum can be considered autonomous.[27]

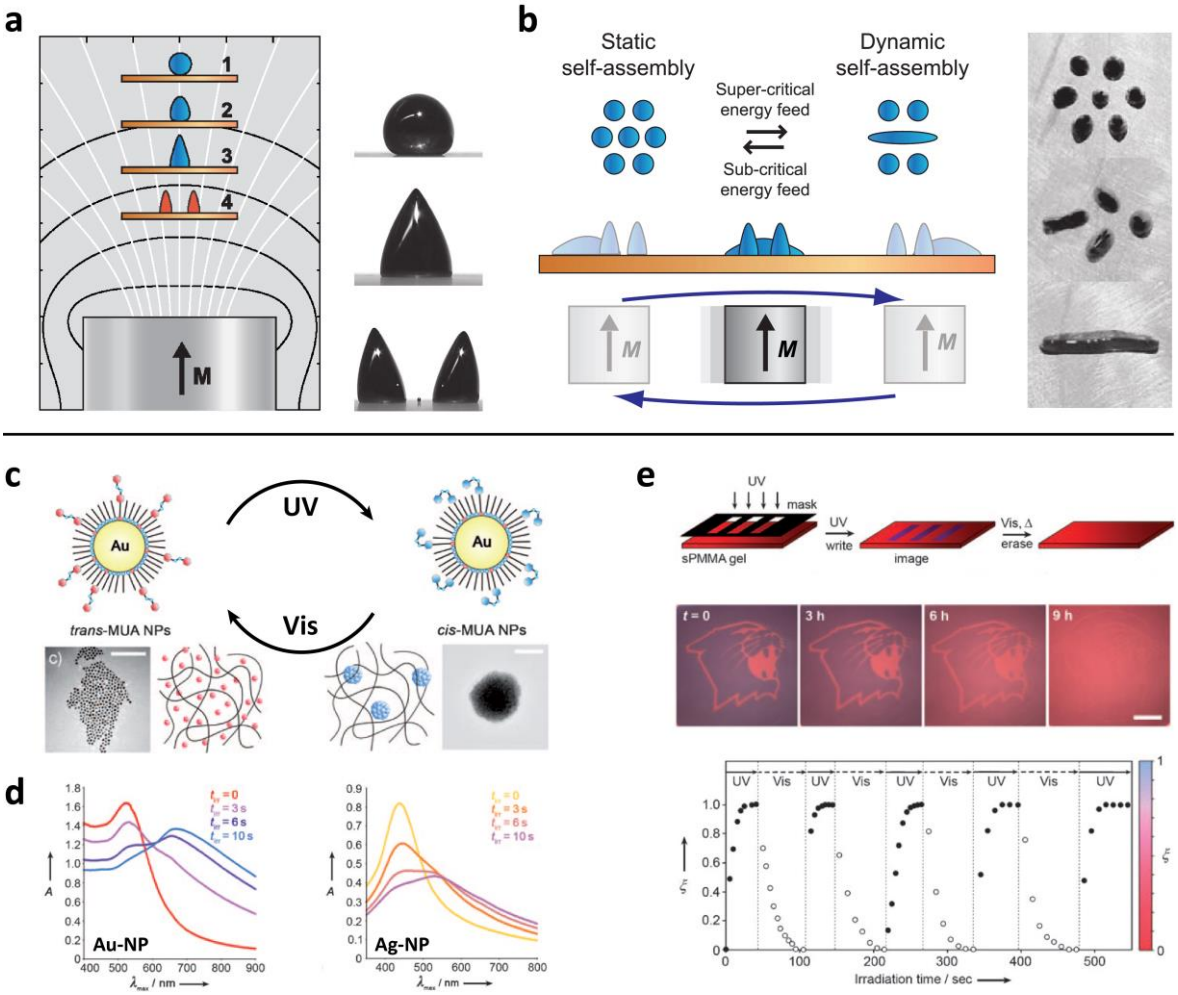

Figure 10: Transient self-assemblies sustained by external energy. a) Static self-assembly of ferrofluid droplets on a superhydrophobic surface. b) Switching between static and dynamic self-assembly. Horizontal oscillation of the magnetic field results in the emergence of dissipative structures. (a-b: Reprinted with permission from Ref.[94]) c) Photo-isomerization of the azobenzene-containing ligand translates into non-equilibrium aggregation of nanoparticles, which can be reverted by irradiation with visible light. d) Duration of UV-illumination and the class of nanoparticles controls the color of the aggregates, measured via UV-Vis spectroscopy. e) Writing on self-erasable Au-NP films via UV-exposure. Cycles of UV/Vis irradiation allow sequential rewriting. (c-e: Reprinted with permission from Ref.[96])

The combination of light-fuelled isomerization and thermodynamic relaxation is the fundamental principle of the metastable nanoparticle ink described by Klajn et al.[96] The photoswitchable molecule *trans*-azobenzene undergoes isomerization into the *cis*-form upon irradiation with UV-light.[97] The rearrangement alters the dipole moment of the molecule and results in a thermodynamically unstable configuration (*cis*), which spontaneously reverts to the *trans*-form. The decoration of Au-NPs with an azobenzene-containing ligand allows translating

the photo-isomerization into non-equilibrium aggregation of nanoparticles upon UV-irradiation as schematically shown in Figure 10c. Duration of the UV-exposure controls the color of the particle aggregates, which shifts from red (non-aggregated) to blue (aggregated), as depicted in Figure 10d. For the preparation of self-erasable thin films, the Au-NPs are embedded in an organogel matrix. Covered with a photo-mask, only NPs in the area exposed to UV-light form metastable aggregates, which facilitates printing self-erasable patterns as illustrated in Figure 10e.

1.6 Scope of the Thesis

Within this work I will demonstrate different strategies, following kinetic and biocatalytic pathways, to preorchestrate transient pH-profiles and integrate temporal signatures into various pH-responsive self-assemblies.

First, I will showcase a kinetic concept to program an alkaline transient pH-state, which encodes the lifetime of block copolymer micelles/vesicles, gold nanoparticle aggregates and peptide nanofibrils (Chapter 2). Though the formation of self-assembled structures is widely investigated, I will for the first time demonstrate a platform approach to integrate a self-regulation mechanism, controlling the lifetime of pH-responsive self-assemblies over several orders of magnitude. I will present, how the kinetic balance of a directly available promoter (base) and an initially dormant deactivator translates into self-regulating alkaline pH-profiles (Figure 11a). Here, ester or lactone molecules serve as dormant species, which are prone to base-catalyzed hydrolysis, releasing the active deactivator (acid). Further, I will investigate, how the structure and concentration of the dormant deactivator controls the rate of hydrolysis, directly modulating the kinetics of the transient pH-state. Finally, I will demonstrate integration of the internal feedback system with different pH-responsive building motifs, to predefine transient structure formation. Hence, the established platform approach allows to program the lifetime of virtually any pH-responsive self-assembling system, operating in the accessible pH-regime.

Within the second concept, I will demonstrate how biocatalytic feedback-driven generation of base facilitates a self-regulating acidic pH-state to encode the lifetime of dipeptide hydrogels and the transient optical response of a block copolymer photonic display. (Chapter 3, 4). Here, the activation of the dormant deactivator (urea) follows a biocatalytic pathway utilizing the enzyme urease. The integration of a biocatalyst is highly beneficial as the bell-shaped pH-dependent enzyme activity provides positive feedback to the system. First, I will investigate how different concentrations of promoter, dormant deactivator and biocatalyst influence the time domain of the transient acidic pH-profile (Figure 11b). Further, I will show the integration of the biocatalytic feedback system with a peptide gelator. Since the concentration of the biocatalyst directly controls the liberation of the active deactivator, I will demonstrate catalytically-controlled temporal programming of dipeptide hydrogels, spanning lifetimes from minutes to hours. Finally, I will present first-time applications of self-regulating hydrogels in the field of transient rapid prototyping and fluidic guidance. In a similar approach I will

investigate the integration of the biocatalytic feedback system with a pH-sensitive block copolymer photonic gel to preorchestrate the lifetime of a transient reflective state and demonstrate a first application towards self-regulating photonic displays (Chapter 4). The presented approach provides precise biocatalytic control over the deactivating pathway. Nevertheless, the activating step still relies on the injection of a simple acidic buffer, though the substitution with a dormant activator would provide advanced control.

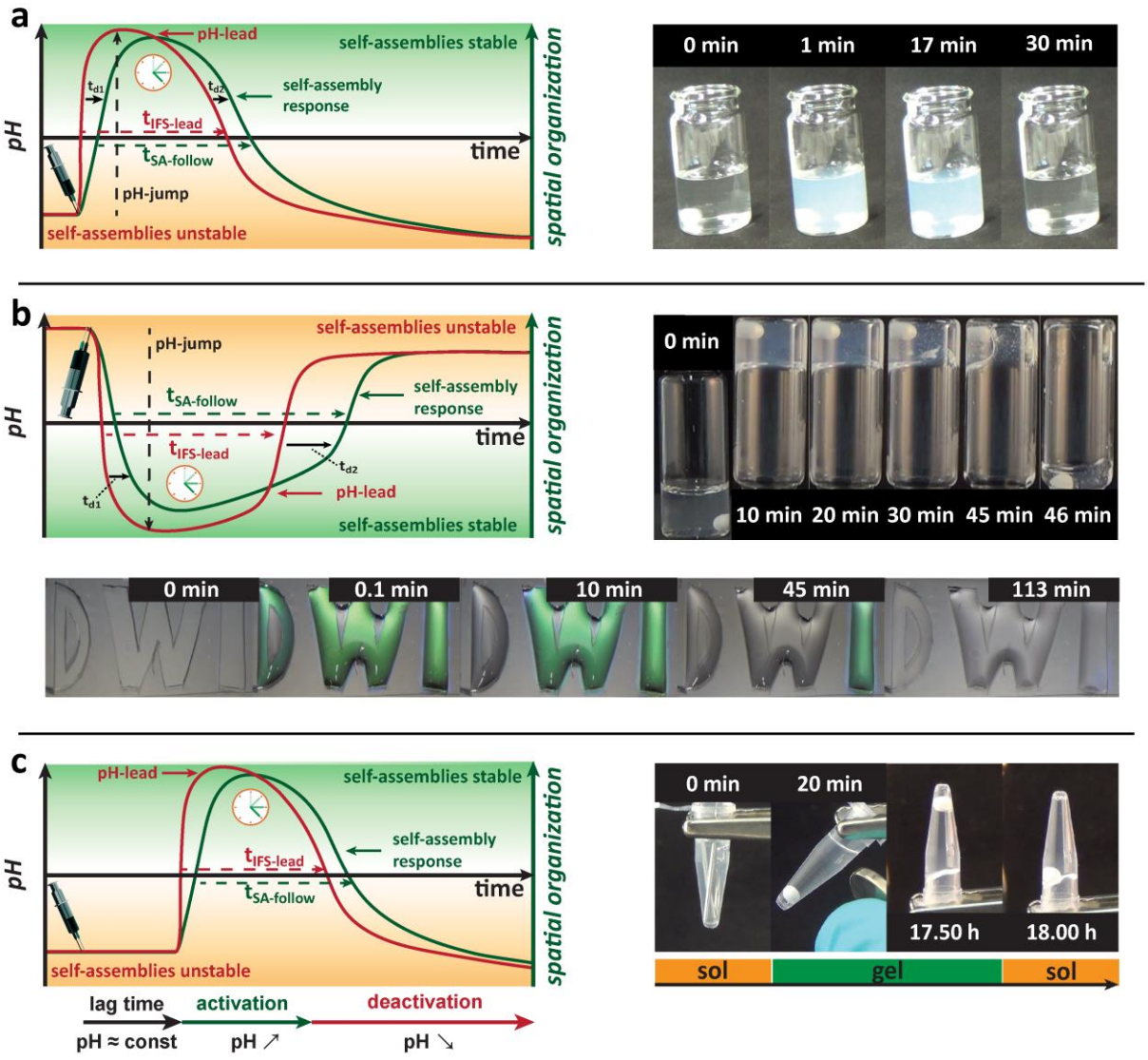

Figure 11: Scope of the thesis: a) Kinetic concept to preorchestrate an alkaline transient pH-state, controlling the lifetime of self-regulating BCP self-assemblies, Au-NP aggregates and peptide nanofibrils. b) The biocatalytic feedback-driven generation of base allows to program transient acidic pH-profiles to encode the lifetime of dipeptide hydrogels and the reflective state of a block copolymer photonic film. c) Balancing two antagonizing biocatalytic reactions regulates a transient alkaline pH-state programming the lifetime of self-regulating DNA-hydrogels.

Within the last part I will investigate the kinetic balance of two antagonistic biocatalytic reactions, to preorchestrate an alkaline pH-state, preceded by an initial lag time (Chapter 5). In the presented biocatalytic reaction network, opposing enzymes convert dormant activators and deactivators into their active forms. Here, the activating step relies on the urease-catalyzed conversion of urea, while the deactivation is achieved to the biocatalytic conversion of ethyl acetate by the enzyme esterase (Figure 11c). First, I will investigate the enzyme ratios required, to meet the kinetic prerequisites realizing transience in the alkaline regime. Further, I will demonstrate how to program the initial lag time for given enzyme and substrate concentrations, increasing the content of available acetic acid buffer introduced to the system. Finally, I will present the integration of the dual-enzymatic feedback with a novel DNA hydrogel, to control the initial lag time prior to hydrogelation.

1.7 Outlook

Within my thesis I investigated different strategies to preorchestrate transient pH-profiles encoding the lifetime of pH-responsive self-assembling systems. Initially, I proved the base-catalyzed hydrolysis of ester-containing molecules in combination with a rapid promoter, to translate into alkaline pH-profiles with predefined lifetimes. The solid dormant deactivator gluconic acid δ-lactone was dissolved in dimethyl sulfoxide (DMSO) to prevent hydrolysis prior to the experiment and to avoid any impact of solubility phenomena. Unfortunately the presence of DMSO renders the feedback system incompatible with delicate self-assemblies such as the oligopeptide hydrogelator. The integration of glucose oxidase in combination with glucose, which is water soluble and not prone to hydrolysis, allows to implement a biocatalytic switch into the feedback system. The biocatalyst facilitates advanced temporal control, broadening the applicability in the absence of organic solvents.

Further I presented acidic pH-profiles with predefined lifetimes following a biocatalytic pathway, utilizing the feedback-driven urease-catalyzed generation of base. Here, in combination with a rapid promoter, the concentration of the biocatalyst ultimately controls the lifetime of the transient pH-state and the synchronized self-assembly. High concentrations of urease enable lifetimes in the range of minutes, however longer timescales are restricted to 11 hours, approaching the minimum enzyme concentration still generating base efficiently. Introducing a further biocatalytic switch prior to the urease-catalyzed negative feedback

provides an efficient delay mechanism and opens pathways towards complex cascade reactions and biocatalytic reaction networks. The enzyme barbiturate amidohydrolase controls the catalytic conversion of barbituric acid into malonic acid and urea. Carefully balancing the kinetics of biocatalytic hydrolysis, starving the availability of urea, and subsequent amide cleavage may extend the range of accessible lifetimes significantly. Further the incorporation of urease into responsive microgels would facilitate advanced spatiotemporal control mechanisms.

In the last part I realized transient alkaline pH-profiles, balancing two antagonistic biocatalytic reactions, the urease-catalyzed generation of base and the release of acid following the conversion of ethyl acetate by the enzyme esterase. Within a follow-up concept a flip-flop system could be realized with the ratio of urease/esterase regulating the course of the transient pH-state being either alkaline or acidic for constant substrate concentrations. Furthermore the immobilization of enzymes within magnetic nanoparticles would open pathways towards advanced spatial control such as pattern formation and directed particle motion.

1.8 References

1. Hu, G.; Pojman, J. A.; Scott, S. K.; Wrobel, M. M., Taylor, A. F., *J. Phys. Chem. B* **2010,** *114*, 14059-14063.
2. Ko, C. H., Takahashi, J. S., *Hum. Mol. Genet.* **2006,** *15*, 271-277.
3. Gallego, M., Virshup, D. M., *Nat. Rev. Mol. Cell Biol.* **2007,** *8*, 139-148.
4. Guillaumond, F.; Dardente, H.; Giguère, V., Cermakian, N., *J. Biol. Rhythms* **2005,** *20*, 391-403.
5. Yamazaki, S.; Numano, R.; Abe, M.; Hida, A.; Takahashi, R.-i.; Ueda, M.; Block, G. D.; Sakaki, Y.; Menaker, M., Tei, H., *Science* **2000,** *288*, 682-685.
6. Reppert, S. M., Weaver, D. R., *Nature* **2002,** *418*, 935-941.
7. Jennifer, A. M.; Carla, B. G., Joseph, S. T., *Annu. Rev. Neurosci.* **2012,** *35*, 445-462.
8. Berridge, M. J.; Bootman, M. D., Roderick, H. L., *Nat. Rev. Mol. Cell Biol.* **2003,** *4*, 517-529.
9. Uhlén, P., Fritz, N., *Biochem. Biophys. Res. Commun.* **2010,** *396*, 28-32.
10. Alberts, B.; Johnson, A.; Lewis, J.; Morgan, D.; Raff, M.; Roberts, K., Walter, P., *Molecular Biology of the Cell*. (ed. 6th, 2015).
11. Bean, B. P., *Nat. Rev. Neurosci.* **2007,** *8*, 451-465.
12. Berridge, M. J., *J. Physiol.* **1997,** *499*, 291-306.
13. Mikoshiba, K., *J. Neurochem.* **2007,** *102*, 1426-1446.
14. Ran, Z.; Stephan, E. L., Andrew, R. M., *Annu. Rev. Biochem* **2007,** *76*, 367-385.
15. Bezprozvanny, l.; Watras, J., Ehrlich, B. E., *Nature* **1991,** *351*, 751-754.
16. Cheeseman, I. M., Desai, A., *Nat. Rev. Mol. Cell Biol.* **2008,** *9*, 33-46.
17. Mitchison, T., Kirschner, M., *Nature* **1984,** *312*, 237-242.
18. Howard, J., Hyman, A. A., *Nature* **2003,** *422*, 753-758.
19. Caplow, M., Shanks, J., *J. Biol. Chem.* **1990,** *265*, 8935-8941.

20. Ravelli, R. B. G.; Gigant, B.; Curmi, P. A.; Jourdain, I.; Lachkar, S.; Sobel, A., Knossow, M., *Nature* **2004,** *428*, 198-202.
21. Akhmanova, A., Steinmetz, M. O., *Nat. Rev. Mol. Cell Biol.* **2015,** *16*, 711-726.
22. Conde, C., Caceres, A., *Nat. Rev. Neurosci.* **2009,** *10*, 319-332.
23. Farina, F.; Gaillard, J.; Guerin, C.; Coute, Y.; Sillibourne, J.; Blanchoin, L., Thery, M., *Nat. Cell Biol.* **2016,** *18*, 65-75.
24. Lotka, A. J., *J. Am. Chem. Soc.* **1920,** *42*, 1595-1599.
25. Prigogine, I., Lefever, R., *J. Chem. Phys* **1968,** *48*, 1695-1700.
26. Prigogine, I., Nicolis, G., *J. Chem. Phys* **1967,** *46*, 3542-3550.
27. Heinen, L., Walther, A., *Soft Matter* **2015,** *11*, 7857-7866.
28. Warren, S. C.; Guney-Altay, O., Grzybowski, B. A., *J. Phys. Chem. Lett.* **2012,** *3*, 2103-2111.
29. Grzybowski, B. A., Huck, W. T. S., *Nat. Nanotechnol.* **2016,** *11*, 585-592.
30. Merindol, R., Walther, A., *Royal Society Reviews* **2017,** accepted.
31. Belousov, B., *Sb. Rf. Radiats. Med.* **1958**.
32. Epstein, I. R., Showalter, K., *J. Phys. Chem.* **1996,** *100*, 13132-13147.
33. Zaikin, A. N., Zhabotinsky, A. M., *Nature* **1970,** *225*, 535-537.
34. Noyes, R. M.; Field, R., Koros, E., *J. Am. Chem. Soc.* **1972,** *94*, 1394-1395.
35. Field, R. J.; Koros, E., Noyes, R. M., *J. Am. Chem. Soc.* **1972,** *94*, 8649-8664.
36. Field, R. J., Noyes, R. M., *J. Chem. Phys* **1974,** *60*, 1877-1884.
37. Epstein, I. R., *Chem. Commun.* **2014,** *50*, 10758-10767.
38. Yoshida, R.; Takahashi, T.; Yamaguchi, T., Ichijo, H., *Adv. Mater.* **1997,** *9*, 175-178.
39. Hirokawa, Y., Tanaka, T., *J. Chem. Phys* **1984,** *81*, 6379-6380.
40. Yoshida, R.; Uchida, K.; Kaneko, Y.; Sakai, K.; Kikuchi, A.; Sakurai, Y., Okano, T., *Nature* **1995,** *374*, 240-242.
41. Yoshida, R.; Sakai, T.; Ito, S., Yamaguchi, T., *J. Am. Chem. Soc.* **2002,** *124*, 8095-8098.
42. Maeda, S.; Hara, Y.; Yoshida, R., Hashimoto, S., *Angew. Chem.* **2008,** *120*, 6792-6795.
43. Field, R., Burger, M., *Oscillations and Traveling Waves in Chemical Systems*. (Wiley, New York, 1985).
44. Murase, Y.; Maeda, S.; Hashimoto, S., Yoshida, R., *Langmuir* **2009,** *25*, 483-489.
45. Maeda, S.; Hara, Y.; Sakai, T.; Yoshida, R., Hashimoto, S., *Adv. Mater.* **2007,** *19*, 3480-3484.
46. Yoshida, R., *Adv. Mater.* **2010,** *22*, 3463-3483.
47. Suzuki, D.; Sakai, T., Yoshida, R., *Angew. Chem. Int. Ed.* **2008,** *47*, 917-920.
48. Tamate, R.; Ueki, T.; Shibayama, M., Yoshida, R., *Angew. Chem.* **2014,** *126*, 11430-11434.
49. Shinohara, S.-i.; Seki, T.; Sakai, T.; Yoshida, R., Takeoka, Y., *Angew. Chem. Int. Ed.* **2008,** *47*, 9039-9043.
50. Sagues, F., Epstein, I. R., *Dalton Trans.* **2003,** 1201-1217.
51. Stuart, M. A. C.; Huck, W. T. S.; Genzer, J.; Muller, M.; Ober, C.; Stamm, M.; Sukhorukov, G. B.; Szleifer, I.; Tsukruk, V. V.; Urban, M.; Winnik, F.; Zauscher, S.; Luzinov, I., Minko, S., *Nat Mater* **2010,** *9*, 101-113.
52. Adams, D. J.; Butler, M. F.; Frith, W. J.; Kirkland, M.; Mullen, L., Sanderson, P., *Soft Matter* **2009,** *5*, 1856-1862.
53. Fletcher, N. L.; Lockett, C. V., Dexter, A. F., *Soft Matter* **2011,** *7*, 10210-10218.
54. Kim, E.; Kang, C.; Baek, H.; Hwang, K.; Kwak, D.; Lee, E.; Kang, Y., Thomas, E. L., *Adv. Funct. Mater.* **2010,** *20*, 1728-1732.
55. Kang, Y.; Walish, J. J.; Gorishnyy, T., Thomas, E. L., *Nat. Mater.* **2007,** *6*, 957-960.
56. Liu, D., Balasubramanian, S., *Angew. Chem. Int. Ed.* **2003,** *42*, 5734-5736.
57. Hartgerink, J. D.; Beniash, E., Stupp, S. I., *Science* **2001,** *294*, 1684-1688.

58. Rabai, G.; Orban, M., Epstein, I. R., *Acc. Chem. Res.* **1990,** *23*, 258-263.
59. Tsukada, M., *Chem. Lett.* **1987,** *16*, 1707-1710.
60. Boissonade, J., De Kepper, P., *J. Phys. Chem.* **1980,** *84*, 501-506.
61. De Kepper, P.; Epstein, I. R., Kustin, K., *J. Am. Chem. Soc.* **1981,** *103*, 2133-2134.
62. Field, R. J., *J. Chem. Educ.* **2000,** *77*, 450.
63. Orbán, M.; Kurin-Csörgei, K., Epstein, I. R., *Acc. Chem. Res.* **2015,** *48*, 593-601.
64. Kurin-Csörgei, K.; Epstein, I. R., Orbán, M., *Nature* **2005,** *433*, 139-142.
65. Crook, C. J.; Smith, A.; Jones, R. A. L., Ryan, A. J., *Phys. Chem. Chem. Phys.* **2002,** *4*, 1367-1369.
66. Tang, Y.; Liu, G.; Yu, C.; Wei, X., Zhang, G., *Langmuir* **2008,** *24*, 8929-8933.
67. Ryan, A. J.; Crook, C. J.; Howse, J. R.; Topham, P.; Jones, R. A. L.; Geoghegan, M.; Parnell, A. J.; Ruiz-Perez, L.; Martin, S. J.; Cadby, A.; Menelle, A.; Webster, J. R. P.; Gleeson, A. J., Bras, W., *Faraday Discuss.* **2005,** *128*, 55-74.
68. Howse, J. R.; Topham, P.; Crook, C. J.; Gleeson, A. J.; Bras, W.; Jones, R. A. L., Ryan, A. J., *Nano Lett.* **2006,** *6*, 73-77.
69. Poros, E.; Horváth, V.; Kurin-Csörgei, K.; Epstein, I. R., Orbán, M., *J. Am. Chem. Soc.* **2011,** *133*, 7174-7179.
70. Kovacs, K.; McIlwaine, R. E.; Scott, S. K., Taylor, A. F., *J. Phys. Chem. A* **2007,** *111*, 549-551.
71. Kovacs, K.; McIlwaine, R.; Gannon, K.; Taylor, A. F., Scott, S. K., *J. Phys. Chem. A* **2005,** *109*, 283-288.
72. Kovacs, K.; McIlwaine, R. E.; Scott, S. K., Taylor, A. F., *Phys. Chem. Chem. Phys.* **2007,** *9*, 3711-3716.
73. McIlwaine, R.; Kovacs, K.; Scott, S. K., Taylor, A. F., *Chem. Phys. Lett.* **2006,** *417*, 39-42.
74. Lagzi, I.; Wang, D.; Kowalczyk, B., Grzybowski, B. A., *Langmuir* **2010,** *26*, 13770-13772.
75. Lagzi, I.; Kowalczyk, B.; Wang, D., Grzybowski, B. A., *Angew. Chem. Int. Ed.* **2010,** *49*, 8616-8619.
76. Vanag, V. K.; Míguez, D. G., Epstein, I. R., *J. Chem. Phys* **2006,** *125*, 194515.
77. Dhanarajan, A. P.; Misra, G. P., Siegel, R. A., *J. Phys. Chem. A* **2002,** *106*, 8835-8838.
78. Kistiakowsky, G. B., Rosenberg, A. J., *J. Am. Chem. Soc.* **1952,** *74*, 5020-5025.
79. Krajewska, B., *J. Mol. Catal. B: Enzym.* **2009,** *59*, 22-40.
80. *J. Mol. Catal. B: Enzym.* **2009,** *59*, 9-21.
81. Fidaleo, M., Lavecchia, R., *Chem. Biochem. Eng. Q.* **2003,** *17*, 311-318.
82. Wrobel, Magdalena M.; Bánsági, T., Jr.; Scott, Stephen K.; Taylor, Annette F.; Bounds, Chris O.; Carranza, A., Pojman, John A., *Biophys. J. 103*, 610-615.
83. Jee, E.; Bánsági, T.; Taylor, A. F., Pojman, J. A., *Angew. Chem. Int. Ed.* **2016,** *55*, 2127-2131.
84. Novak, B., Tyson, J. J., *Nat. Rev. Mol. Cell Biol.* **2008,** *9*, 981-991.
85. Semenov, S. N.; Wong, A. S. Y.; van der Made, R. M.; Postma, S. G. J.; Groen, J.; van Roekel, H. W. H.; de Greef, T. F. A., Huck, W. T. S., *Nat. Chem.* **2015,** *7*, 160-165.
86. Ikeda, M.; Tanida, T.; Yoshii, T.; Kurotani, K.; Onogi, S.; Urayama, K., Hamachi, I., *Nat. Chem.* **2014,** *6*, 511-518.
87. Amir, L.; Tam, T. K.; Pita, M.; Meijler, M. M.; Alfonta, L., Katz, E., *J. Am. Chem. Soc.* **2009,** *131*, 826-832.
88. Motornov, M.; Zhou, J.; Pita, M.; Gopishetty, V.; Tokarev, I.; Katz, E., Minko, S., *Nano Lett.* **2008,** *8*, 2993-2997.
89. Debnath, S.; Roy, S., Ulijn, R. V., *J. Am. Chem. Soc.* **2013,** *135*, 16789-16792.
90. Williams, R. J.; Smith, A. M.; Collins, R.; Hodson, N.; Das, A. K., Ulijn, R. V., *Nat.*

Nanotechnol. **2009,** *4*, 19-24.
91. Pappas, C. G.; Sasselli, I. R., Ulijn, R. V., *Angew. Chem. Int. Ed.* **2015,** *54*, 8119-8123.
92. Boekhoven, J.; Brizard, A. M.; Kowlgi, K. N. K.; Koper, G. J. M.; Eelkema, R., van Esch, J. H., *Angew. Chem. Int. Ed.* **2010,** *49*, 4825-4828.
93. Boekhoven, J.; Hendriksen, W. E.; Koper, G. J. M.; Eelkema, R., van Esch, J. H., *Science* **2015,** *349*, 1075-1079.
94. Timonen, J. V. I.; Latikka, M.; Leibler, L.; Ras, R. H. A., Ikkala, O., *Science* **2013,** *341*, 253-257.
95. Grzybowski, B. A.; Stone, H. A., Whitesides, G. M., *Nature* **2000,** *405*, 1033-1036.
96. Klajn, R.; Wesson, P. J.; Bishop, K. J. M., Grzybowski, B. A., *Angew. Chem. Int. Ed.* **2009,** *48*, 7035-7039.
97. Klajn, R.; Stoddart, J. F., Grzybowski, B. A., *Chem. Soc. Rev.* **2010,** *39*, 2203-2237.

2 Generic Concept to Program the Time Domain of Self-Assemblies with a Self-Regulation Mechanism

The results presented in this chapter were published in the article: T. Heuser et al., *Nano Letters*, **2015**, 15, 2213-2219

2.1 Introduction

The recent decade has witnessed great progress in static near-equilibrium self-assembly, and we increasingly understand how to construct very complex soft matter via molecular programming using competing interactions, coassemblies, and hierarchical length scales.[1-17] This has furnished real-life materials with unprecedented functionalities, inaccessible without balanced interplay of molecular interactions and delicate control over nano/meso-structuration.[18-22] However, reaching new levels of functionalities and complexity requires to go beyond structuring under static conditions and to find pathways to orchestrate the time domain of self-assemblies via internal and external feedback mechanism. Success in this largely unsolved challenge would open up possibilities for self-regulating, dynamic, and adaptive behavior. The challenge to control the time domain of self-assemblies can be approached by managing the kinetics of opposing assembly/disassembly reactions, the implementation of internal feedback systems or the use of energy dissipation to sustain structures only as long as a chemical fuel is available. The most notable approach towards temporal patterns uses the coupling of specifically designed self-assemblies to nonlinear chemical oscillators. Most success was reported using the Belousov-Zhabotinsky reaction to generate pulsating hydrogels or control aggregate formations.[23] Such nonlinear oscillators are, however, very rare and attempts to tune their time scale quickly lead to collapse of their feedback systems.[23-28]

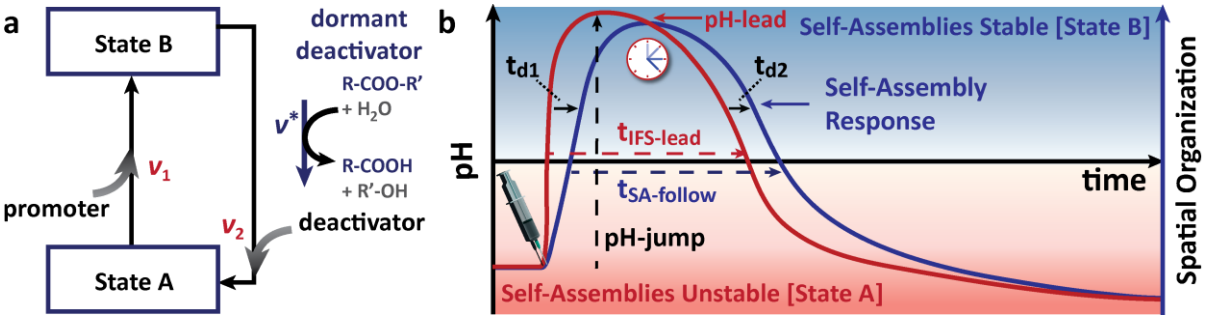

Scheme 1: Kinetic control to program self-regulating self-assemblies in time by simultaneous injection of rapid promoters and dormant deactivators (DDs). a) Stringent kinetic boundary conditions $\nu_1 >> \nu_2$ to achieve transient self-assemblies can be lifted using DDs. The relevant kinetic condition changes to $\nu_1 >> \nu^*$, $\nu_1 \approx \nu_2$ becomes irrelevant. Ultimately, an excess of the deactivator leads to the self-regulated disassembly. b) Simultaneous addition of promoter and DD leads to a transient pH-profile (red), which the self-assembly follows with system-specific offsets (t_{d1}, t_{d2}).

Dissipative self-assemblies are forcefully kept away from equilibrium by continuous energy input.[29-32] They are prominent in nature (e.g. microtubules) but profoundly difficult to create artificially.[30-32] Most difficult to realize are chemically fueled dissipative self-assemblies in closed systems. These require establishing a delicate balance between a promoting (ν_1) and a competing deactivating (ν_2) step to allow a nonlinear evolution with the formation of a transient self-assembled state that self-regulates/decays without any further external signal (Scheme 1). In some cases, the deactivating step must be a slow hydrolysis of an activated species. They are particularly rare as tedious optimization is needed to prevent direct annihilation of the promoter in the deactivating environment, and the boundary condition of $\nu_1 > \nu_2$ for transient self-assembly formation remains an outstanding challenge (Figure 14).[32, 33] For instance, van Esch and coworkers used MeI to temporally methylate carboxyl acid functions of a gelator and trigger a self-assembly that is subsequently reversed by hydroxide triggered hydrolysis.[32] Overall, the need for system-specific optimization is the major bottleneck to push sophisticated chemically fuelled dissipative self-assemblies into applications.

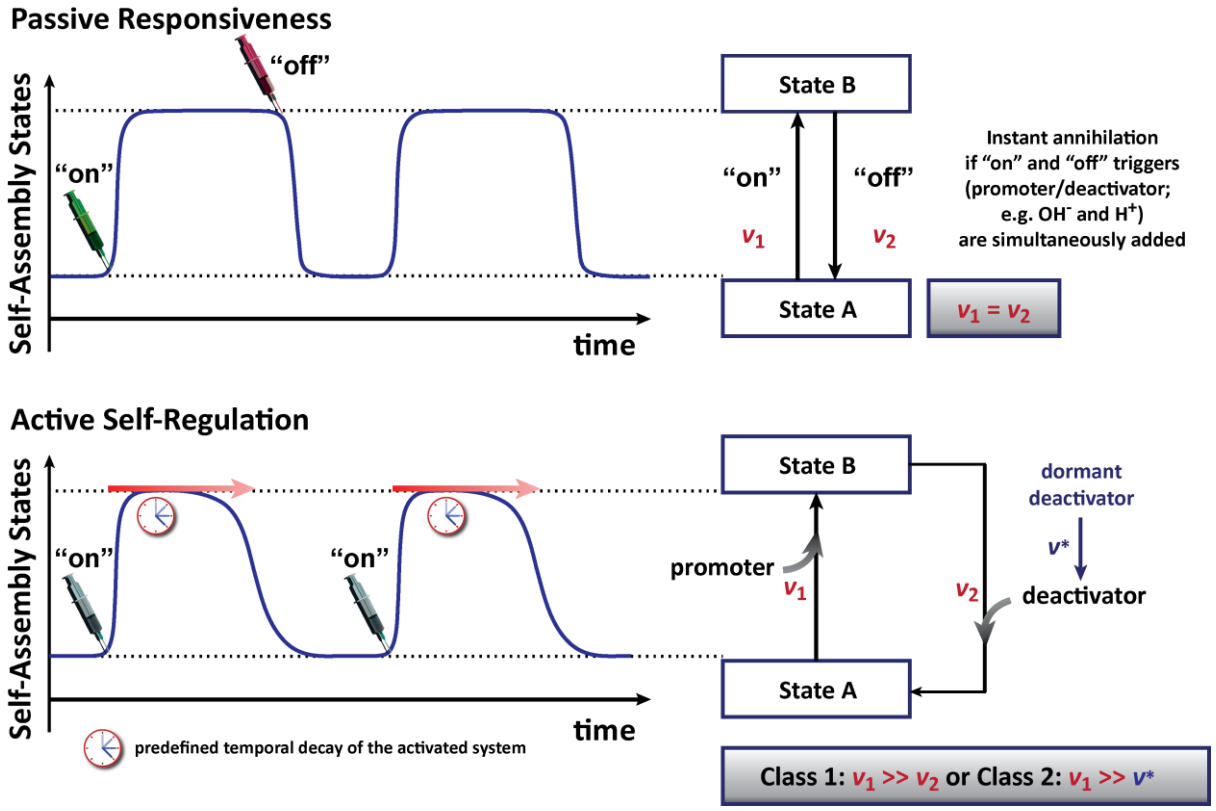

Figure 12: Responsive vs. self-regulated, temporally programmed self-assemblies. (TOP) Classical responsive systems requiring sequential "on" and "off" triggers to induce changes from state A to state B and back. For a simple responsive system, the "on" switch (promoter) induces a change from state A to state B. State B remains infinitely stable in a closed system. Only once the "off" switch is triggered, the state B returns to state A. The process is reversible. If both promoter and deactivator are added simultaneously (e.g. acid plus base; heating plus cooling), there is no change in the system as the two triggers basically annihilate instantaneously. (BOTTOM) Self-regulated systems, which require only one "on"-switch and contain internal feedback information for temporal self-regulation. Multiple switching is allowed. Two kinetic scenarios are relevant: (i) Class 1 is a system without dormant deactivator, in which precise chemical design, specific promoter and deactivator pairs and optimization are needed to satisfy the stringent kinetic boundary condition: $v1 >> v2$.[32] An ultimate excess of the deactivator leads to disassembly of state B once all the promoter is consumed. (ii) Class 2 is our platform system using dormant deactivators, which releases the real deactivator in a controlled fashion (here via hydrolysis). For such systems, the challenges of precise tailoring of the chemical structure and promoter/deactivator reaction pairs and the kinetic constraints of $v1 >> v2$ are lifted and replaced by a much simpler and general approach ($v_1 >> v^*$). Again, an ultimate excess of the deactivator leads to disassembly of state B once all the promoter is consumed. As a major advantage, it can be coupled to a range of systems satisfying the targeted stimuli, independent of the detailed chemical structure.

Such challenging, non-equilibrium concepts with potential internal control of the temporal fate

contrast classical stimuli responsiveness in static near-equilibrium self-assembly, which is the conceptual cornerstone of present-day switchable advanced materials based on external triggers (details in Figure 12). For a simple responsive system, the "on" switch (promoter) induces a change from state A to state B. State B remains infinitely stable in a closed system. Hence, self-regulation is not found and the time domain does not feature autonomous control. Only once the "off" switch is triggered externally (deactivator), the state B returns to state A. If both switches are added simultaneously (e.g., acid plus base; heating plus cooling), there is no change in the system as the two triggers basically annihilate instantaneously ($\nu_1 = \nu_2$). However, appreciating the differences between sophisticated dissipative self-assemblies, self-oscillating reactions, and classical responsive materials allows to identify emerging possibilities arising at their interface. This may bring forward new types of facile self-assembly concepts and materials with more dynamic properties and internal control over the temporal fate, mainly empowered by mastering kinetic control over activating and deactivating steps.

To this end, we herein introduce a facile and generic approach to achieve temporally programmed, self-regulating, self-assembling systems by playing a kinetic trick and by precisely modulating their surroundings. We take charge of the activating and deactivating pathway and conceive "dormant deactivators" (DD), which slowly decay (ν^*) and liberate an active deactivator (Scheme 1a). Dormant is defined[34] as a physical function, here the deactivation, being suspended or slowed down. This simplifies the kinetic boundary conditions to achieve a transient self-assembling state upon simultaneous addition of both activator and dormant deactivator to $\nu_1 \gg \nu^*$. During the preprogrammed course, the self-assemblies form (fast promoter) and then decay (dormant deactivator). We demonstrate that the duration of this transient non-equilibrium state can be tuned over four orders of magnitude, from minutes to days, similar to encoding a precise self-destruction mechanism.

2.2 Experimental Section

Materials: Methyl formate (MF, 98%), Gluconic acid δ-lactone (δ-GL, ≥99.0%), Glucoronic acid γ-lactone (γ-GL, ≥99.0%), β-Butyrolactone (β-BL, 98%), ε-Caprolactone (ε-CL 97%), TRIS (tris(hydroxymethyl) aminomethane) hydrochloride) buffer substance (pH 8.8), 3-(Cyclohexylamino)-1-propanesulfonic acid (CAPS) buffer substance, were purchased from Aldrich and used as received. The oligopeptide Ac-QQ-Orn-F-Orn-W-Orn-F-QQQ-NH_2 based on L amino acids was purchased from CASLO and prepared by solid phase synthesis using established techniques. MilliQ water was used for all experiments. BCP-1 was synthesized based on Atom Transfer Radical Polymerization (ATRP), starting from a PEO-macroinitator, based on established techniques.[35] BCP-2 was polymerized using sequential Radical Addition Fragmentation Transfer Polymerization (RAFT) of OEGMA and DEAEMA, and using commercial 4-Cyano-4-(phenylcarbonothioylthio) pentanoic acid as chain transfer agent (Aldrich).[36, 37] The functionalized Au-NPs were synthesized according to literature procedures.[38-40]

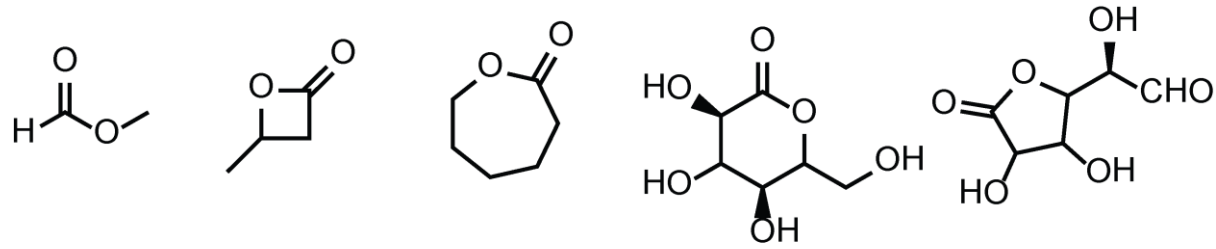

Figure 13: Selection of dormant deactivators, together with their pK_a values of the corresponding acids and solubility in water.

General procedure for temporal programming of dynamic self-assemblies. The calculated amounts of promoter and dormant deactivator solutions were loaded into gas-tight micro-syringes and simultaneously injected into the vessel containing the self-assembling components. Liquid dormant deactivators (DDs) are injected directly, whereas solid DDs are dissolved close to their saturation concentration in DMSO at 0.5 g/mL (TRIS, CAPS, δ-GL).

Simultaneous pH and transmission/absorption measurements to monitor the time-dependent evolution of time-programmed self-assemblies. All pH measurements were recorded on a Methrom Titrando 905 equipped with an optrode for simultaneous transmission analysis. The

wavelength of the optrode can be set to the following wavelength (470, 502, 520, 574, 590, 610 and 660 nm). We used 520 nm for standard transmission analysis to monitor turbidity. Changes in Au-NP dispersions were monitored at 590 nm in a Varian Cary 50 Bio UV/Vis spectrometer. The selected wavelength corresponds to the largest difference between the absorption spectra of both plasmon states (Figure 17e). Immediately prior temporal programming, the stable Au-NP dispersion stored at pH = 12.5 (isolated Au-NPs, reddish solution) was titrated with HCl to pH = 3 to induce clustering (blue solution), aged at this pH for 8 seconds, and subsequently, the IFS was injected. All operations where done inside the cuvette inserted into the spectrometer. Mixing was accomplished with pipettes. The Au-NP dispersions should be stored at alkaline pH to prevent excess clustering and precipitation. Note that dilution effects are visible due to injection of promoter and deactivator solutions (Figure 17d).

Transmission Electron Microscopy: Dispersions of micelles, vesicles, Au-NPs and self-assembled peptides were observed after deposition on glow-discharged carbon-coated cupper grids and imaged in transmission mode on a Zeiss Libra 120kV TEM at 120 kV using zero-loss energy filtering. For cryogenic-TEM, a small droplet was vitrified using a glow-discharged lacey grid and liquid ethane with a Vitrobot. The grid was transferred and imaged under cryogenic conditions.

Light Scattering: Dynamic and static light scattering was performed utilizing a goniometer ALV-GCS3 from ALV. All measurements were performed with a constant angle of 90° and a temperature of 20 °C. The hydrodynamic size distribution was evaluated using the CONTIN algorithm. The samples were prepared by injecting the IFS into a cuvette placed within the ALV instrument. The presented data presents an average of at least three measurements.

Fourier-Transform Infrared (FTIR) spectroscopy was performed on a Nexus 470 spectrometer with a resolution of 4 cm^{-1}.

2.3 Results and Discussion

We focus on a transient change of pH in the alkaline regime using DDs slowly hydrolyzing to acid (Scheme 1b). The simultaneous injection with a fast promoter, that is, a directly available base, creates a kinetically controlled transient pH-state with a fast rise and a controlled decay (due to an ultimate excess of DD). The hydrolysis speed of the DD is pH-dependent and the combination with a rapid promoter increase the pH and triggers an accelerated decomposition. This leads to an overall negative feedback. Hence, we term the full system a simple yet efficient internal feedback system (IFS) that can be coupled to virtually all pH-triggered self-assemblies operating in the targeted pH regime. We use the term internal to clearly express that the system operates in closed conditions and without the need of another external trigger for disassembly as in classical responsive self-assembly. This enables a unique platform concept to temporally program self-assemblies in closed systems over at least four orders of magnitude in time, from minutes to days. We showcase temporal programming for block copolymer self-assemblies (micelles and vesicles), and extend it as a generic platform to nanoparticles and peptides, all being key building blocks for advanced nanoscale and molecular materials.[2, 5, 11, 18, 41] The key ingredients to our platform approach are DDs; dormant expresses a retarded physical function.[34] These are selected from ester-containing molecules that slowly hydrolyze to furnish acid (v*, active deactivators; Figure 13).

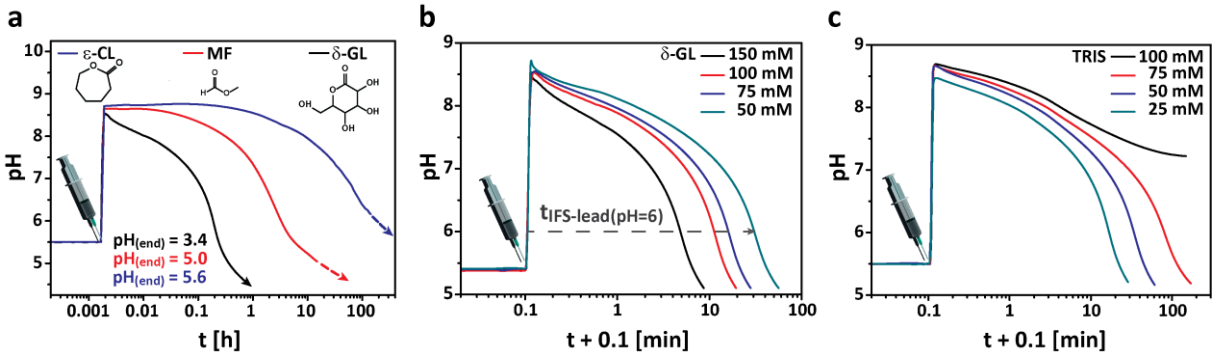

Figure 14: Programming the time-scales of non-equilibrium transient pH-profiles. a) Molecular structure of the DD controls the hydrolysis kinetics (ring strain and electronic activation) and regulates the timescale from minutes (δ-GL) to hours (MF) to days (ε-CL). Conditions: 20mM TRIS (pH=8.8) as promoter and 100mM DD. b) The DD concentration controls the decay kinetics at constant promoter concentration. Conditions: 20 mM TRIS (pH=8.8) as promoter and different concentrations of δ-GL as DD. c) Buffer capacity regulates the plateau length of the transient pH-profile at constant c(DD). Conditions: Different concentrations of TRIS (pH=8.8) as promoter and 100 mM δ-GL as DD.

Their structure controls the hydrolysis rate and acidity (pK_a value) and governs the pH-decay kinetics and final pH together with their concentration (Figure 14). The magnitude of the pH jump depends on the amount and type of added base, and alkaline buffers can be used as promoter to extend the plateau. Suitable promoters can be selected from a wide range of basic buffers if ion-specific effects need to be considered. Figure 14a depicts the influence of molecular structure for three DDs. Simultaneous injection of 100 mM DD and 20 mM TRIS buffer pH = 8.8 (fast promoter; TRIS = tris(hydroxymethyl)aminomethane hydrochloride) leads to a transient alkaline pH-state with a rapid decay within minutes for gluconic acid δ-lactone (δ-GL), whereas methyl formate (MF) decays within hours, and ε-caprolactone (ε-CL) requires days.

δ-GL is used in food industry and was applied earlier for shear-free acidification of solutions in a linear gradient.[42, 43] Most notable is the work by Adams[43, 44] targeting a more homogeneous gelation of dipeptides at low pH by slow acidification using δ-GL. Such a linear decrease is only able to trigger one transition, assembly or disassembly, and results in a rather similar process and properties compared to switching states in classical static self-assemblies. However, the combination with a fast promoter allows a new level of kinetic balance and enables a spike that, when coupled to a self-assembly operating in this transient pH-regime, allows it to pass two phase transitions consecutively and with high confidence (assembly/disassembly), furnishing a transient, intermediate self-assembly with a programmable time signature and encoded lifetimes of the self-assemblies. Self-regulation can be achieved with high fidelity and for various self-assembling systems.

Besides different DDs, a wide tunability is given by varying the ratio of promoter to DD. Longer plateau times occur upon lowering the concentration of the DD at constant buffer/ promoter strength (Figure 14b). Similarly, an increase in the buffer/promoter capacity at constant DD concentration also leads to longer plateau times (Figure 14c). Excess buffer prevents a decay. In summary, the duration of this transient state, $t_{IFS\text{-}lead}$, depends on the concentration and structure of the DD and can be substantially prolonged and tailored to a desired pH level using specific buffers as promoter and increasing the ratio of promoter to DD. For successful temporal programming ($t_{SA\text{-}follow}$), the pH-switchable self-assemblies need to be in state A and couple with a phase transition within the pH jump to temporally reach state B. Kinetic delays occur (t_{d1} and t_{d2}) depending on the particular self-assembling system (Scheme 1b).

It is important to distinguish our approach from chemical clocks or self-oscillating reactions, both in terms of approach and possible application. Self-oscillating systems only operate in a narrow window and a tuning of the periodicity of the oscillations over orders of magnitude is near impossible to achieve.[23, 24, 26-28, 45] Additionally, typical continuous pH oscillators are open and require constant feeding of reactants.[24-28, 46] Even though the chemistry of pH oscillators would in principal also allow creating a primary transient state upon a single injection, the accessible time scales and pH regime remain limited. For instance, we did not succeed in establishing reliable time scales for the methylene glycol−sulfite system.[46] Moreover, these pH oscillators typically contain oxidants, which may in principal interfere with more delicate self-assembling systems susceptible to oxidation in the range of the oxidation potentials of the oscillator.

Therefore, a simultaneous control over the time scale spanning four orders of magnitude and of the pH jump height (herein crossing seven pH units; see below) requires going beyond the possibilities of established oscillators and motivates exploring the tunability and capabilities of our benign activator/dormant deactivator system. The major advantage is that simple exchange of the DD allows to change the time scales completely while keeping other parameters constant due to unlike activation for hydrolysis. Second, and more importantly, the potential applications are completely different. While oscillating reactions yield pulsating systems,[23] useful for hydrodynamic pumping, for example, our targeted programmable state focuses on generating transient self-regulating states and time-programmed memory effects into materials.

Conceptually, our systems are different than chemical dissipative self-assemblies, by having the whole system (aqueous environment plus self-assembling material) out-of-equilibrium, whereas only the self-assembling material is out-of-equilibrium in dissipative self-assemblies. We first demonstrate temporal programming using our IFS approach for block copolymer solution self-assemblies (BCPs). BCPs are remarkably interesting materials, combining facile synthesis and switchability with hierarchical self-assembly and applications, for example, in nanolithography, photonics, hydrogels, or drug delivery.[6, 8, 11, 19-21, 41]

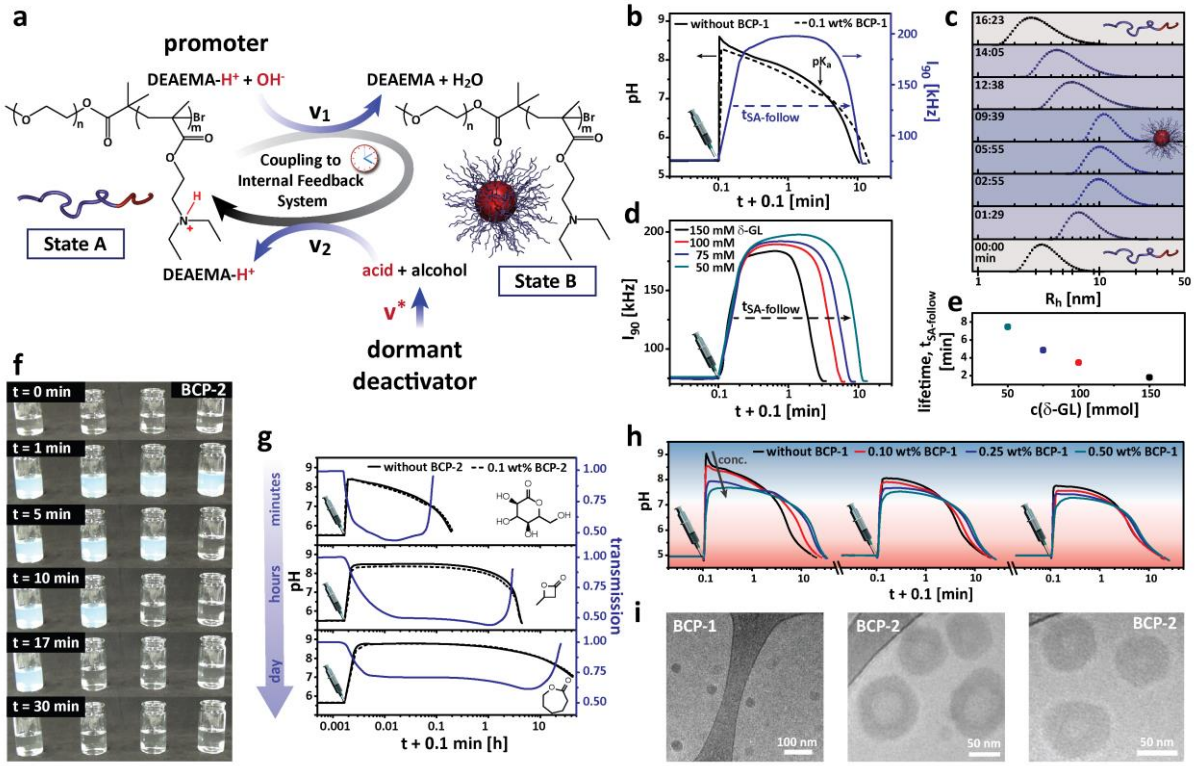

Figure 15: Temporal programming of self-regulating BCP self-assemblies using IFSs. BCP concentration is 0.1 wt%. a) Unimer-to-micelle-to-unimer transition upon deprotonation of DEAEMA-H^+ in BCP-1 due to promoter consumption and subsequent dynamic reprotonation by deactivator consumption. b) Unimer-to-micelle-to-unimer transition as a response to an IFS for BCP-1, tracked by pH-measurement and static LS at 90° ($I_{90°}$), and c) hydrodynamic radii distributions. Conditions: 20 mM TRIS (pH=8.8)/50 mM δ-GL. (d,e) The DD concentration regulates the lifetime of the transient micellar state. Conditions: 20 mM TRIS (pH=8.8)/various concentrations of δ-GL. f) Time-laps snapshot series of four temporally programmed vesicle self-assemblies of BCP-2. Conditions: 100 mM TRIS (pH=8.8) and 90, 100, 150, 300 mM δ-GL (left to right). g) Order-of-magnitude changes of the lifetimes of vesicles controlled by the chemical structure of the DD. Conditions: 100 mM TRIS (pH=8.8)/300 mM of various DDs as indicated. h) Repeated jumps for different concentrations of BCP-1. Conditions: 20 mM TRIS (pH=8.8)/100 mM δ-GL. i) Cryo-TEM images of micellar (BCP-1) and vesicular (BCP-2) morphologies.

We synthesized two different pH-switchable BCPs: EO114-*b*-DEAEMA99 (BCP-1, M_n = 26000 g/mol) and POEGMA9-*b*-DEAEMA224 (BCP-2; M_n = 46000 g/mol. Numbers denote degree of polymerization; EO, poly(ethylene oxide); OEGMA, poly(oligoethylene oxide methacrylate); DEAEMA, poly-(diethylaminoethyl methacrylate)). EO and OEGMA are fully water-soluble at room temperature, whereas DEAEMA turns solvophobic/insoluble at pH > 7.0

(Figure 16)[47]. This allows switchable self-assemblies with a transition intended to fit our IFS.

We designed the BCPs according to their DEAEMA weight fractions to be in the star-like (BCP-1) and crew-cut (BCP-2) regime to target spherical micelles and vesicles.[35] Simultaneous addition of promoter and DD allows programmable autonomous self-regulation of the corresponding BCP self-assemblies in time (Figure 15a). We combine in-situ light scattering with pH measurements to analyze the nonlinear evolution self-assemblies when coupled to an IFS (Figure 15b). Ex-situ dynamic light scattering (DLS) reveals a unimer-to- micelle transition in the range of 7.0 − 7.5 for BCP-1 (Figure 16).[47] Upon simultaneous injection of the promoter/DD pair (20 mM TRIS (pH = 8.8)/ 50 mM δ-GL), distinct changes in the pH evolution are observed in the presence of the BCP. First, the pristine IFS shows a higher pH jump than the one containing the BCP. This is due the presence of protonated DEAEMA-H^+ segments that consume OH^- of the promoter to switch solvophobic and induce self-assembly. Even if acid/base reactions are among the simplest chemical reactions, it becomes evident that injection of insufficient promoter prevents the formation of self-assembled structures. Second, a buffer plateau appears around pH ≈ 7.2 during the pH decay, which corresponds to the pK_a value of the DEAEMA and whose duration depends on the amount of DEAEMA. We further discuss the influence of the BCP concentration below. More importantly, the light scattering intensity ($I_{90°}$) displays a similar plateau-like profile, following the pH profile with a slight offset. This slight delay arises from kinetic retardation of the micelle-to-unimer-to-micelle transitions (t_{d1} and t_{d2}; Scheme 1b). Higher light scattering originates from larger structures and indicates the presence of self-assemblies that are identified as spherical micelles by cryogenic transmission electron microscopy (cryo-TEM, Figure 15i). Simultaneous in-situ hydrodynamic size distribution analysis by DLS reveals unimers at the start ($\langle R_h \rangle_w \approx 3$ nm), subsequent micelle formation and stable micelles ($\langle R_h \rangle_w \approx 12$ nm), and disassembly after 10 min, coinciding with the drop in scattering intensity (Figure 15c). The distributions correspond to the ones measured ex-situ (Figure 16). We exemplify temporal programming by changing the δ-GL concentration, which allows regulating the self-assembly lifetimes ($t_{SA\text{-}follow}$) in the range of minutes (Figure 15d,e). During this process and in the plateau of stable self-assemblies, there is a constant exchange of H^+/OH^- between the various components, that is, the buffer molecules as promoter, the liberated acid and the DEAEMA units as interacting self-assembling system. At longer time scales the dynamic reprotonation by the liberated deactivating acid takes over, and deactivates the self-assembly by protonating the DEAEMA units, as well as protonates all TRIS-NH_2 promoter molecules. Order-of-magnitude changes can be achieved conveniently using other

DDs as shown below for BCP-2.

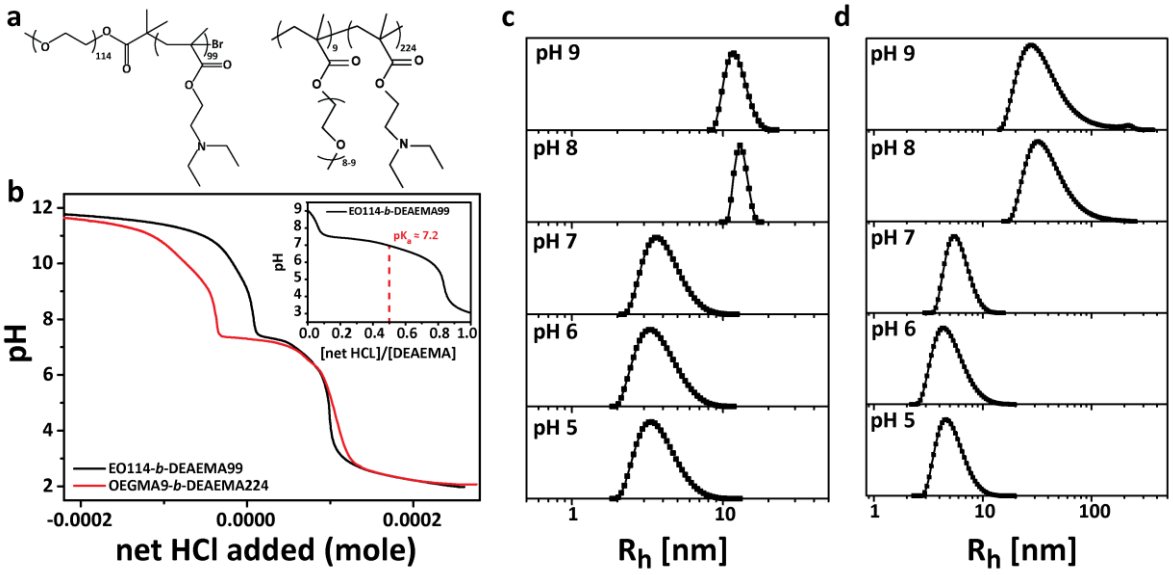

Figure 16: Structure, titration curves and ex-situ DLS analysis of BCP-1 and BCP-2. a) Molecular structure of EO114-*b*- DEAEMA99 (BCP-1, M_n = 26000 g/mol) and OEGMA9-*b*-DEAEMA224 (BCP-2); M_n = 46000 g/mol b) Titration curves of 0.25 wt% BCP-1 and BCP-2 solution. The higher content of DEAEMA in BCP-2 leads to a larger buffer plateau around pH ≈ 7.2. The inset depicts the same titration curve as a function of the degree of ionization, revealing a pK_a-value close to 7.2 (here for BCP-1). (c-d) Mass-weighted DLS CONTIN plots as a function of the pH-value for BCP-1 (c) and BCP-2 (d). A distinct unimer-to-micelle (c) and unimer-to-vesicle (d) transition occurs at pH values greater 7.0, whereupon species with larger hydrodynamic radius are identified $\langle R_h \rangle_{w,BCP-1}$ = 12 nm, $\langle R_h \rangle_{w,BCP-2}$ = 30 nm (pH 8 and 9). See main manuscript for cryo-TEM characterization.

Next we change to BCP-2 containing a majority fraction of switchable DEAEMA (>90 wt %), being in the so-called crew-cut regime.[35] BCP-2 provides the advantage that the typically larger sizes formed by crew-cut aggregates, in particular rod-like structures and vesicles, are macroscopically visible due to turbidity. DLS indeed shows larger sizes of $\langle R_h \rangle_w \approx 30$ nm and cryo-TEM evidences vesicles (Figure 15i; Figure 16). This allows (i) following the temporal self-regulation by the naked eye (Figure 15f) and (ii) simplifies the experiments as turbidity can be directly used to quantify the temporal evolution. Figure 15f displays snapshots of BCP-2 programmed with different δ-GL concentrations to decay at times between 5 to 30 min (Figure SI 1). Much longer lifetimes can be reached by changing the DD to β-BL (β-butyrolactone) and ε-CL, allowing transient states of 3 h and 1 day (Figure 15g). This shift in time scale reflects the molecularly controlled decomposition kinetics of the pure compounds (Figure 14a) and

demonstrates the unique ability to program self-regulation over four orders of magnitude in time.

Repeated jumps are possible upon reinjection of the IFS as illustrated for different concentrations of BCP-1 (Figure 15h). We perform this reactivation to exclude any negative effects of the promoter/deactivator pairs on the self-assembling components. The creation of stable oscillations is beyond the focus of this contribution. Interestingly, the pH jumps decrease and the curves show more pronounced plateaus (lifetimes of the self-assembly are longer) for higher BCP concentrations. The decrease in the pH jump is caused by the consumption of the promoter by higher concentrations of the protonated DEAEMA-H^+ segments, whereas the longer plateau is associated with two phenomena. First, the ester hydrolysis is base-catalyzed and occurs more quickly at higher pH. Second, more DEAEMA units cause a longer buffering region around neutral pH ($pK_a \approx 7.2$) during the decay, stabilizing the hydrolysis of the DD at low speed before the acid-catalyzed decomposition takes over. The overall pH jump and plateau length decrease for repeated jumps due to remaining excess of DD.

Next, we demonstrate the general applicability to self-regulate and temporally program other self-assembling systems by applying IFSs to (i) gold nanoparticles (Au-NPs) and program optical plasmon effects by reversible deaggregation/aggregation and (ii) oligopeptides undergoing reversible β-sheet nanofibrillization. Both material classes are cornerstones for advanced materials with applications in optical sensors, conducting nanowires and for biomedical applications.[1, 2, 5, 18] We use Au-NPs ($\langle R \rangle_{n,\,TEM} = 3.9$ nm) functionalized with a phenol-ligand,[26] which undergoes deprotonation at high pH ($pK_a \approx 8.3$), inducing declustering via electrostatic repulsion (Figure 17a). This can be followed macroscopically by a color change from blue to red due to the loss of interparticle coupling of the plasmons, as further quantified by UV−vis (Figure 17e). Cryo-TEM depicts typical clusters at acidic conditions (Figure 17b). The weak acidity of the phenol group requires more alkaline buffers (CAPS (3-(cyclohexylamino)-1-propanesulfonic acid), pH = 11) for sufficient ionization and to trigger the transition. In addition to changing the buffer, we now show temporal programming using a variation in buffer strength while maintaining the same concentration of DD (200 mM MF). The evolution is conveniently monitored using simultaneous pH measurement and optical absorption at 590 nm (largest difference between both spectra) to follow the dissolution of the Au-NP clusters (Figure 17c−f).

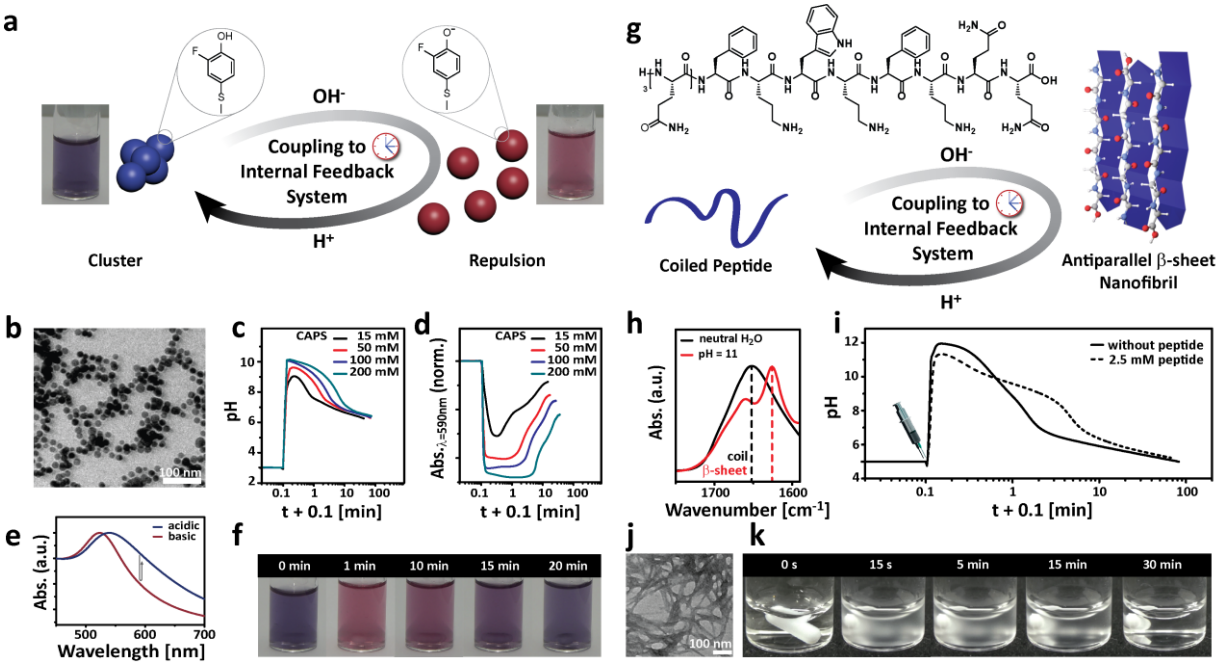

Figure 17: General ability for temporal programming of self-assembly lifetimes demonstrated for Au-NPs and oligopeptides. a) Phenol-functionalized Au-NPs show clusters at acidic pH, which reversibly break due to electrostatic repulsion at high pH when subjected to suitable IFS. b) Cryo-TEM illustrating Au-NP clusters at pH = 5. (c−d) Temporal programming using different buffer strength of CAPS at constant concentration of 200 mM MF as DD. pH profiles (c) and de/reclustering monitored via absorbance at 590 nm (d). e) UV−vis spectra at acidic and alkaline pH showing the blue (539 nm) and red plasmon peak (525 nm). f) Snapshot series at 60 mM CAPS and 100 mM MF. g) Structure and temporally programmed reversible switching of an oligopeptide from coil-to-β-sheet-to-coil traced by (h) FTIR spectroscopy, (i) pH-profile, (j) TEM of nanofibrils formed at alkaline pH, and (k) macroscopic turbidity as seen in the snapshot series. Conditions: 2.5 mM oligopeptide, 25 mM NaOH, and 100 mM β-Bl.

The differences in the pH jump height reflect the increased concentration of switchable units and the in-situ absorption/pH measurements demonstrate successful programming on time scales from ca. 15 to 45 min upon increasing the buffer strength of the promoter from 15 to 200 mM. Differences in absorption at start and end are mainly due to dilution effects based on adding the IFS. Even very delicate self-assemblies can be programmed in time as shown for an oligopeptide that undergoes a distinct isotropic-to-nematic transition due to base-induced fibrillization caused by switching its conformation from coil to β-sheets (Figure 17g−k).[48] The particular peptide displays a transition at pH ≈ 7.6, due to deprotonation of the amine groups and either forms nematic fluids (>0.9 mM) or nematic gels (>6.6 mM). We achieve temporal programming using NaOH as promoter and β-BL as DD. The formation of nanofibrils goes

along with macroscopically observable turbidity (Figure 17k). After 30 min, the turbidity vanishes and a solution of original clarity is obtained, indicating the complete redissolution of the nanofibrils, again corresponding to the transient pH profile. TEM images and FTIR spectroscopy verify the intermediate presence of β-sheet-based peptide nanofibrils and confirm the programming of a transient self-assembled nanofibrillar state.

2.4 Conclusion

In summary, we presented a general concept to program the time domain of pH-switchable self-assemblies over four orders of magnitude and equip them with a mechanism for autonomous self-regulation in closed systems. We realize this by controlling the kinetics of assembly and disassembly reaction, and more precisely by starving the availability of the deactivator using a dormant species. This conceptual approach enables a new level of control for switchable self-assembling systems and allows advancements toward more dynamic materials, spawning self-regulating and time-programmed (self-erasing) memory functions. We expect potential applications in photonic memories, self-erasing patterns, burst release hydrogels for delivery applications, and for noninvasive, in-situ analysis of self-assembly processes, for example, in a closed liquid-cell TEM, confocal and super-resolution microscopy and scattering experiments. The approach can be generalized by expanding to dormant deactivators releasing base and other dormant species (e.g., chelators, redox-active compounds). We reason that the balanced combination of different dormant activators and deactivators will allow to increase control over the system by also controlling the activation time scale (ν_1) and programming an "on" time. Even though not targeted by us, the increasing understanding of dormant species and strengthening artificial feedback mechanisms may lead to new designs for chemical oscillators. The successful orchestration of the time domain, and understanding self-regulation and artificial feedback mechanisms of diverse kinds affords the needed counterpart to widely pursued efforts toward ever more complex 3D hierarchical self-assemblies in space. The combination of both is of fundamental interest to promote and understand complex and more dynamic systems. For our systems, one of the most intriguing challenges will be to couple the time-scale of the self-assembly state to the induction of a secondary time-dependent process to at some point approach nonlinear evolutions.

2.5 Supporting Information

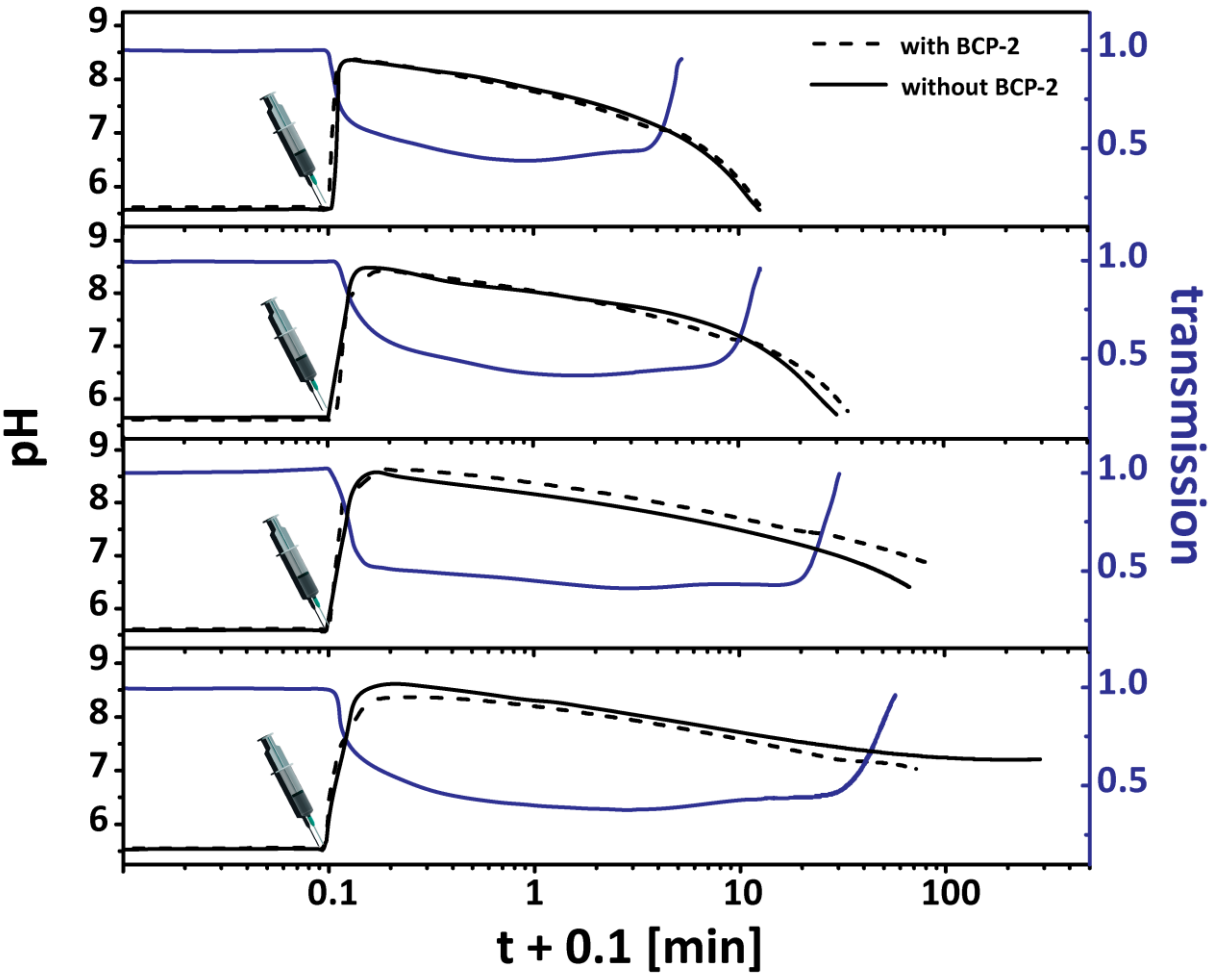

Figure SI 1: Temporal programming of self-regulating vesicles of BCP-2 using internal feedback systems (IFS). BCP concentration is 0.1 wt%. Unimer-to-vesicle-to-unimer transition tracked by pH- and turbidity measurements. The drop in the blue curve (turbidity) corresponds to vesicle formation, while the subsequent increase to the original level (full transmission) corresponds to vesicle dissolution. Different times for self-regulation are programmed using four different concentrations of the dormant deactivator in the IFS. Conditions: 100 mM TRIS (pH = 8.8) and 300, 150, 100, 90 mM δ-GL (top to bottom). Movie SI1 and Figure 2f contain complementary data.

2.6 References

1. Aida, T.; Meijer, E. W., Stupp, S. I., *Science* **2012,** *335*, 813-817.
2. Grzelczak, M.; Vermant, J.; Furst, E. M., Liz-Marzán, L. M., *ACS Nano* **2010,** *4*, 3591-3605.
3. Mann, S., *Nat. Mater.* **2009,** *8*, 781-792.
4. Whitesides, G. M., Grzybowski, B., *Science* **2002,** *295*, 2418-2421.
5. Glotzer, S. C., Solomon, M. J., *Nat. Mater.* **2007,** *6*, 557-562.
6. André H. Gröschel; Andreas Walther; Tina I. Löbling; Felix H. Schacher; Holger Schmalz, Müller, A. H. E., *Nature* **2013,** *503*, 247–251.
7. Liu, K.; Nie, Z.; Zhao, N.; Li, W.; Rubinstein, M., Kumacheva, E., *Science* **2010,** *329*, 197-200.
8. Rupar, P. A.; Chabanne, L.; Winnik, M. A., Manners, I., *Science* **2012,** *337*, 559-562.
9. Fukino, T.; Joo, H.; Hisada, Y.; Obana, M.; Yamagishi, H.; Hikima, T.; Takata, M.; Fujita, N., Aida, T., *Science* **2014,** 499-504.
10. Cui, H.; Chen, Z.; Zhong, S.; Wooley, K. L., Pochan, D. J., *Science* **2007,** *317*, 647-650.
11. Bates, F. S.; Hillmyer, M. A.; Lodge, T. P.; Bates, C. M.; Delaney, K. T., Fredrickson, G. H., *Science* **2012,** *336*, 434-440.
12. Chen, Q.; Bae, S. C., Granick, S., *Nature* **2011,** *469*, 381-384.
13. Gröschel, A. H.; Schacher, F. H.; Schmalz, H.; Borisov, O. V.; Zhulina, E. B.; Walther, A., Müller, A. H. E., *Nat. Commun.* **2012,** *3*, 710.
14. Gilroy, J. B.; Gädt, T.; Whittell, G. R.; Chabanne, L.; Mitchels, J. M.; Richardson, R. M.; Winnik, M. A., Manners, I., *Nat. Chem.* **2010,** *2*, 566-570.
15. Hermans, T. M.; Broeren, M. A. C.; Gomopoulos, N.; van der Schoot, P.; van Genderen, M. H. P.; Sommerdijk , N. A. J. M.; Fytas, G., Meijer, E. W., *Nat. Nanotechnol.* **2009,** *4*, 721-726.
16. Walther, A.; Drechsler, M.; Rosenfeldt, S.; Harnau, L.; Ballauff, M.; Abetz, V., Müller, A. H. E., *J. Am. Chem. Soc.* **2009,** *131*, 4720-4728.
17. Morris, K. L.; Chen, L.; Raeburn, J.; Sellick, O. R.; Cotanda, P.; Paul, A.; Griffiths, P. C.; King, S. M.; O'Reilly, R. K.; Serpell, L. C., Adams, D. J., *Nat. Commun.* **2013,** *4*, 1480.
18. Boekhoven, J., Stupp, S. I., *Adv. Mater.* **2014,** *26*, 1642-1659.
19. Kang, Y.; Walish, J. J.; Gorishnyy, T., Thomas, E. L., *Nat. Mater.* **2007,** *6*, 957-960.
20. Valkama, S.; Kosonen, H.; Ruokolainen, J.; Haatainen, T.; Torkkeli, M.; Serimaa, R.; ten Brinke, G., Ikkala, O., *Nat. Mater.* **2004,** *3*, 872-876.
21. Park, S.; Lee, D. H.; Xu, J.; Kim, B.; Hong, S. W.; Jeong, U.; Xu, T., Russell, T. P., *Science* **2009,** *323*, 1030-1033.
22. Walther, A.; Bjurhager, I.; Malho, J.-M.; Pere, J.; Ruokolainen, J.; Berglund, L. A., Ikkala, O., *Nano Lett.* **2010,** *10*, 2742-2748.
23. Yoshida, R., *Adv. Mater.* **2010,** *22*, 3463-3483.
24. Rabai, G.; Kustin, K., Epstein, I. R., *J. Am. Chem. Soc.* **1989,** *111*, 3870-3874.
25. Padirac, A.; Fujii, T.; Estévez-Torres, A., Rondelez, Y., *J. Am. Chem. Soc.* **2013,** *135*, 14586-14592.
26. Lagzi, I.; Kowalczyk, B.; Wang, D., Grzybowski, B. A., *Angew. Chem. Int. Ed.* **2010,** *49*, 8616-8619.
27. Rabai, G.; Orban, M., Epstein, I. R., *Acc. Chem. Res.* **1990,** *23*, 258-263.
28. Poros, E.; Horváth, V.; Kurin-Csörgei, K.; Epstein, I. R., Orbán, M., *J. Am. Chem. Soc.* **2011,** *133*, 7174-7179.
29. Fialkowski, M.; Bishop, K. J. M.; Klajn, R.; Smoukov, S. K.; Campbell, C. J.,

Grzybowski, B. A., *J. Phys. Chem. B* **2006,** *110*, 2482-2496.
30. Grzybowski, B. A.; Stone, H. A., Whitesides, G. M., *Nature* **2000,** *405*, 1033-1036.
31. Timonen, J. V. I.; Latikka, M.; Leibler, L.; Ras, R. H. A., Ikkala, O., *Science* **2013,** *341*, 253-257.
32. Boekhoven, J.; Brizard, A. M.; Kowlgi, K. N. K.; Koper, G. J. M.; Eelkema, R., van Esch, J. H., *Angew. Chem. Int. Ed.* **2010,** *49*, 4825-4828.
33. Debnath, S.; Roy, S., Ulijn, R. V., *J. Am. Chem. Soc.* **2013,** *135*, 16789-16792.
34. dormant as definded in the Oxford Dictionary *oxforddictionaries.com.* Oxford University Press, 2014
35. Walther, A.; Goldmann, A. S.; Yelamanchili, R. S.; Drechsler, M.; Schmalz, H.; Eisenberg, A., Müller, A. H. E., *Macromolecules* **2008,** *41*, 3254-3260.
36. Chiefari, J.; Chong, Y. K.; Ercole, F.; Krstina, J.; Jeffery, J.; Le, T. P. T.; Mayadunne, R. T. A.; Meijs, G. F.; Moad, C. L.; Moad, G.; Rizzardo, E., Thang, S. H., *Macromolecules* **1998,** *31*, 5559-5562.
37. Moad, G.; Rizzardo, E., Thang, S. H., *Aust. J. Chem.* **2005,** *58*, 379-410.
38. Jana, N. R., Peng, X., *J. Am. Chem. Soc.* **2003,** *125*, 14280-14281.
39. Sato, M.; Kawashima, Y.; Goto, J.; Yamane, Y.; Chiba, Y.; Jinno, S.; Satake, M., Iwata, C., *Eur. J. Med. Chem.* **1995,** *30*, 403-414.
40. Wang, D.; Kowalczyk, B.; Lagzi, I., Grzybowski, B. A., *J. Phys. Chem. Lett.* **2010,** *1*, 1459-1462.
41. Walther, A.; Yuan, J.; Abetz, V., Müller, A. H. E., *Nano Lett.* **2009,** *9*, 2026-2030.
42. Hao, J.; Hoffmann, H., Horbaschek, K., *J. Phys. Chem. B* **2000,** *104*, 10144-10153.
43. Adams, D. J.; Butler, M. F.; Frith, W. J.; Kirkland, M.; Mullen, L., Sanderson, P., *Soft Matter* **2009,** *5*, 1856-1862.
44. Cardoso, A. Z.; Alvarez Alvarez, A. E.; Cattoz, B. N.; Griffiths, P. C.; King, S. M.; Frith, W. J., Adams, D. J., *Farad. Discuss.* **2013,** *166*, 101-116.
45. Lagzi, I.; Wang, D.; Kowalczyk, B., Grzybowski, B. A., *Langmuir* **2010,** *26*, 13770-13772.
46. Kovacs, K.; McIlwaine, R. E.; Scott, S. K., Taylor, A. F., *J. Phys. Chem. A* **2007,** *111*, 549-551.
47. Vamvakaki, M.; Papoutsakis, L.; Katsamanis, V.; Afchoudia, T.; Fragouli, P. G.; Iatrou, H.; Hadjichristidis, N.; Armes, S. P.; Sidorov, S.; Zhirov, D.; Zhirov, V.; Kostylev, M.; Bronstein, L. M., Anastasiadis, S. H., *Farad. Discuss.* **2005,** *128*, 129-147.
48. Aggeli, A.; Bell, M.; Carrick, L. M.; Fishwick, C. W. G.; Harding, R.; Mawer, P. J.; Radford, S. E.; Strong, A. E., Boden, N., *J. Am. Chem. Soc.* **2003,** *125*, 9619-9628.

3 BIOCATALYTIC FEEDBACK-DRIVEN TEMPORAL PROGRAMMING OF SELF-REGULATING PEPTIDE HYDROGELS

The results presented in this chapter were published in the article: T. Heuser et al., Angew. Chem. Int. Ed., **2015**, 54, 13258 - 13262

3.1 Introduction

Stimuli-responsiveness in self-assemblies and materials is one of the cornerstones in soft matter research, as it enables fundamental investigations of structure formation[1, 2] and the targeting of switchable materials with advanced functionalities as needed in photonics,[3, 4] for hydrogels,[5-8] actuation (bilayers)[9, 10] and controlled release.[11, 12] Such switchability relies on the responsiveness of self-assemblies to external signals, such as temperature, the pH value, or light, and is well understood for a range of systems.[13, 14] On a conceptual level, such property changes are rather passive: Classical stimuli-responsive systems always need an outside trigger to induce a one-way transition between thermodynamically stable states (e.g. assembly/disassembly). The resulting state will be infinitely stable, and a counter-trigger is needed to revert the system (Figure SI 2). The simultaneous addition of a trigger and a counter-trigger (e.g. H^+/OH^-) typically leads to their instantaneous annihilation. Hence, autonomous behavior of the time domain and self-regulating behavior is not found. In stark contrast, natural non-equilibrium systems,[15-17] which are orchestrated via kinetically and catalytically controlled conversions, feedback mechanisms and constant energy dissipation display orchestrated dynamics in the time domain. They present prominent examples of self-regulation and adaptive behavior in general, thus, offering inspiration for new concepts towards in the design of dynamic materials.

Hydrogels formed by self-assembly or crosslinking are vital for a range of technologies, for example, in food, materials, bio and life sciences, and serve as model materials for the study of fundamental approaches to structure matter.[18-20] Despite intense development, it has remained a challenge to advance their properties from classical, passive responsiveness to create systems that show autonomous dynamics and self-regulation. Most prominent is the coupling of tailored hydrogels to the serendipitously discovered Belousov-Zhabotinsky reaction, to generate pulsating hydrogels useful for pumping or transport.[21-23] More recent oscillators target rational design by defined chemical or enzymatic reaction networks.[24] Routs towards single transient states in closed systems include kinetically controlled transformations of peptide nanofibril precursors[25, 26] or dissipative structure formation.[27] We recently showed that transient states can be programmed in time by playing a different kinetic trick.[28] We demonstrated autonomously self-regulating, transient pH-states in alkaline media through the simultaneous injection of fast promoters and slow, dormant deactivators (DDs). Such transient pH jumps can be coupled to virtually all self-assembling systems operating in the targeted pH regime, whereupon they form and decay on a pre-programmed course in closed systems as encoded by the pH-profile. The main advantage is that such rationally programmed pH-states open a facile and generic pathway to impart artificial self-regulation and programmed lifetimes to diverse switchable self-assemblies.

Herein we provide a new approach and demonstrate catalytic and feedback-driven control over a transient, self-regulating pH-state in the acidic regime, and use it in conjunction with the self-assembly of dipeptide gelators. We achieve programmable time signatures and reveal progress from an earlier self-assembly level to a materials level by now showing full gelation and hydrogel lifetimes that can be programmed with very high confidence across orders of magnitude in time in closed systems. We also identify first applications of such time-programmed self-regulating hydrogels by developing injectable solutions for temporal blocking and fluidic guidance within fluidic systems, for burst release systems, and for self-erasing micromolded gels.

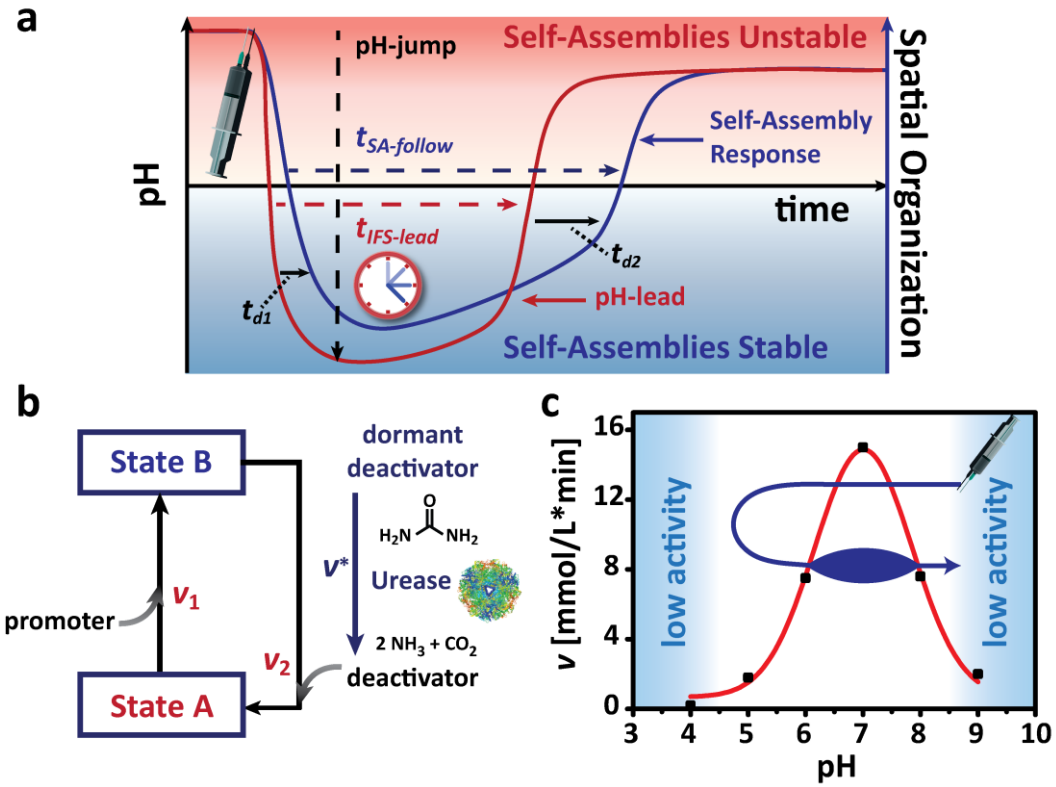

Scheme 2: Enzymatic, feedback-controlled programming of transient pH-profiles for the temporal programming of self-assemblies: (a) The simultaneous injection of a promoter and a DD programs a transient acidic pH profile (red line, $t_{IFS\text{-}lead}$). The self-assembly follows (blue line, $t_{SA\text{-}follow}$) with kinetic offsets, t_{d1} and t_{d2}. (b) Temporal programming of pH-switchable self-assemblies by controlling the availability of the deactivator. The kinetic balance of the promoting and deactivating reaction is $v_1 >> v^*$; $v_1 \approx v_2$ becomes irrelevant. Ultimately, the excess of DD leads to recovery of the pH value. (c) Bell-shaped pH-dependent urease activity with the hypothetical jump indicated.[29]

We focus on transient states in the acidic pH-regime, as obtained by the kinetic balance of a fast promoter (acidic buffer) and dormant deactivator, which are added simultaneously (Scheme 2a, Figure SI 2). The active deactivator (base) is generated in a highly time-controlled manner by the urease-catalyzed conversion of urea into CO_2 and NH_3 (Scheme 2b). This rate (v^*) can be controlled by the biocatalyst concentration, and is highly pH dependent (Scheme 2c).[30] Base generation provides negative pH-feedback and lifts the pH value back up without any external interference (closed system). Urease was used earlier to control homogeneous base generation,[31] and continuous addition with acid in open stirred reactors allowed the production of oscillations.[32-34] However, we are not targeting linear pH changes or oscillations, but precisely programmed, non-linear transient states. Such an approach has not been described previously and involves further considerations.

More importantly, we couple these states with a switchable dipeptide gelator to program hydrogel lifetimes. We term the overall system an internal feedback system (IFS). Which "internal" clearly express that outside triggers are not needed. This transient acidic state goes conceptually beyond complementing our earlier transient alkaline state,[28] for which we relied on the constant hydrolysis of an unstable compound to provide the active deactivator. The first major advantage of the present approach is the catalytic nature of the process, which provides a unique way to fine-tune the speed of base generation through the enzyme concentration.[35] Second, the bell-shaped curve of the enzymatic activity is interesting, as it provides low enzyme activity at high and low pH values (pH < 3.5 or pH > 9) (Scheme 2c). Hence, the system is forcefully activated from the nearly inactive alkaline state (pH > 9) into the activity window (pH > 3.5) upon injection of the promoter. The bell-shaped activity curve leads to a beneficial steep pH-recovery, as the activity is self-enforcing (positive feedback) when the enzyme passes from an area of low activity at low pH values to high activity at intermediate pH values. Finally, the rate is also self-diminishing in terms of the pH-value, as base generation pushes the enzyme out of its active window.

3.2 Experimental Section

Materials: Urea (>99.0%), urease (from *Canavalia ensiformis*) and citric acid monohydrate (≥ 99.0 %) were purchased from Aldrich. Trisodium citrate dihydrate (99.0 %) was purchased from Alfa Aesar. Hydrochloric acid (0.1 N) was purchased from Merck. Sodium hydroxide (0.1 N) was purchased from VWR Chemicals. The peptide Fmoc-Leu-Gly-OH was purchased from Bachem AG. All chemicals were used as received.

Protocol for enzymatically controlled temporal programming of self-assemblies: Mixtures of calculated amounts of urea and citric acid buffer were loaded into Hamilton micro-syringes and injected into a solution of urease and the self-assembling Fmoc-dipeptide. All solutions were prepared freshly before each measurement. The evolutions of the pH profiles were recorded on a 12-channel pH monitoring system by EA Instruments. All graphs show the average data of at least three measurements.

Cryogenic Transmission electron microscopy: For morphological observation, zero-loss energy-filtered transmission electron microscopy (TEM) images were recorded with a LIBRA 120 operating at 120 kV using a bottom mounted CCD camera. Cryo-TEM samples were prepared by rapid vitrification in liquid ethane from aqueous dispersion (0.2 wt%) using plasma-treated lacey grids and a vitrobot system.

3.3 Results and Discussion

We first focus on programming the time-scale, $t_{IFS\text{-}lead}$, and the pH-jump of the transient acidic pH profile. The depth of the pH-jump is limited by the properties of the urease (from *canavalia ensiformis)* to a level at which the enzyme still shows sufficient activity to enable a pH feedback. Therefore, we injected urease (15000-50000 catalytic units/g; 0.1 g/L) into urea solutions (20 mM) with different starting pH-values as adjusted by HCl (Figure 18a). Three different regimes can be observed: (I) Above a pH_{start} value of 3.5, a steep increase to a plateau at approximately pH ≈ 9 occurs (grey curves). (II) In the range of pH_{start} 2.5 - 3.5, an increase still occurs; however, it begins with an increasingly elongating plateau for lower pH_{start} values, followed by an abrupt and steep transition. (III) No increase occurs for $pH_{start} < 2.5$, thus indicating that the enzyme is inactive. The plateau at low pH values in the intermediate regime (II) is caused by the initially low catalytic activity of the urease and slow base generation. At $pH_{start} > 3.5$, the enzyme is directly in the pH-window of high catalytic activity and the increase occurs immediately. All curves level off at the same alkaline pH, because the enzyme leaves its active zone and an ammonia buffer forms around pH ≈ 9. Therefore, the depth of the pH-jump is limited to pH > 2.5 to allow for the return, and the depth of the pH-jump needs to be very precise to enable reliable programming of the transient state. Next, we establish the full IFS by a single injection of a urea-containing acidic buffer solution (promoter + DD) into basic urease solutions at $pH_{start} = 9.5$, which is in the alkaline low activity area of urease. We choose acidic buffers over pure acid as rapid promoters because they enable (i) a jump to a certain pH level with a high confidence, and (ii) the extension of $t_{IFS\text{-}lead}$ by increasing the buffer capacity. Specifically, we selected a citric acid/sodium citrate buffer (CA/Na_3C), because preliminary investigations revealed a superior homogeneity of the targeted dipeptide hydrogels as compared to those formed in phosphate buffers (possibly a counterion effect). CA/Na_3C buffers can be adjusted over a wide pH value and ionic strength range by the combination of different ratios of CA/Na_3C and different total concentration. Figure 18b depicts the influence of the buffer concentrations (CA/Na_3C 4:1) on the IFS (60 mmol urea, 0.3 g/L urease). Several phenomena are observed. First, as expected, increasingly deeper pH-jumps occur as the buffer capacity is increased (see Figure SI 3 for the quantification and discussion of this behavior for different CA/Na_3C mixtures). More importantly, the transient plateau at low pH values indeed extend upon the injection of buffers with higher capacity, because the buffers scavenge the generated base.

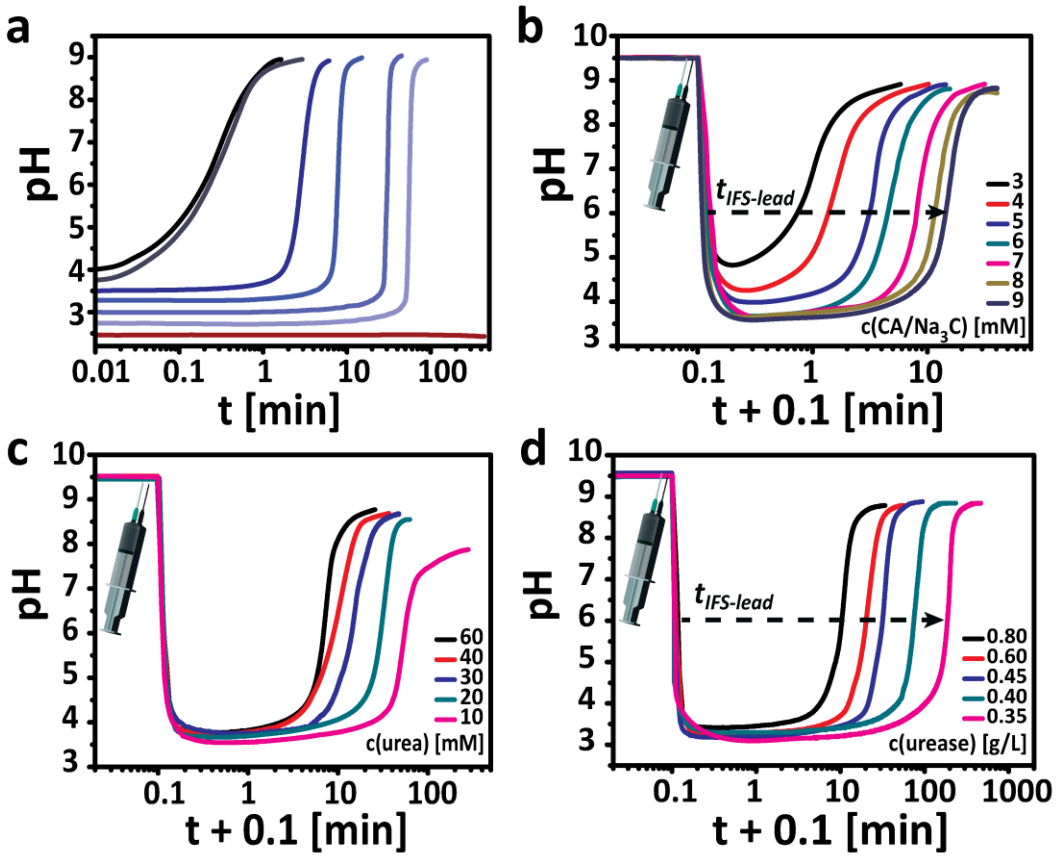

Figure 18: Programming of transient acidic pH states: (a) pH_{start} value controls the enzyme activity and the rate of base generation (20 mM urea; 0.1 g/L urease). (b) The concentration of CA/Na_3C-buffer regulates the timescale (60 mM urea, 0.3 g/L urease and various concentrations of CA/Na_3C-buffer (4:1) as promoter. (c) Influence of the substrate concentration on timescales. (0.3 g/L urease, 7 mM CA/Na_3C (4:1) buffer and various urea concentrations). (d) Catalytic control over the timescale by changing the urease concentration (60 mM urea, 12 mM CA/Na_3C (9:1) buffer).

Since all curves are in regime I of the enzymatic activity (pH-jump > 3.5; high activity), the elongation of the plateau time can mainly be attributed to the increasing buffer capacity. This result demonstrates that the use of buffers is one key to the extension of $t_{IFS-lead}$. We further studied the influence of the substrate concentration (DD, urea, Figure 18c) under otherwise constant conditions and find elongating plateaus for lower substrate concentrations. This result reflects the Michaelis-Menten kinetics, which rationalizes an asymptotical increase of the reaction rate with substrate concentration. The Michaelis Menten constant of the urease is in the range of 2.9 - 3.6 mM.[29, 36] Interestingly, low urea concentrations (10 mM) limit the pH-value rise owing to the small amount of base-generating substrate. To exclude any ambiguities, we keep the substrate concentration constant at 60 mM. The crucial advantage of a biocatalytic pH-IFS is that the generation of the active deactivator is coupled to the maximum turnover

number (TON) of the enzyme. Hence, the enzyme concentration ultimately governs the rate and provides the most precise means to fine-tune the reaction rate. Furthermore, varying the urease concentration under otherwise constant conditions minimizes any adverse effects of the pH-dependent activity induced by jumps with different buffer concentrations (Figure 18a,b; Figure SI 3). Figure 18d clearly shows that $t_{IFS\text{-}lead}$ can be tuned with high confidence from 10 to 190 min, by changing the enzyme concentration from 0.35 to 0.80 g/L (at pH = 6).

In summary, the careful screening of the reaction conditions establishes how the amount of activator (buffer), the depth of the pH-jump, and most importantly, the enzyme concentration can be used to program the timescale of the transient non-equilibrium pH profile. The accessible timescales range from several minutes to hours. Further tuning to days appears feasible by increasing the buffer capacity and lowering the urease concentration. Multiple jumps are possible upon reinjection of the activator when an excess of DD is added at the beginning of the reaction (Figure SI 4). To approach the time-programmed generation of self-assemblies and hydrogels, we couple our IFS to a carefully selected dipeptide, Fmoc-Leu-Gly-OH,[37] which forms well-defined, self-assembled, twisted ribbon-type nanofibrils and hydrogels at low pH values as a result of the removal of electrostatic repulsion (Figure 19 a,c). The transition to a nanofibrillar gel state occurs at approximately pH 5.8 and a peptide concentration of about 0.6 wt%. The dipeptide changes the pH-evolution of the system as a result of coupling with the IFS (Figure 19 b). The pH-jump depth and the plateau are coupled to the peptide concentration and its respective pK_a value. Both effects are due to the dipeptide carboxylate groups, which consume protons of the promoting CA/Na_3C buffer during the first jump. Thus causing self-assembly into nanofibrils (sol→gel). Later on, they contribute to the buffer capacity and delay the return to high pH value, thereby also delaying the disassembly. (gel→sol; see Figure SI 6 for concentration-dependent titration curves). Macroscopically, upon injection of the IFS, the aqueous dipeptide solutions rapidly form self-supporting hydrogels, which then revert back to the sol state as programmed by the IFS and confirmed by the rheology (Figure SI 5). The associated transient gel time, t_{gel}, were quantified by simple tube inversion tests (Figure 19 d,e) to range from 20 min to 11 hours as programmed by changing the urease concentration from 1 to 0.45 g/L. There are only small differences between the degelation (gel→sol; t_{gel}) and the programmed timescale of the IFS ($t_{IFS\text{-}lead}$), thus indicating only small kinetic offsets during disassembly (t_{d2}, Scheme 2a).

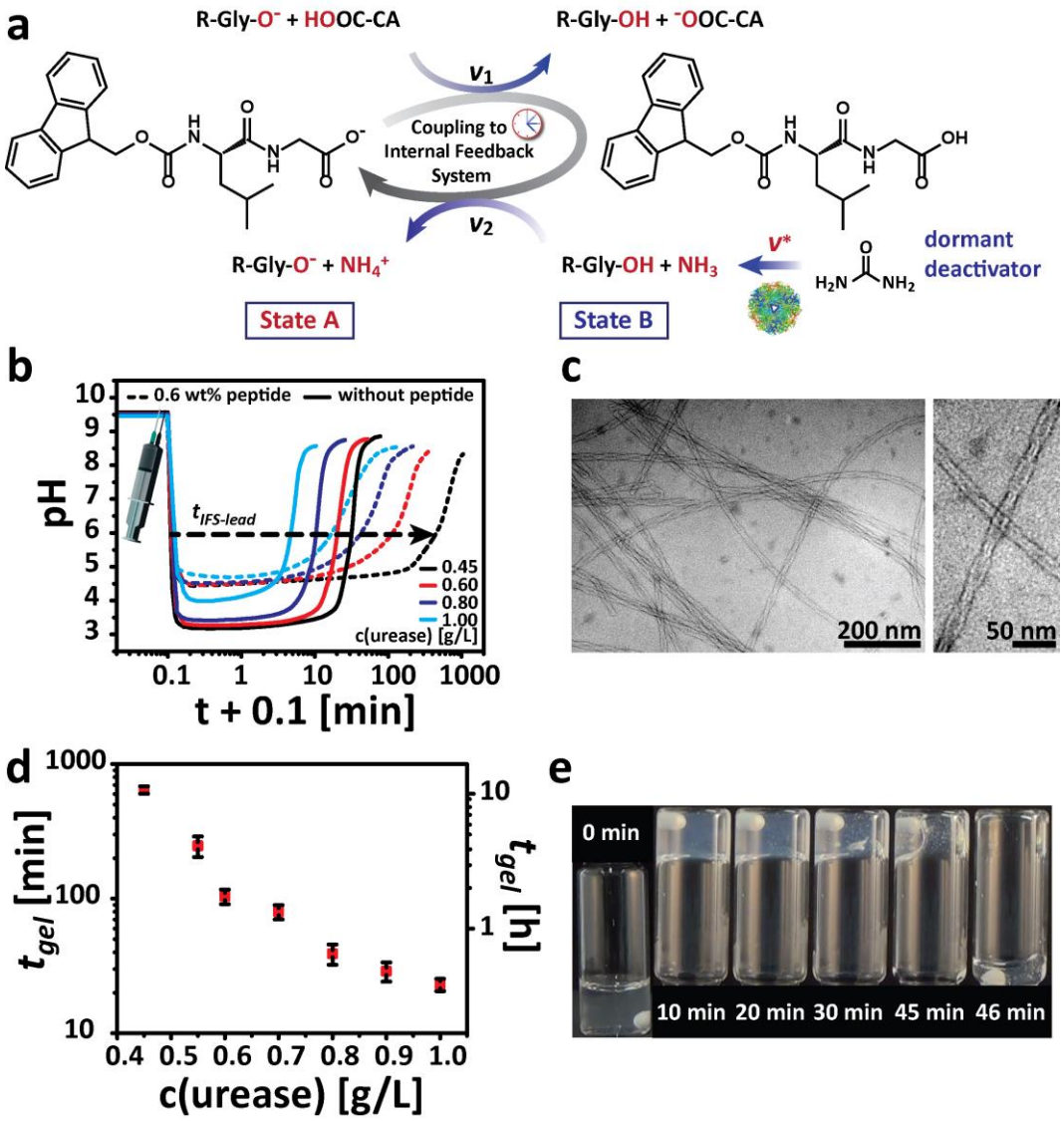

Figure 19: Temporal programing of Fmoc-Leu-Gly-OH dipeptide self-assemblies and hydrogels. (a) Coupling of the dipeptide with the acidic-IFS. (b) Influence of the peptide on the pH-timeprofiles as programmed by the use of different urease concentrations. (c) Cryo-TEM images revealing the twisted structure of self-assembled nanofibrils (d) Gel lifetimes as determined by tube inversion tests (e) Series of snapshots of a temporally programmed peptide hydrogel at a urease concentration of 0.8 g/L. Conditions for b, d, e: 60 mM urea, 12 mM CA/Na_3C (9:1) buffer and different urease concentrations as indicated.

Next, we demonstrate first applications of the time-programmed dynamic hydrogels in fluidic systems, for burst release and for transient rapid prototyping. In both technical and biological fluidic networks (e.g. blood vessels) the time-programmed regulation of fluidic pathways may be desirable to enable the guidance or time-programmed blocking of liquids and reactants. Fields of application can be diverse, from reaction engineering to separation, fluid logics,[38] or

clamp-free blocking of blood flow during catastrophic injury. To this end, we first developed an injectable variant of the time-programmed hydrogel by using double-barrel syringes with the peptide and urease in compartment A and an acidic solution of urea in compartment B. Upon extrusion through a micromixing needle, these two compartments mix and gelation occurs as a result of a decrease in the pH value. The simultaneous mixing of urea and urease then in turn slowly returns the medium to alkaline state and redissolves the formed gel. For better visualization, we added a pH-tracer dye (resazurin).

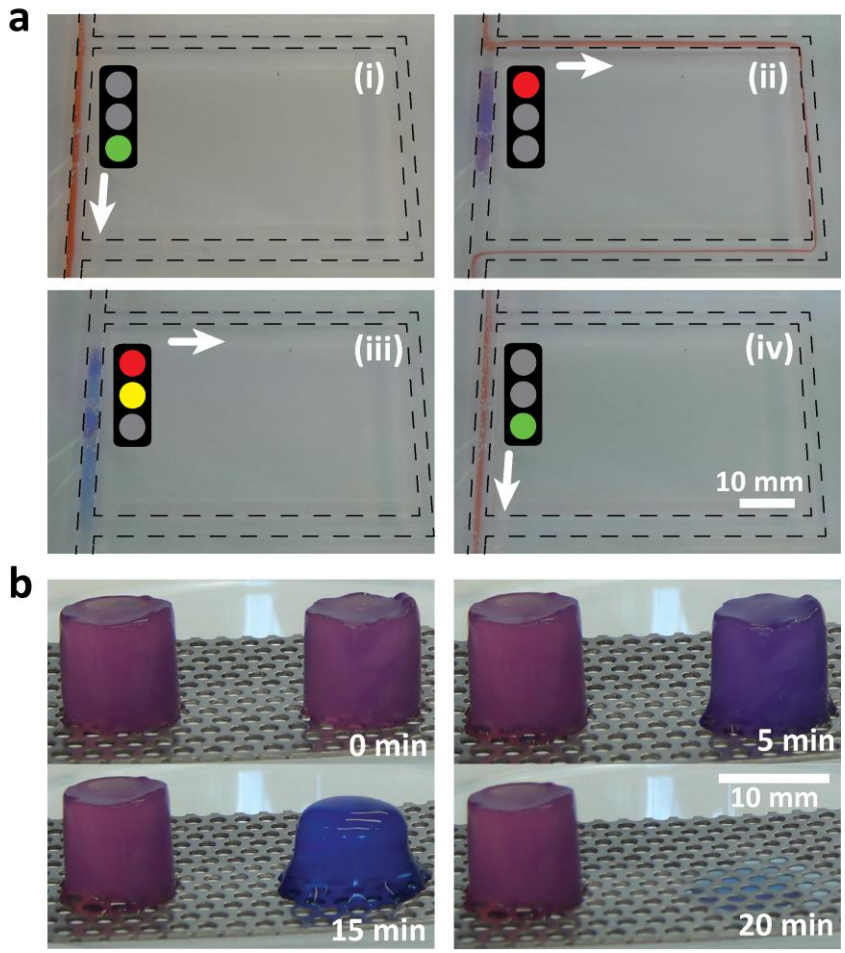

Figure 20: Fluidic guidance, burst release and transient rapid prototyping using time-programmed hydrogels: (a) Fluidic Guidance: (i) the fluid prefers the direct pathway. (ii) The bypass is used upon blocking the dominant channel with the time-programmed hydrogel. (iii,iv) Upon dissolution of the hydrogel the direction of the original fluid stream is recovered (1.3 g/L urease, 60 mM urea, 12 mM CA/Na_3C-buffer (CA/Na_3C = 9/1), 1.5 wt% Fmoc-Leu-Gly, 150 µM resazurin blue, congo red as indicator dye for the fluid stream). (b) Self-erasing hydrogels for burst release and transient rapid prototyping. Snapshot series of two micromolded cylinders without (left) and with IFS (right) (1 wt% Fmoc-Leu-Gly, 1.3 g/L urease, 12 mM CA/Na_3C-buffer (CA/Na_3C = 9/1) and 60 mM urea (right)).

To demonstrate the applicability of our system to fluidic guidance, we designed a poly(dimethylsiloxane) device with a short dominant fluid channel and an alternative bypass, which is unfavorable for the fluid stream owing to a significant pressure difference (Figure 20a). Sealing of the dominant fluid channel with a time-programmed hydrogel plug forces the fluid stream along the bypass for as long as programmed by the IFS, before it is redirected to the original path as a result of dissolution of the time programmed hydrogel by the use of its internal trigger. Operations and repair could be performed behind the gel plug in the meantime, reactants could be diverted as needed, and fluid logic systems could be programmed.[38, 39] Furthermore, self-erasing hydrogels open an avenue to burst release systems and transient rapid prototyping. A comparison between a classical responsive micromolded hydrogel and a time-programmed self-erasing hydrogel is shown in Figure 20b. The classical gel will remain stable untill an outside trigger is given, whereas the self-regulating hydrogel disappears on a time–programmed pathway, thus giving rise to a sudden and predictable burst release of encapsulated material (a dye in this case). The series of snapshots in Figure 20b again demonstrates the clear differences between passively responsive hydrogels and the self-regulating, dynamic hydrogels described herein.

3.4 Conclusion

In conclusion, we demonstrated how to precisely program acidic pH profiles in time by the feedback-driven, biocatalytically controlled slow generation of base in combination with fast acidic promoters in closed systems. We coupled such transient pH profiles to a responsive peptide gelator, thus enabling the programming of gel lifetimes. This approach can be viewed as an important advance with respect to stimuli-responsive materials, as it provides access to dynamic, self-regulating materials based on internal triggers. We also showed that time-programmed and self-erasing, injectable and micromoldable hydrogels are useful for burst release or fluidic guidance. Since our approach modulates the surroundings of the material and does not chemically alter its structure beyond protonation, we believe it to be a simple and generic method that could be used to program the lifetimes of other self-assemblies that form at low pH values. It also promotes an understanding of challenging dynamic materials and systems. In future, advanced control over self-assembling systems with respect to time could be possible by the combination of dormant activators and deactivators, which would enable the definition of the “on-time” before the self-assembly forms.

3.5 Supporting Information

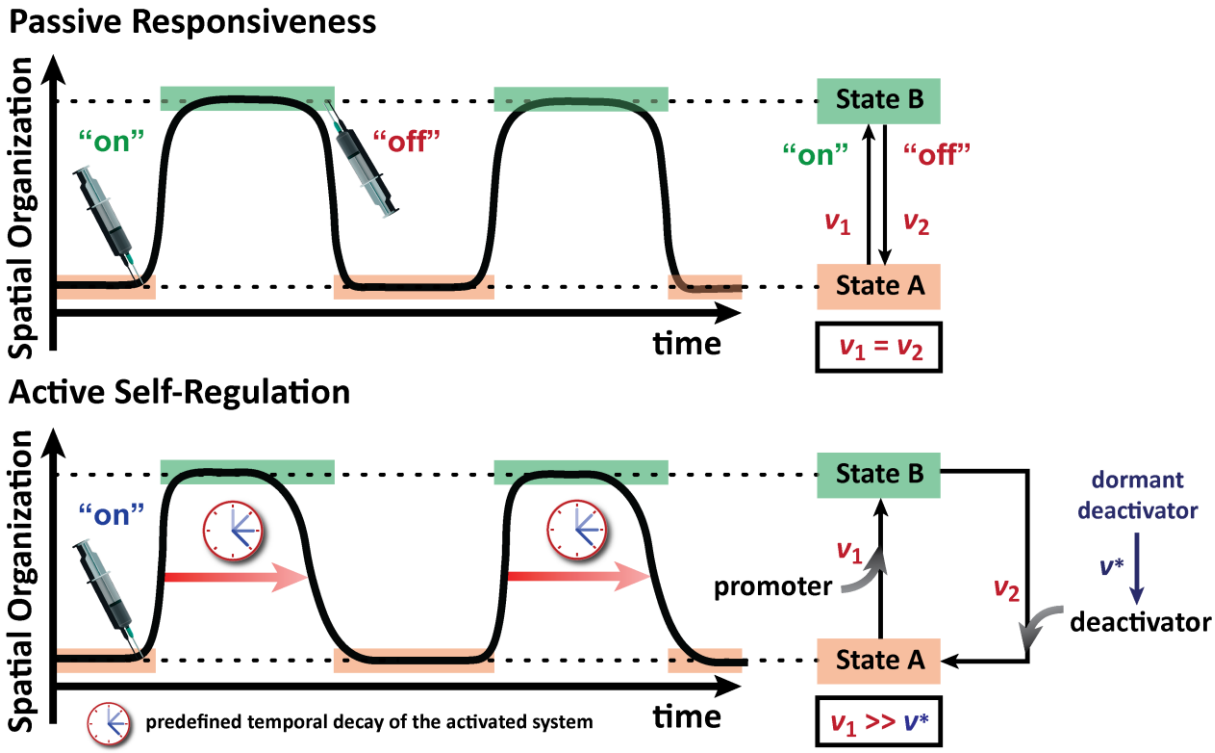

Figure SI 2: Stimuli responsiveness vs. active self-regulation: (i) Classical "static" responsive systems switch from state A to state B in response to antagonistic stimuli. The "on" switch (e.g. heating or addition of acid) induces the switch from state A to B. Once reached, state B remains infinitely stable in time in a closed system. The antagonistic "off" switch (e.g. cooling or addition of base) reverts the system back to the initial state. Upon simultaneous application of both promoting and deactivating trigger, they will annihilate instantaneously ($v_1=v_2$) and a system change does not occur. (ii) Our system only requires a single "on" trigger, which already contains all relevant feedback information required for autonomous self-regulation in closed systems. A simultaneous addition of fast activators (acid buffers) with the dormant deactivator programs a transient pH profile, which the self-assembly follow. We here rely on the enzymatic conversion of urea into ammonia to produce the active deactivating compound in a highly time-controlled, catalytic manner. The kinetic boundary conditions simplifies to $v_1>>v^*$.

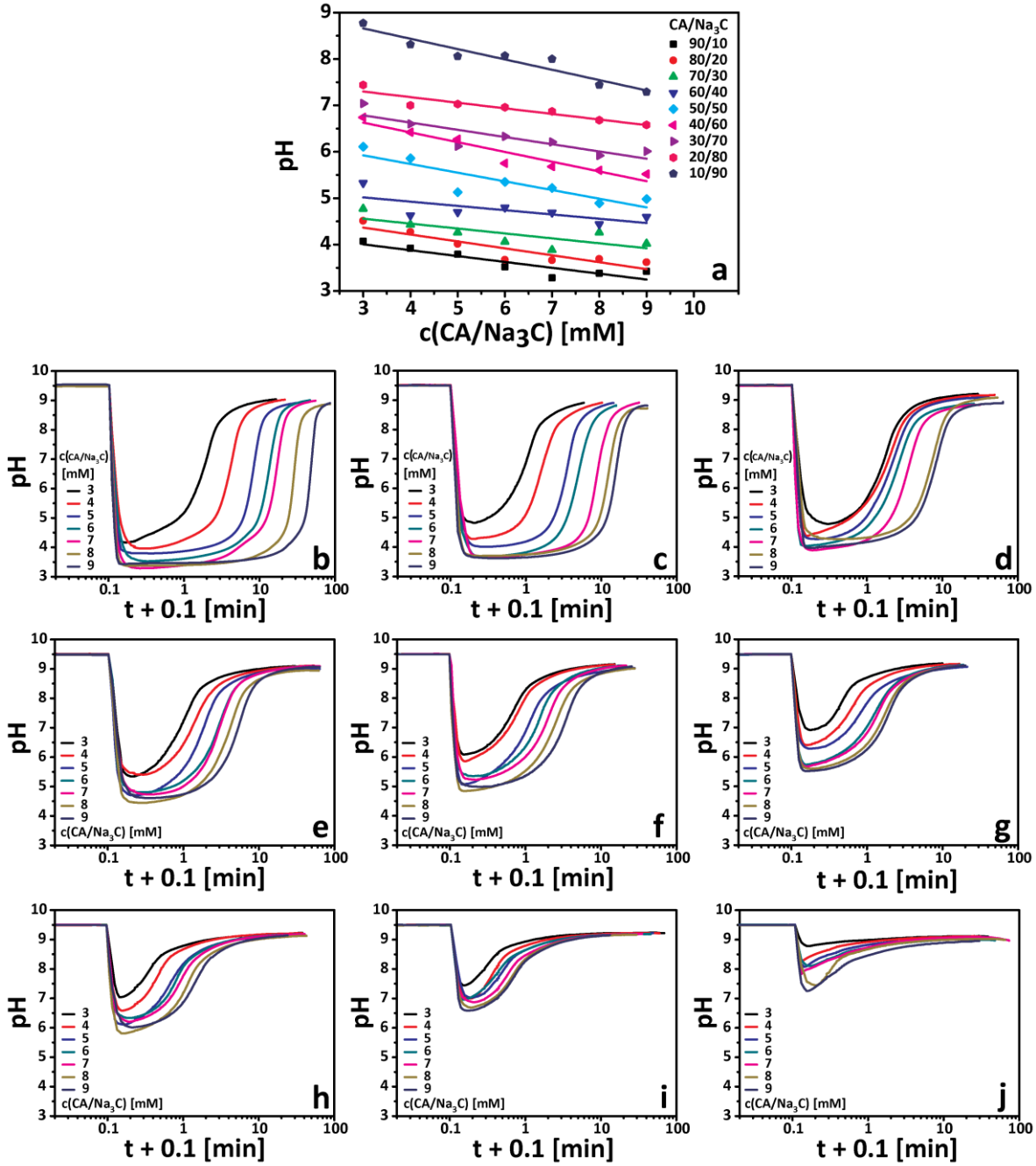

Figure SI 3: The overall buffer concentration and composition influences the depth of the pH-jump and the plateau-time: (a) Depth of the pH-jumps for various internal feedback systems as a function of the overall buffer concentration (c(CA/Na_3C)) and for different buffer compositions as indicated. This plot is constructed based on Figures b-j. (b-j) pH-feedback curves for various buffer concentrations (c(CA/Na_3C) = 3 - 9 mM) prepared at different ratios of CA to Na_3C: (b) 90/10, (c) 80/20 , (d) 70/30, (e) 60/40, (f) 50/50, (g) 40/60, (h) 30/70, (i) 20/80 and (j) 10/90. Conditions: 0.3 g/L urease and 60 mM urea.

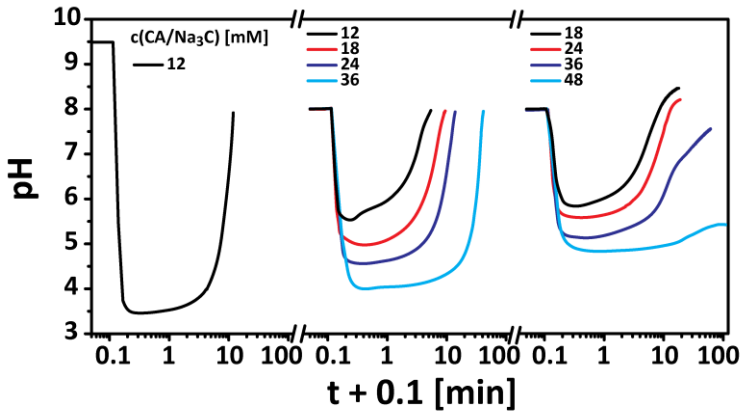

Figure SI 4: Multiple jumps upon reinjection of the fast promoter: An excess of the dormant deactivator (120 mM) enables multiple jumps by simple reinjection of various amounts of the fast promoter (citric acid buffer) after the pH value has returned to basic pH. The overall buffer concentration defines the depth of the pH-jump as shown for four different sets of measurements. In order to overcome the basicity of the continuously released base, the concentration of the promoter is increased for every jump (e.g. red curve: 18 mM CA/Na_3C for the second and 24 mM CA/Na_3C for the third jump). The last light blue curve (3rd injection with 48 mM) shows that an excess of acid was added and that the pH can no longer return to basic pH. Conditions: 0.6 g/L urease, 120 mM urea and various concentrations of citric acid buffer (CA/Na_3C = 0.98M/0.02M).

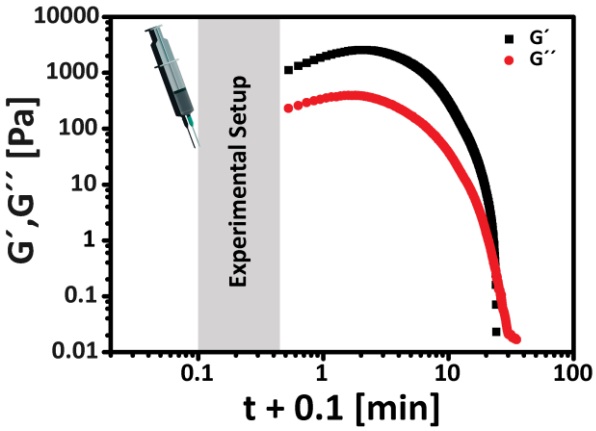

Figure SI 5: Evolution of G´ and G´´ in time: Rheological measurement for 0.6 wt% peptide, 0.9 g/L urease, 60 mM urea and 12 mM CA/Na_3C-buffer (CA/Na_3C = 9/1). Due to the experimental setup, the period subsequent to the injection can not be measured as indicated by the shaded area. Upon injection of the IFS and formation of the dipeptide hydrogel, the storage modulus (G´) is considerably higher than the loss modulus (G´´), both in a range as reported in literature for Fmoc-dipeptides. Due to the subsequent release of base by the enzymatic conversion of urea, the carboxylic peptide groups are deprotonated and the gel/sol transition occurs as indicated by the intersection of both moduli.

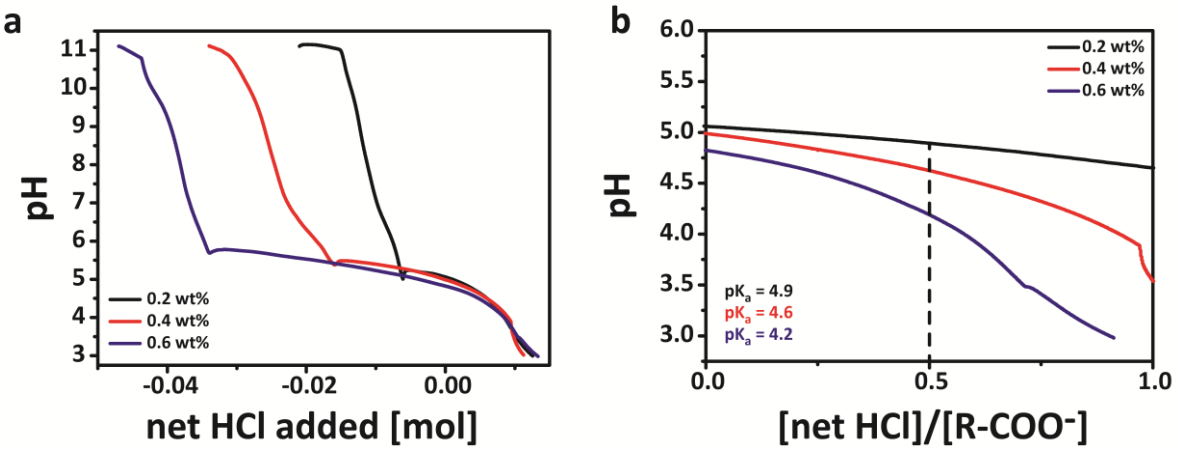

Figure SI 6: Titration curves of Fmoc-Leu-Gly: (a) Titration curves of 0.2, 0.4, and 0.6 wt% solutions of Fmoc-Leu-Gly. All peptide samples were dissolved at pH = 11 (0.1 N NaOH) and titrated against 0.1 N HCl. A higher peptide concentration results in a pronounced buffer plateau with pH transitions at pH = 5.7 (0.6 wt%), pH = 5.4 (0.4 wt%) and pH = 5.0 (0.2 wt%). (b) Titration curves depicted as a function of the degree of ionization. The pK_a values depend on the Fmoc-dipeptide concentration and are shifted to higher values in comparison to the theoretical pK_{a_th} of 3.82, which is in agreement with literature.

3.6 References

1. Stoffelen, C.; Voskuhl, J.; Jonkheijm, P., Huskens, J., *Angew. Chem. Int. Ed.* **2014,** *53*, 3400-3404.
2. Chen, L.; Morris, K.; Laybourn, A.; Elias, D.; Hicks, M. R.; Rodger, A.; Serpell, L., Adams, D. J., *Langmuir* **2010,** *26*, 5232-5242.
3. Kang, Y.; Walish, J. J.; Gorishnyy, T., Thomas, E. L., *Nature Materials* **2007,** *6*, 957-960.
4. Arsenault, A. C.; Puzzo, D. P.; Manners, I., Ozin, G. A., *Nat Photon* **2007,** *1*, 468-472.
5. Huynh, C. T.; Nguyen, M. K., Lee, D. S., *Macromolecules* **2011,** *44*, 6629-6636.
6. Shifeng, Y.; Taotao, W.; Long, F.; Jie, Z.; Kunxi, Z.; Xuesi, C.; Lei, C., Jingbo, Y., *Biomacromolecules* **2014,** *15*, 4495-4508.
7. Zhang, S.; Greenfield, M. A.; Mata, A.; Palmer, L. C.; Bitton, R.; Mantei, J. R.; Aparicio, C.; de la Cruz, M. O., Stupp, S. I., *Nature Materials* **2010,** *9*, 594-601.
8. Lutz, J.-F., Börner, H. G., *Prog. Polym. Sci.* **2008,** *33*, 1-39.
9. Huck, W. T. S., *Mater. Today* **2008,** *11*, 24-32.
10. Moya, S.; Azzaroni, O.; Farhan, T.; Osborne, V. L., Huck, W. T. S., *Angew. Chem. Int. Ed.* **2005,** *44*, 4578-4581.
11. Zhu, Y.; Shi, J.; Shen, W.; Dong, X.; Feng, J.; Ruan, M., Li, Y., *Angew. Chem. Int. Ed.* **2005,** *44*, 5083-5087.
12. Bae, Y.; Fukushima, S.; Harada, A., Kataoka, K., *Angew. Chem. Int. Ed.* **2003,** *42*, 4640-4643.
13. Li, Y.; Lokitz, B. S., McCormick, C. L., *Angew. Chem.* **2006,** *118*, 5924-5927.
14. Stuart, M. A. C.; Huck, W. T. S.; Genzer, J.; Muller, M.; Ober, C.; Stamm, M.; Sukhorukov, G. B.; Szleifer, I.; Tsukruk, V. V.; Urban, M.; Winnik, F.; Zauscher, S.; Luzinov, I., Minko, S., *Nature Materials* **2010,** *9*, 101-113.

15. Fletcher, D. A., Mullins, R. D., *Nature* **2010,** *463*, 485-492.
16. Mitchison, T., Kirschner, M., *Nature* **1984,** *312*, 237-242.
17. Whitesides, G. M., Grzybowski, B., *Science* **2002,** *295*, 2418-2421.
18. Wang, C.; Stewart, R. J., Kopecek, J., *Nature* **1999,** *397*, 417-420.
19. Smith, A. M.; Williams, R. J.; Tang, C.; Coppo, P.; Collins, R. F.; Turner, M. L.; Saiani, A., Ulijn, R. V., *Adv. Mater.* **2008,** *20*, 37-41.
20. Aggeli, A.; Bell, M.; Boden, N.; Carrick, L. M., Strong, A. E., *Angew. Chem. Int. Ed.* **2003,** *42*, 5603-5606.
21. Shinohara, S.-i.; Seki, T.; Sakai, T.; Yoshida, R., Takeoka, Y., *Angew. Chem. Int. Ed.* **2008,** *47*, 9039-9043.
22. Maeda, S.; Hara, Y.; Yoshida, R., Hashimoto, S., *Angew. Chem.* **2008,** *120*, 6792-6795.
23. Maeda, S.; Hara, Y.; Sakai, T.; Yoshida, R., Hashimoto, S., *Adv. Mater.* **2007,** *19*, 3480-3484.
24. Semenov, S. N.; Wong, A. S. Y.; van der Made, R. M.; Postma, S. G. J.; Groen, J.; van Roekel, H. W. H.; de Greef, T. F. A., Huck, W. T. S., *Nat. Chem.* **2015,** *7*, 160-165.
25. Debnath, S.; Roy, S., Ulijn, R. V., *J. Am. Chem. Soc.* **2013,** *135*, 16789-16792.
26. Pappas, C. G.; Sasselli, I. R., Ulijn, R. V., *Angew. Chem. Int. Ed.* **2015,** DOI: 10.1002/ange.201500867
27. Boekhoven, J.; Brizard, A. M.; Kowlgi, K. N. K.; Koper, G. J. M.; Eelkema, R., van Esch, J. H., *Angew. Chem. Int. Ed.* **2010,** *49*, 4825-4828.
28. Heuser, T.; Steppert, A.-K.; Molano Lopez, C.; Zhu, B., Walther, A., *Nano Lett.* **2015,** *15*, 2213-2219.
29. Fidaleo, M., Lavecchia, R., *Chem. Biochem. Eng. Q.* **2003,** *17*, 311-318.
30. Kistiakowsky, G. B., Rosenberg, A. J., *J. Am. Chem. Soc.* **1952,** *74*, 5020-5025.
31. Russell, A. J.; Erbeldinger, M.; DeFrank, J. J.; Kaar, J., Drevon, G., *Biotechnol. Bioeng.* **2002,** *77*, 352-357.
32. Hu, G.; Pojman, J. A.; Scott, S. K.; Wrobel, M. M., Taylor, A. F., *J. Phys. Chem. B* **2010,** *114*, 14059-14063.
33. Johnson, J. M.; Kinsinger, N.; Sun, C.; Li, D., Kisailus, D., *J. Am. Chem. Soc.* **2012,** *134*, 13974-13977.
34. de la Rica, R., Matsui, H., *Angew. Chem. Int. Ed.* **2008,** *47*, 5415-5417.
35. Huang, T.-C., Chen, D.-H., *Journal of Chemical Technology & Biotechnology* **1991,** *52*, 433-444.
36. Krajewska, B., *J. Mol. Catal. B: Enzym.* **2009,** *59*, 9-21.
37. Tang, C.; Ulijn, R. V., Saiani, A., *Langmuir* **2011,** *27*, 14438-14449.
38. deMello, A. J., *Nature* **2006,** *442*, 394-402.
39. Lenshof, A., Laurell, T., *Chem. Soc. Rev.* **2010,** *39*, 1203-1217.

4 PHOTONIC DEVICES OUT OF EQUILIBRIUM: TRANSIENT MEMORY, SIGNAL PROPAGATION AND SENSING

The results presented in this chapter were published in the article: T. Heuser et al., *Adv. Mat.,* **2017**, DOI: 10.1002/adma.201606842

4.1 Introduction

Bright color patterns in nature originate from interactions of pigments or ordered structures with light.[1, 2] While pigmentary color arises from selective absorption by dermal chromatophores, structural color (iridescence) appears due to selective refraction at diffraction gratings and multilayer reflectors as found in beetles, butterflies and cephalopods.[3-5] Additionally, a few species can actively tune their patterns by hormonal or neural control.[6-8] Structural color in synthetic photonic crystals relies on the same fundamental principle that is periodic variation of the refractive index in a dimension similar to the wavelength of visible light. Destructive interference leads to a full or partial photonic band gap, which prevents the propagation of photons of a specific wavelength in any or certain directions, respectively.[9, 10] Such wave guiding is important for a wide range of applications as full color displays,[11-13] sensors,[14-16] in solar cells[17, 18] and energy storage.[19, 20]

Self-assembly has proven to be a powerful and versatile technique for the fabrication of tunable photonic crystals operating in the visible range. Strategies include the assembly of uniform colloidal particles into closely packed arrays (opals), or using such opals to template polymers in the interstitial phase followed by etching of the particles to generate inverse opals, as well as block copolymers (BCPs) where microphase segregation drives the formation of periodic structures.[21-23] Striving for functional and tunable materials, photonic crystals in which the position of the stop band can be tuned by external stimuli are of particular interest.[11, 16, 24-26] Lamellar structures formed by the diblock copolymer polystyrene-*b*-poly(2-vinyl pyridine)

(PS-*b*-P2VP) have attracted considerable interest due to their responsive ionization behavior (swelling) at the P2VP functions. While switchability with pH,[27] temperature,[28] ionic strength,[29] and counter ions[30] has been demonstrated, it has remained challenging to even adjust the timescale of switching[27] after a certain trigger is applied.

The next crucial advances can be made upon the implementation of autonomous behavior, which essentially requires to preorchestrate switching mechanisms in the time domain of a system.[31] If mastered, new system properties would become reachable, including sustained signal propagation (still in an adaptive manner with possibilities to respond to outside) or transient states/memories with programmable lifetimes. On a materials scale, this would allow new levels of functionalities for sensing, logic and computation, or for tamper-proof security features.

Conceptually, such autonomous functionalities can no longer be engineered using classical concepts of responsive materials, such as direct acid/base switching, but require to orchestrate triggers and counter triggers in time in a non-linear fashion to achieve self-regulating behavior. In natural systems, such non-linear phenomena arise from chemical reaction networks, in which temporal control relies on the concurrence of positive and delayed negative feedback. Hence it becomes clear that one needs to integrate responsive photonic materials with out-of-equilibrium chemical reaction networks into a system to enable the desired progress in the direction of autonomous systems behavior.

Here, we demonstrate the system integration of a non-linear, autocatalytic pH-modulating feedback system with a pH-sensitive BCP photonic gel to reach sustained signal propagation, sensing, and temporal control of the lifetimes of a transient reflective state. Urease with a pH-dependent activity and with a pH-modulating reaction (conversion of urea into ammonia and carbon dioxide) is at the core of the non-linear chemistry (Scheme 3a, orange curve). This autocatalytic and feedback-controlled urease switch has previously been used for studying pH-oscillators in continuously fed stirred tank reactors, for pH front propagation, and on a materials level for frontal polymerization and hydrogels with lifetimes.[32-37] Its robustness makes it ideal to investigate increasingly complex materials systems concepts. We distinguish different approaches to couple the urease switch to the soft photonic materials. We first use an overall negative feedback loop starting from the alkaline regime to generate a transient reflection state with preprogrammed and tunable lifetimes (self-erasing memory; Scheme 3a, green curve).

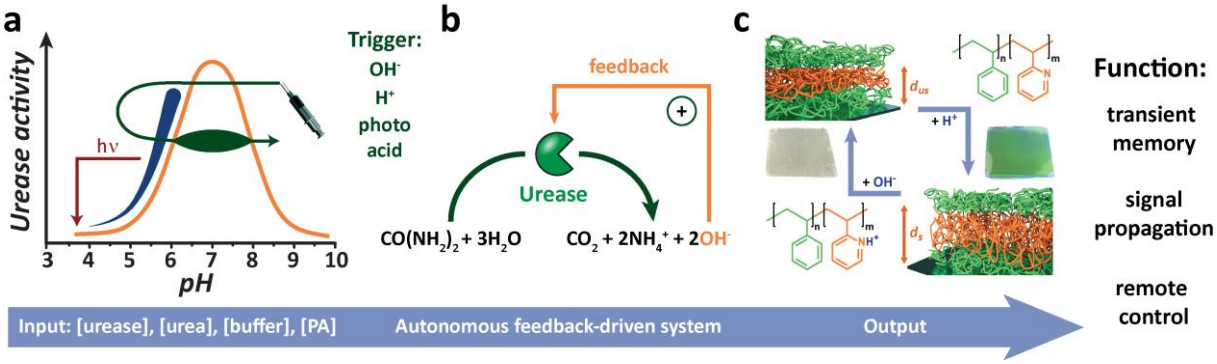

Scheme 3: Integration of non-linear, feedback-controlled, pH-modulating biocatalysis with pH-responsive BCP photonic mirrors allows new autonomous functionalities in photonic devices: (a) System integration: Orange curve: The pH-dependent bell-shaped urease activity[33] provides overall negative feedback (urea → OH^-). Green curve: Starting from high pH, the injection of acid in cooperation with the pH-modulating urease/urea reaction allows to extinguish the transient reflection state of a photonic mirror (that occurs at low pH). Blue curve: The autocatalytic amplification serves as a positive feedback for pH signal propagation when starting from low pH and adding base. Red arrow: External modulation of the autocatalytic amplification using the counteracting photoacid (PA) 2-nitrobenzaldehyde (light sensing). (b) Different concentrations of enzyme, substrate, buffer and photoacid (PA) compose the input information. The autocatalytic conversion of urea into ammonia gives rise to autonomous behavior, and is controlled in its speed by the urease concentration. The input information encodes transient temporal signatures and propagating pH-waves in aqueous media. (c) Protonation of the pyridine group in a PS-*b*-P2VP BCP photonic film results in anisotropic volume expansion of the hydrophilic P2VP layer. The domain thickness, and the refractive index contrast encode the refracted wavelength of the visible light, and the reflective color serves as an output signal.

We then show that a positive feedback mechanism (autocatalytic amplification) can be triggered from the acidic state, and allows to send reflection/dark signal fronts across centimeter-long channels with a tunable propagation speed and without loss of velocity (Scheme 3a, blue curve). The incorporation of a photo-responsive component even allows to remotely stop the signal using external illumination (Scheme 3a, red arrow). Hence, by merging two previously independent fields, non-linear feedback controlled chemistry and photonic materials, we open the design space for achieving new system functionalities, here focusing on a transient memory, signal propagation and remote light sensing. (Scheme 3).

4.2 Experimental Section

Materials: Urease (from *canavalia ensiformis*), urea (99.0 – 100.5%), (3-iodopropyl)trimethoxysilane (≥ 95%), propylene glycol monomethyl ether acetate (≥ 99.5%), iodine (≥ 99.99%), 2-nitrobenzaldehyde (98%), bromocresol purple (90%), Triton X-100 (10 % in H_2O) and citric acid monohydrate were purchased from Sigma Aldrich. Trisodium citrate dihydrate (99.0%) was purchased from Alfa Aesar, hydrochloric acid (0.1 N) from Merck and sodium hydroxide (0.1 N) from VWR Chemicals. Poly(styrene-*b*-2-vinyl-pyridine); PS(55000)-P2VP(56000) was purchased from Polymer Source and Hellmanex III solution from Hellma Analytics.

Film preparation: The glass substrates were cleaned following a standard procedure including alternating washing steps with Hellmanex solution and water under ultra-sonication for 15 minutes prior to the final treatment in ethanol and subsequent drying under air pressure. The photonic BCP films were prepared as described in literature. The glass slides were placed in a desiccator in presence of a small beaker containing (3-iodopropyl)trimethoxysilane. Vacuum was applied for several minutes and the films were allowed to remain in the silane-atmosphere for 10 min to improve BCP adhesion. Subsequently, the glass slides were spin-coated with a 50 mg/mL BCP solution (dissolved in propylene glycol monomethyl ether acetate) at 3000 rpm for 15 s and 500 rpm for further 75 s. In the end the films were annealed in a chloroform atmosphere for 24 hours at room temperature.

Scanning Electron Microscopy: Images of the cross-section of the block copolymer films were recorded on a SU9000 SEM by Hitachi. The cross-section was milled with an ion beam of an IM4000 Ion Milling System from Hitachi. To increase the contrast between the PS and the P2VP layer, the latter was stained with I_2 vapor.

Temporal programming of the reflectance of pH-responsive block copolymer photonics via enzymatically controlled internal feedback: The CA/Na_3C buffer was prepared with 0.98 M citric acid monohydrate and 0.02 M trisodium citrate dihydrate dissolved in 0.1 M hydrochloric acid. The resulting mixture was diluted with water before calculated amounts of urea were dissolved to yield final concentrations of 3 M urea in 0.5 M CA/Na_3C buffer. Specific amounts of the resulting CA/Na_3C buffer and urea were loaded into Hamilton syringes and injected into an aqueous urease solution (varied concentration) containing the BCP photonic films and 0.5 g

L^{-1} bovine serum albumin (added as sacrificial protein to protect urease). The feedback pH profiles as well as pH titrations were monitored with a Methrom Titrando 905 combined with in-situ reflectance measurement by an Ocean Optics device.

Propagating pH waves: Specific amounts of urease were added in a solution containing 5 mM of citric acid monohydrate, 35 mM of urea (and 0.1 mM of bromocresol purple when needed). The resulting solution was injected in a 2 x 3 x 100 mm PDMS channel on top of a BCP photonic gel and covered with a glass slide. Propagation was started by the injection of 10 µL 0.1 M NaOH at one end of the channel.

Stopping the pH wave propagation with a photoacid: 1 mM citric acid monohydrate, 29 mM hydrochloric acid, 2 wt% Triton X-100, 42 mM 2-nitrobenzaldehyde (from a solution at 600 mM in ethanol), 27 mM urea and 1.2 g L^{-1} urease were successively added in MilliQ water. The propagation experiments were then performed as previously described. Shining UV light for 10-20 min from 10 cm distance stops the propagation. (Wavelength 365 nm, irradiance 150 W m^{-2}, model SpecBright LF1, ProPhotonics, Ireland)

Photoacid in stirred solution: 3 mM citric acid, 2 wt% Triton X-100, 10 mM 2-nitrobenzaldehyde (from a solution at 600 mM in ethanol), 27 mM urea and 1.2 g L^{-1} urease were mixed in MilliQ water shortly before starting the experiment. To prevent the pH jump the vials were UV-illuminated for 10 min from 10 cm distance, (150 W m^{-2}, wavelength 365 nm, model SpecBright LF1, ProPhotonics, Ireland).

4.3 Results and Discussion

The photonic films are based on a PS528-*b*-P2VP533 diblock copolymer (the numbers denote the number average degree of polymerizations), and were prepared by spin-coating and solvent annealing as described earlier.[30] The corresponding cross-sectional scanning electron microscopy (SEM) image reveals an in-plane lamellar microdomain structure with a periodicity, d_{us}, of 60 nm in the dried state at an overall thickness of 1 µm (Figure 21a). The dry films are transparent. The presence of the pyridine groups implements a strong responsiveness towards changes of the surrounding pH, and leads to a selective hydrophobic/hydrophilic switching of the P2VP layer, and subsequent swelling. Hence, below the pK_a value (pK_a ≈ 5.2 in dilute solution, pK_a = 3.2 in the photonic film)[27] of the pyridine groups, electrostatic repulsion and

ingress of water result in a volume expansion, leading to a photonic band gap in the visible region as a result of both the increased refractive index contrast and the properly enlarged dimensions, d_s. The position of the photonic stop band is related to the pH as illustrated in Figure 21b. Upon increasing the pH from strongly acidic conditions (pH = 3, λ_{max} = 647 nm), the maximum reflection measured at 90° shows a pronounced blue shift due to deswelling before the film becomes transparent above pH = 4.5.

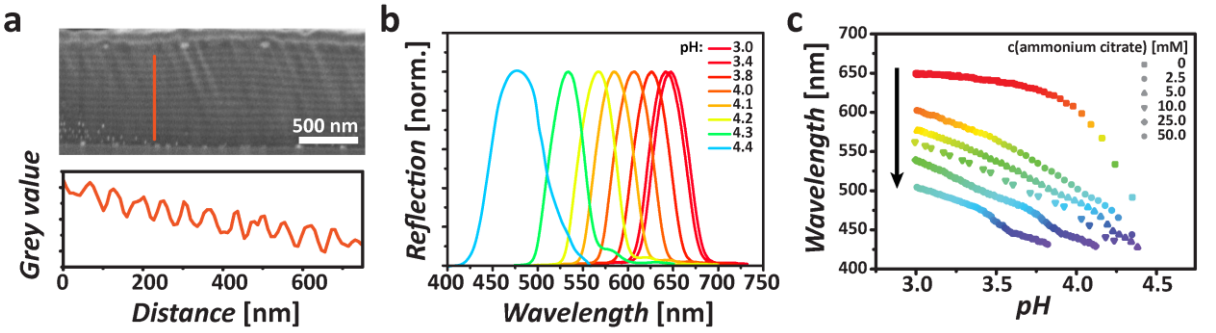

Figure 21: pH-dependent structural color: (a) The SEM image of the ion-beam milled cross-section of the PS-*b*-P2VP film reveals the lamellar multilayered structure after I_2 staining with an average periodicity of 60 ± 5.9 nm after horizontal grey scale analysis. (b) pH-dependent stop band position upon addition of NaOH (measured at 90°). (c) pH-dependent stop bands in presence of different amounts of ammonium citrate during titration from the acidic state (HCl) with NaOH (measured at 90°). The concentration of the ammonium citrate was chosen to mimic the ionic strength introduced later (see below).

Besides variation of the surrounding pH-value, the photonic films exhibit a strong sensitivity towards changes of the ionic strength of the aqueous medium. This is important in the context of applying the urease-controlled feedback mechanisms later on, because those will encompass the addition of significant amounts of citric acid (activator) and the generation of NH_4^+/OH^- (generated during feedback). To simulate the salinity conditions during the subsequent application of the non-linear chemistry, we performed titration experiments with simultaneous reflection measurements in the presence of different concentrations of ammonium citrate (Figure 21c). The position of the stop band for a given pH shows a pronounced blue shift with increasing ammonium citrate concentrations, which originates from the osmotic deswelling of the P2VP layers.[29, 38, 39] A broad tunability of the stop band position is maintained for ammonium citrate concentrations up to 10 mM, which is thereby set as the maximum concentration of citric acid used later.

Toward an integration of feedback-controlled chemical systems with the photonic materials, we first demonstrate how an overall negative feedback loop of the urease switch can be used to encode transient lifetimes into the reflective state of the BCP photonic mirror (Scheme 3a, green curve). We utilize in-situ pH measurements in combination with an optical reflection probe (90°) to correlate the pH value of the surrounding solution with the wavelength of the reflected light. We start from the alkaline state (pH = 9.5), and set up a system containing the photonic mirror immersed in a urease solution. At these conditions, the urease is nearly inactive and the photonic mirror is collapsed and transparent. Subsequently, the system is activated upon injection of a citric acid/trisodium citrate buffer (CA/Na_3C = 0.98/0.02) containing the urea to reach final concentrations of 10 mM and 60 mM, respectively. The injected CA/Na_3C buffer rapidly lowers the pH value (pH ≈ 3.6) and protonates the P2VP layer promoting the lamellar expansion responsible for the appearance of the macroscopic reflective color (v_1, Figure 22a) in the range of 560 nm (Figure 22b). This wavelength is in good agreement with the titration experiment of systems of similar ionic strength at the respective pH value (10 mM ammonium citrate; Figure 21c). At the same time, the urease is activated by injection of the acid (see activity profile in Scheme 3a), and starts producing ammonia with a catalytically controlled reaction speed (v*, Figure 22a). Importantly, this reaction rate can be controlled by changing the urease concentration, while leaving all other system parameters constant. Subsequently, the pH rises again in an autonomous and time-controlled fashion, leading to a temporally delayed deprotonation of the pyridine groups and deswelling of the hydrophilic layer. As a result the photonic mirror returns to the transparent state at a pH of around pH = 4.5 in a closed and autonomous system (Figure 22b).

In a classical acid/base switching, using for instance HCl and NaOH, such an autonomous behavior would not be possible, because activation/swelling by addition of acid and deactivation/deswelling by addition of base are not properly (de)coupled or preorchestrated in time. Basically, both triggers, acid and base, would directly annihilate each other and quickly result in a final state. Herein, the balance of activator strength (buffer) and deactivator formation (enzyme concentration) controls the lifetime of the transient optical state. Temporal control over the autonomous lifetimes of the reflective state of the photonic gels – a simplistic transient photonic memory – can be achieved by simply changing the urease concentration. A decrease in the urease concentration from 0.9 – 0.3 g L^{-1} leads to a strong increase of the lifetimes of the reflective state from 10 minutes up to 4 hours.

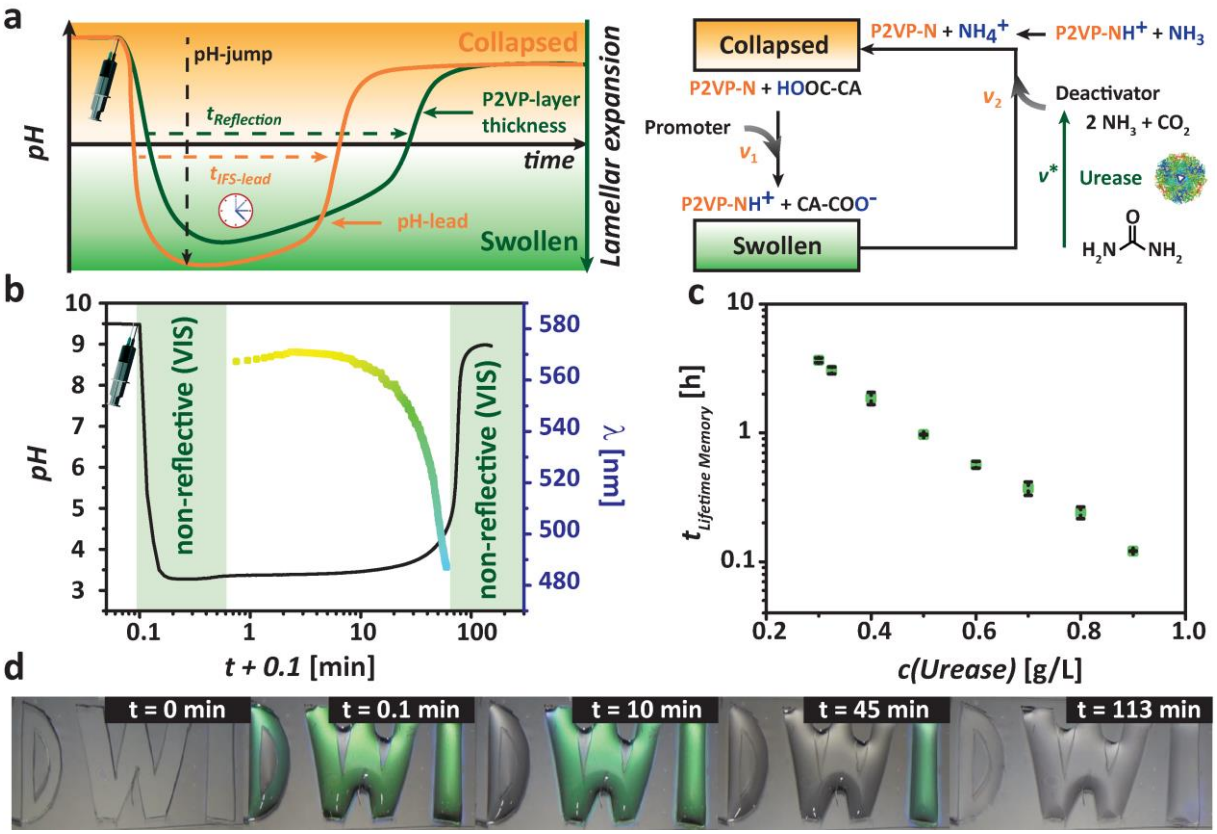

Figure 22: Temporal control of the lifetimes of the reflectance of BCP photonic gels in autonomous systems: (a) Injection of a promoter substance (acid buffer) with the dormant deactivator (urea) results in a transient pH state (orange line, $t_{IFS\text{-}lead}$). The structural response of the switchable P2VP layer (green line, $t_{Reflection}$) follows with a kinetic delay. The relevant kinetic balance required for the temporal decoupling of the promoting and the deactivating reaction, which is mandatory for a transient state, is given by $v_1 >> v^*$. (b) Control over the lifetime of the optical reflection of a BCP photonic film, exemplarily shown for 0.50 g L^{-1} urease, 60 mM urea, 10 mM CA/Na_3C buffer (0.98/0.02). (c) The urease concentration controls the lifetime of the transient optical response. Conditions: 60 mM urea, 10 mM CA/Na_3C (0.98/0.02). (d) Snapshot series of a photonic display, programmed with different enzyme concentrations to different transient lifetimes. Conditions: 60 mM urea, 4 mM CA/Na_3C buffer (0.95/0.05) and 0.30, 0.15 and 0.10 g L^{-1} urease.

The small error bars (standard deviation of three measurements) indicate the high reproducibility of the temporally programmed photonic states. To further showcase the reliability of encoding lifetimes and progress towards devices, we demonstrate a first approach towards a patterned photonic display. Figure 22d shows a snapshot series of a photonic mirror covered with a PDMS mask featuring three letters. The three letters are covered with pH-feedback solutions of various urease concentrations that encode different lifetimes. Indeed this results in consecutive disappearance of the reflected color as preprogrammed by the

concentration of the urease. Overall this is a first demonstration of a versatile information pattern technique, where the information can be encoded in a programmable and self-erasing fashion.

Next we utilize the inherent positive feedback of the urease switch for sustained color expansion/signal propagation along PDMS channels using a self-reinforcing pH-wave starting from a metastable acidic state (Scheme 3a, blue curve). Such chemical wave propagation on out-of-equilibrium basis is known both for inorganic[40, 41] as well as biocatalytic systems,[42-44] including homogeneous urease systems.[37] Yet, here we integrate this property with a photonic mirror to form a signal propagation device with minimal interference between the display and the out-of-equilibrium process, and later on expand it to a remote stopping mechanism.

Overall, there are two major requirements for a stable and fast propagation of a wave front in combination with a controlled excitation. First, the wave front requires an autocatalytic amplification driven by a positive feedback mechanism to self-sustain the signal strength, as simple diffusion would dilute the signal until it vanishes over space. Second, successful signal initiation requires controlled metastable conditions, where the system can be triggered to rapidly switch to high pH, but remains at low pH in the absence of the respective trigger.

A delicate balance is needed to realize this situation for urease. On one hand, the enzyme gets denatured at prolonged exposure at too low pH, and the signal cannot propagate, on the other hand, the system does not remain in stasis if the starting pH is too high, as the enzyme is active enough to spontaneously generate a switch without an external trigger (Scheme 3a).[42] Following critical optimization, we found that lowering the pH of the urea/urease solution to pH = 3.1 using citric acid yields a static and yet excitable state with negligible enzyme activity. The addition of a small amount of base (NaOH 5 µL at 100 mM) at one end of the channel (fabricated by placing a PDMS mask on the BCP film) triggers the biocatalytic positive feedback process. The base locally activates the enzymes, which start converting urea into ammonia and further increase the pH, thereby also increasing the enzyme activity (positive feedback). The produced base diffuses towards adjacent areas (while protons diffuse in the opposite direction to neutralize them) activating nearby enzymes, which start the same process (Figure 23a). This self-accelerating cascade leads to a stable front propagation. Behind the wave front the pH rises to the end of the activity window of the enzyme, leading to a stable pH. In addition to using the color provided by the pH-responsive photonic film, we also compare the wave fronts using a water-soluble pH-color indicator (bromocresol purple; pK_a = 6.3; Figure 23b-e).

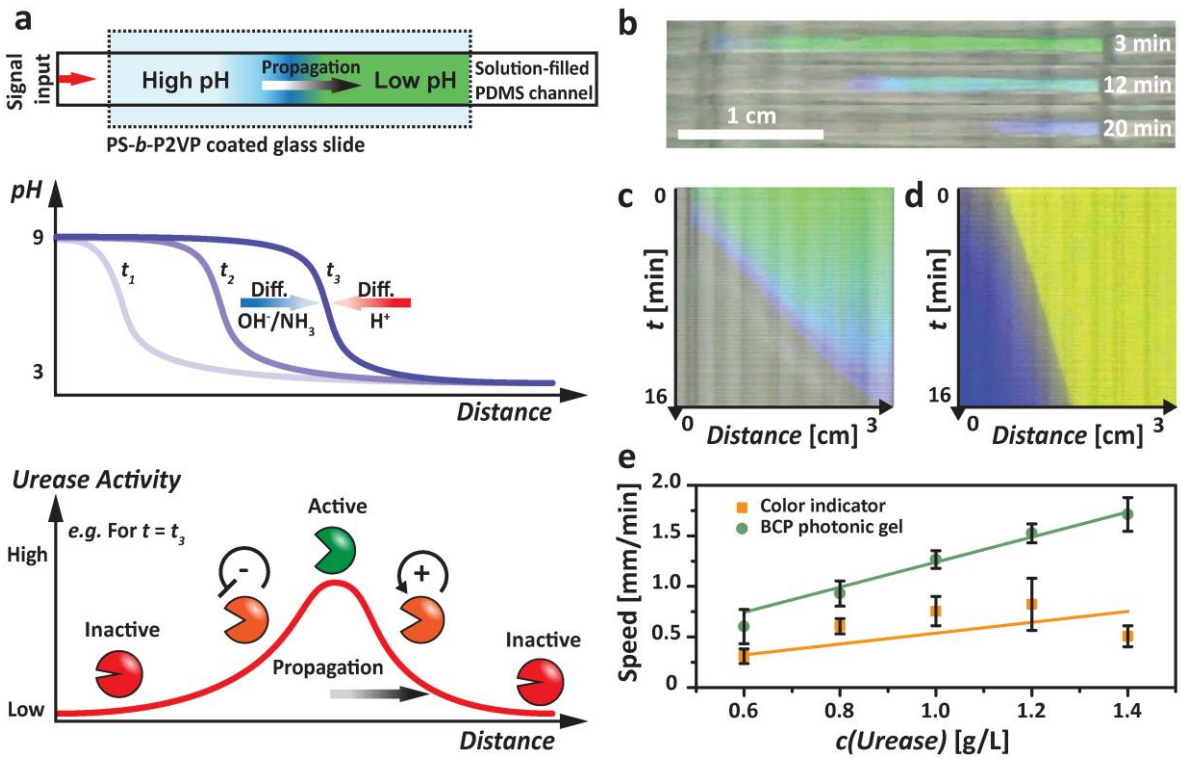

Figure 23: Long distance signal transport via propagating pH waves: (a) From top to bottom. Schematic representation of the PDMS channel device with propagating pH wave and photonic display (top view). Below, the corresponding pH profile in the channel at different times ($t_3 > t_2 > t_1$) together with the direction of diffusion of H^+, OH^- and NH_3 for $t = t_3$. At the bottom the profile of urease activity where the enzyme self-activates (positive feedback) at the front of the wave and self-inactivates after, as the pH jumps to the end of the activity window of urease. (b) Photographs of a propagating pH wave at different times (solution containing 1.4 g L^{-1} of urease, 35 mM of urea, 5 mM of citric acid) and (c) the corresponding kymographs for the BCP photonic gel and (d) for bromocresol purple with the time on the vertical axis and the front position on the horizontal axis. (e) Propagation speed of the pH wave as function of the urease concentration with 35 mM of urea and 5 mM of citric acid for the BCP photonic gel and the color indicator

The photographs of the photonic channels at different times depict the propagation of the wave front over time in a semi-quantitative fashion (Figure 23b). A more quantitative impression can be gained with kymographs, which plot the position of the pH front in the channel (vertical axis) as a function of the time (horizontal axis, Figure 23c). This plot clearly evidences a constant speed of the chemical front that is characteristic for positive feedback-driven propagation where enzymes remain active throughout the duration of the experiment. Interestingly, a kymograph for the same conditions using bromocresol purple as pH-color

indicator displays slower pH front propagation than with the photonic crystal (lower slope, Figure 23d), signifying some undesirable chemical interference.
To further understand this phenomenon, and also identify ways of tuning the speed, we recorded a full series of experiments with different urease concentrations (Figure 23e). As expected, the propagation speed increases with the enzyme concentration. Yet, the systems using the color indicator are systematically slower and present higher standard deviation (three experiments). This indicates that bromocresol purple (and certainly other color indicators) indeed poisons the urease and decreases its activity. The highest speed using the photonic mirror as reporter is more than double compared to the bromocresol purple and also twice as high as reported when using cresol red (up to 1 mm/min).[37] Overall this reveals an important advantage of using the pH-responsive photonic films. They are non-leaching and hence minimize interference with the enzymatic out-of-equilibrium processes, leading to stable and faster propagation.

In the next step we implemented a remote control of the biocatalytic out-of-equilibrium photonic device by adding a UV-sensitive photoacid, able to interfere with the autocatalyzed base generation (Scheme 3a, red curve). Figure 24a displays its molecular structure (2-nitrobenzaldehyde) and the proton release mechanism upon UV-illumination.[45] Due to its poor water solubility, we added 2 wt% of Triton X-100 to disperse the photoacid homogeneously. The basic effect for modulating the out-of-equilibrium reaction front using the photoacid is depicted for a homogenous solution in Figure 24c. Shining UV light on a well-stirred solution containing the photoacid, urea and urease at pH = 3.3 lowers the pH slightly below 3.0, thereby preventing the spontaneous transition to high pH. However, exposure to UV light after the transition to high pH has little effect on the overall pH, because of the large quantities of base generated by the self-amplifying urease/urea reaction.

The transfer to the photonic devices is schematically shown in Figures 24b,d. In absence of UV the acid remains caged in the micelles and has limited interaction with the enzyme, and the addition of small quantities of base can trigger the autocatalytic transition to high pH. However, UV illumination at specific spots leads to acid release, which inactivates the enzymes, and prevents further signal conduction. Note that the control experiment (UV illumination without photoacid) did not allow to stop the pH propagation, confirming the importance of the light-sensitive signal modulator.

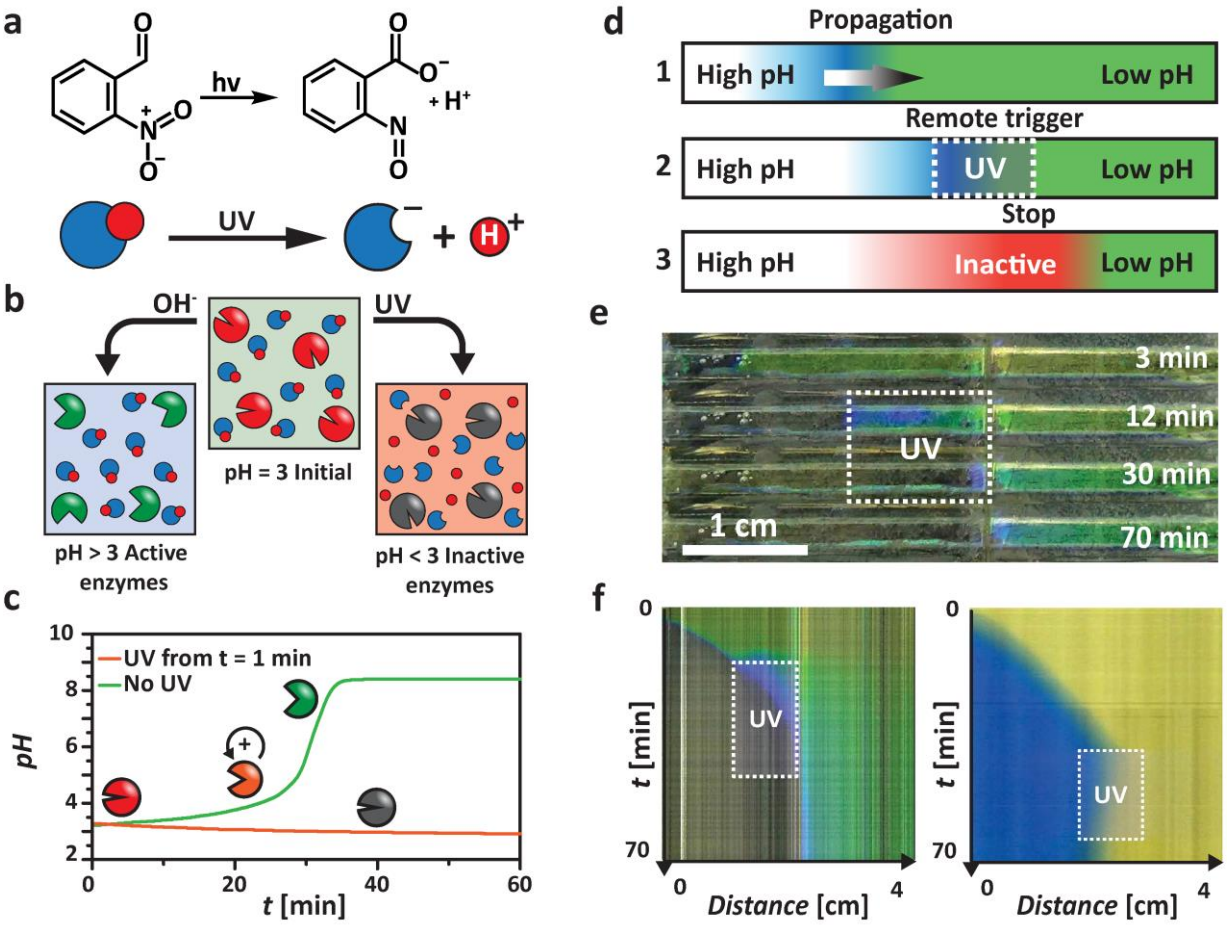

Figure 24: Arresting signal conduction through a remotely triggerable modulator: (a) Acid release from the photoacid 2-nitrobenzaldehyde upon UV-illumination (365 nm). (b) System design: Addition of a small amount of base before UV-illumination allows to drive optical signals via pH wave propagation. UV-illumination of the system before addition of the starter (base) releases the acid and prevents further activation. (c) Inhibition of the spontaneous time-programmed biocatalytic switch by UV-illumination (365 nm, 20 min, from 10 cm distance about 150 W m^{-2}) of a solution containing 1.2 g L^{-1} urease, 35 mM urea, 3 mM citric acid, 2 wt% Triton X-100, and 10 mM 2-nitrobenzaldehyde. (d) Schematic representation of UV-light-induced stopping of the propagating signal in the PDMS channel. (e) Macroscopic photographs of the propagation stop in the channel device for a system containing 1.2 g L^{-1} urease, 27 mM urea, 1 mM citric acid, 29 mM hydrochloric acid, 2 wt% Triton X-100, and 42 mM 2-nitrobenzaldehyde. (f) The corresponding kymographs showing a pH wave stopped by UV-illumination at 365 nm from 10 cm distance (150 W m^{-2}) for 20 min in the photonic gel system and the bromocresol system.

A corresponding example for a stopped signal propagation is displayed in Figure 24e, and further quantified by the kymographs in Figure 24f. Again, the system containing the color indicator displays a slower propagation speed due to decreased urease activity. Upon UV

illumination, the propagation front can be stopped. Interestingly, one can notice that the color front travels through the illuminated area in the photonic device, while it stops in the center of the illuminated area when using the color indicator (Figure 24f). However, the apparent crossing of the front in the photonic device does not come from insufficient ability to stop the propagating pH front, but the disappearance of the photonic reflectance is caused by the ions released from the activated photoacid, which locally increase the ionic strength and decrease the swelling of the photonic crystal (Figure 21c). The effect of the ionic strength is already visible at early stages before the front reaches this area, as it causes a blue shift immediately after illumination (Figure 24e). Further neutralization of incoming ammonia then decreases the photonic band gap below visible wavelengths. Indeed there is no equivalent effect with bromocresol purple and the pH front stops in the center due to a balance of acid and base, and decreased activity of the enzyme in the acidified regime.

4.4 Conclusion

In summary, we demonstrated a first system integration of an out-of-equilibrium, biocatalytic pH-feedback system with a soft photonic display, featuring an additional light-control mechanism. Depending on the operating conditions of the urease switch, versatile new autonomous behaviors can be programmed, such as time-programmed self-erasing memories and photonic information patterning, pH-signal propagation with adjustable speeds and light sensing by remotely stopping propagating fronts with UV-light. These concepts can be expanded towards advanced sensory mechanisms, for soft matter logic and computation, or for advanced photonic displays. On a broader scale, we believe that these proof-of-concept examples combining non-linear chemistry with advanced responsive materials provide conceptual inspiration to challenge thinking towards other out-of-equilibrium material systems targeting active and autonomous behavior.

4.5 References

1. Mäthger, L. M.; Denton, E. J.; Marshall, N. J., Hanlon, R. T., *J. R. Soc., Interface* **2009,** *6,* 149-S163.
2. Hanlon, R. T.; Cooper, K. M.; Budelmann, B. U., Pappas, T. C., *Cell Tissue Res.* **1990,** *259,* 3-14.
3. Kinoshita, S.; Yoshioka, S., Kawagoe, K., *Proc. R. Soc. B* **2002,** *269,* 1417-1421.
4. Vukusic, P., Sambles, J. R., *Nature* **2003,** *424,* 852-855.
5. Vukusic, P.; Sambles, J. R.; Lawrence, C. R., Wootton, R. J., *Proc. R. Soc. B* **1999,** *266,* 1403-1403.

6. Hanlon, R. T.; Chiao, C. C.; Mäthger, L. M.; Barbosa, A.; Buresch, K. C., Chubb, C., *Philos. Trans. R. Soc., B* **2009,** *364*, 429-437.
7. Teyssier, J.; Saenko, S. V.; van der Marel, D., Milinkovitch, M. C., *Nat. Commun.* **2015,** *6*.
8. Stuart-Fox, D., Moussalli, A., *Philos. Trans. R. Soc., B* **2009,** *364*, 463-470.
9. Armstrong, E., O'Dwyer, C., *J. Mater. Chem. C* **2015,** *3*, 6109-6143.
10. Lee, J.-H.; Koh, C. Y.; Singer, J. P.; Jeon, S.-J.; Maldovan, M.; Stein, O., Thomas, E. L., *Adv. Mater.* **2014,** *26*, 532-569.
11. Arsenault, A. C.; Puzzo, D. P.; Manners, I., Ozin, G. A., *Nat. Photon.* **2007,** *1*, 468-472.
12. Lee, I.; Kim, D.; Kal, J.; Baek, H.; Kwak, D.; Go, D.; Kim, E.; Kang, C.; Chung, J.; Jang, Y.; Ji, S.; Joo, J., Kang, Y., *Adv. Mater.* **2010,** *22*, 4973-4977.
13. Park, T. J.; Hwang, S. K.; Park, S.; Cho, S. H.; Park, T. H.; Jeong, B.; Kang, H. S.; Ryu, D. Y.; Huh, J.; Thomas, E. L., Park, C., *ACS Nano* **2015,** *9*, 12158-12167.
14. Fan, Y.; Tang, S.; Thomas, E. L., Olsen, B. D., *ACS Nano* **2014,** *8*, 11467-11473.
15. Hong, W.; Chen, Y.; Feng, X.; Yan, Y.; Hu, X.; Zhao, B.; Zhang, F.; Zhang, D.; Xu, Z., Lai, Y., *Chem. Commun.* **2013,** *49*, 8229-8231.
16. Arsenault, A. C.; Clark, T. J.; von Freymann, G.; Cademartiri, L.; Sapienza, R.; Bertolotti, J.; Vekris, E.; Wong, S.; Kitaev, V.; Manners, I.; Wang, R. Z.; John, S.; Wiersma, D., Ozin, G. A., *Nat. Mater.* **2006,** *5*, 179-184.
17. Kang, D.-Y.; Lee, Y.; Cho, C.-Y., Moon, J. H., *Langmuir* **2012,** *28*, 7033-7038.
18. Varghese, L. T.; Xuan, Y.; Niu, B.; Fan, L.; Bermel, P., Qi, M., *Adv. Opt. Mater.* **2013,** *1*, 692-698.
19. Yang, L.; Ge, D.; Zhao, J.; Ding, Y.; Kong, X., Li, Y., *Sol. Energy Mater. Sol. Cells* **2012,** *100*, 251-257.
20. Kang, D.-Y.; Kim, S.-O.; Chae, Y. J.; Lee, J. K., Moon, J. H., *Langmuir* **2013,** *29*, 1192-1198.
21. Ge, J., Yin, Y., *Angew. Chem. Int. Ed.* **2011,** *50*, 1492-1522.
22. Aguirre, C. I.; Reguera, E., Stein, A., *Adv. Funct. Mater.* **2010,** *20*, 2565-2578.
23. von Freymann, G.; Kitaev, V.; Lotsch, B. V., Ozin, G. A., *Chem. Soc. Rev.* **2013,** *42*, 2528-2554.
24. Kobler, J.; Lotsch, B. V.; Ozin, G. A., Bein, T., *ACS Nano* **2009,** *3*, 1669-1676.
25. Lotsch, B. V., Ozin, G. A., *Adv. Mater.* **2008,** *20*, 4079-4084.
26. Valkama, S.; Kosonen, H.; Ruokolainen, J.; Haatainen, T.; Torkkeli, M.; Serimaa, R.; ten Brinke, G., Ikkala, O., *Nat. Mater.* **2004,** *3*, 872-876.
27. Kim, E.; Kang, C.; Baek, H.; Hwang, K.; Kwak, D.; Lee, E.; Kang, Y., Thomas, E. L., *Adv. Funct. Mater.* **2010,** *20*, 1728-1732.
28. Walish, J. J.; Fan, Y.; Centrone, A., Thomas, E. L., *Macromol. Rapid Commun.* **2012,** *33*, 1504-1509.
29. Kang, Y.; Walish, J. J.; Gorishnyy, T., Thomas, E. L., *Nat. Mater.* **2007,** *6*, 957-960.
30. Lim, H. S.; Lee, J.-H.; Walish, J. J., Thomas, E. L., *ACS Nano* **2012,** *6*, 8933-8939.
31. Heinen, L., Walther, A., *Soft Matter* **2015,** *11*, 7857-7866.
32. Heuser, T.; Steppert, A.-K.; Molano Lopez, C.; Zhu, B., Walther, A., *Nano Lett.* **2014**.
33. Heuser, T.; Weyandt, E., Walther, A., *Angew. Chem. Int. Ed.* **2015,** *54*, 13258-13262.
34. Hu, G.; Pojman, J. A.; Scott, S. K.; Wrobel, M. M., Taylor, A. F., *J. Phys. Chem. B* **2010,** *114*, 14059-14063.
35. Jee, E.; Bánsági, T.; Taylor, A. F., Pojman, J. A., *Angew. Chem. Int. Ed.* **2016,** *55*, 2127-2131.
36. Muzika, F.; Bansagi, T.; Schreiber, I.; Schreiberova, L., Taylor, A. F., *Chem. Commun.* **2014,** *50*, 11107-11109.
37. Wrobel, Magdalena M.; Bánsági, T., Jr.; Scott, Stephen K.; Taylor, Annette F.; Bounds,

Chris O.; Carranza, A., Pojman, John A., *Biophys. J.* **2012,** *103*, 610-615.
38. Starodoubtsev, S. G.; Khokhlov, A. R.; Sokolov, E. L., Chu, B., *Macromolecules* **1995,** *28*, 3930-3936.
39. Sasaki, S.; Koga, S.; Imabayashi, R., Maeda, H., *J. Phys. Chem. B* **2001,** *105*, 5852-5855.
40. Zaikin, A. N., Zhabotinsky, A. M., *Nature* **1970,** *225*, 535-&.
41. Epstein, I. R.; Vanag, V. K.; Balazs, A. C.; Kuksenok, O.; Dayal, P., Bhattacharya, A., *Acc. Chem. Res.* **2012,** *45*, 2160-2168.
42. Kovacs, K.; Leda, M.; Vanag, V. K., Epstein, I. R., *Phys. D* **2010,** *239*, 757-765.
43. Miguez, D. G.; Vanag, V. K., Epstein, I. R., *Proc. Natl. Acad. Sci. U. S. A.* **2007,** *104*, 6992-6997.
44. Padirac, A.; Fujii, T.; Estevez-Torres, A., Rondelez, Y., *J. Am. Chem. Soc.* **2013,** *135*, 14586-14592.
45. Techawanitchai, P.; Idota, N.; Uto, K.; Ebara, M., Aoyagi, T., *Sci. Technol. Adv. Mater.* **2012,** *13*.

5 Antagonistic Enzymes in a Biocatalytic pH Feedback System Program Autonomous DNA Hydrogel Life Cycles

submitted

5.1 Introduction

Biocatalysis is a key regulatory mechanism in biology empowering spatiotemporal self-organization of complex structures and functions, such as in metabolism, cell division and morphogenesis.[1, 2] Accordingly, biocatalytic reaction networks (BRN) constitute a powerful strategy to integrate advanced control mechanisms into self-assembling and soft matter systems. Enzymes being at the heart of these BRNs provide regulatory functions, that is positive feedback (autocatalysis, amplification) or negative feedback and inhibition, and can be coupled to energy dissipation by consumption of fuel molecules (co-factors, substrates).[3] These biocatalytic control mechanisms allow for installation of feedback loops, bistability, threshold sensing, memory, time-dependent states and operation outside equilibrium, thereby equipping classical soft matter materials with capacities for active, adaptive and autonomous behavior.[4-6]

Advantageously, enzymes operate under mild conditions and allow to induce self-assembly both under thermodynamic and kinetic control, which helps to build up more defect-free or temporary structures by site-specific reactions and selective tuning of reaction rates.[7] These benefits become even more obvious for mixtures of several enzymes, enabling the bottom-up construction of logic gates and oscillatory circuits by relatively simple man-made BRNs and cascades.[8-11]

In particular, the development of gel materials has benefited in the recent past from the increasing understanding of kinetic, feedback-driven and dissipative biocatalytic control, and brought about novel programmable gel topologies with emergent properties, such as autonomous and transient formation cycles, as well as adaptive, time-dependent mechanical properties.[5, 6] At this point, it is important to distinguish between enzymes that directly modify the molecular building blocks of the gel and those that modulate the environment to trigger gelation. Ulijn and co-workers demonstrated transient peptide gels under biocatalytic control using a single enzyme, α-chymotrypsin, which catalyzed the formation and the hydrolysis of a peptide hydrogelator in a coordinated fashion.[12, 13] Huck's group pursued a different strategy for programming complex hydrogel responses, and embedded the crosslinking chemistry of a polyacrylamide based hydrogel directly into a feedback-driven BRN with trypsin at its core, which resulted in programmable gel-sol-gel transitions.[14]

Focusing on the modulation of the surrounding, we recently introduced a platform concept to install kinetically controlled non-linear pH-profiles, and coupled those with a palette of pH-switchable self-assemblies to impart them with programmable lifetimes from minutes to days.[15-18] We described both transient alkaline and acidic pH profiles by combination of fast activators and dormant deactivators (DD). While activation of the systems was thus far instantaneous, using a fast activator (e.g. alkaline or acidic buffers), the deactivation was delayed by a time-dependent formation of an active deactivator i.e., the reverse pH stimulus, from a dormant species. System control has been advancing from chemical DDs to enzyme-catalyzed conversion of the DD (e.g. urea/urease switch), giving rise to autocatalytic behavior and advanced internal pH feedback systems (pH-IFS). On an application level, we could demonstrate self-erasing, micro-moldable peptide gels useful for microfluidic guidance and controlled release, as well as intelligent photonic displays featuring memories and remote light control.[16, 17]

Crucial advances in all of the above systems can be made with respect to controlling the autonomous behavior. Ideally one would be able to orthogonally program the lag time before a self-assembly (or material) forms as well as the lifetime of the following transient state. Taylor, Pojman and co-workers reported one of the first approaches, using slow, urease-catalyzed base formation from urea to control hydrogel formation via a base-assisted crosslinking.[19] Due to the presence of ester linkages, the polymer network degraded over time at alkaline conditions,

reverting the gel to the sol state. The system follows an irreversible pathway (A→B→C) and cannot be reactivated.

Additionally, progressing towards self-assembling materials that provide highest control over spatial structuring would enable new types of functional behavior based on precise molecular interactions. To this end, DNA hydrogels are promising owing to their high level of molecular programmability, inherent biocompatibility, diverse and orthogonal biochemical addressability, and interesting application prospects.[20, 21] The sequence-specific molecular programmability in combination with functional units (aptamers, DNAzymes, stimuli-responsive sequences) render DNA hydrogels useful for complex functional material responses, such as bio-sensing, drug release, mediating cell adhesion, and unusual mechanical behavior including reversible shape-memory effects.[22-26]

Herein, we demonstrate a significant advance in autonomous hydrogel materials and describe a DNA hydrogel system with a fully programmable temporal life cycle. To this end, we design a new type of biocatalytic pH internal feedback system (bio-pH-IFS) based on two antagonistic enzymes, that encodes the time signature of the transient pH-responsive DNA hydrogel. This bio-pH-IFS provides higher levels of system control by orthogonal programming of the timescale of the pH increase ("ON" signal) and pH decrease ("OFF" signal) of a transient alkaline pH profile. Upon integration with the pH-responsive DNA hydrogel, this allows the independent programming of the initial lag time and of the lifetime of the transient material state. We will first showcase precise temporal programming of the transient alkaline pH state using the BRN, and then proceed to the integrated system with the DNA hydrogel, leading to autonomous, time-controlled gel states with distinct programmable lag and lifetimes.

Scheme 4 displays the concept to achieve full temporal control over a transient self-assembling material state in alkaline conditions by coupling to a bio-pH-IFS which is composed of two counteracting enzymes forming the underlying BRN. The BRN serves as a non-linear pH modulator mastering the kinetic framework for a programmable transient alkaline pH state, and provides independent and selectively addressable activation (pH increase) and deactivation (pH decrease) signals. It is composed of urease from Canavalia ensiformis, catalyzing the formation of NH_3 and CO_2 from urea (activation, pH increase), and pig liver esterase, catalyzing the hydrolysis of ethyl acetate (EA) into ethanol and acetic acid (deactivation, pH decrease). The

BRN is fueled by its substrates, urea and EA, termed dormant activator (DA) and dormant deactivator (DD), respectively, because of the controllable formation rates (v_{DA} and v_{DD}) of the active pH species, OH^- and H^+.

This strategy allows to reach new levels of control compared to our previous transient pH systems[15-18], because we herein no longer use a directly available alkaline or acidic buffer for the pH jump (instantaneous activation), but extend the principle of dormant components to a programmable activation reaction (dormant activator). This enables advanced control over the timescales of activation, and ultimately provides lag times to the material system. The combination of both antagonistic enzymes into a single system leads to a complex non-linear pH modulation. Two main factors however permit to reach a programmable system with high levels of control (T = const.). First, due to the catalytic nature of both processes, it is relatively easy to selectively adjust the speeds of both reactions. Second, the pH-dependent activity profiles of both enzymes need to be known to understand how their reaction rates change during pH changes. While the urease shows maximum conversion at intermediate pH (bell-shaped profile), the esterase has a low reaction speed at low pH and an almost constant plateau at pH > 6 (Figure SI 8).

In light of the aforementioned principles, we hypothesized that it is possible to program transient pH profiles with distinct lag times ($t_{lag\ time}$) before a pH increase occurs, as well as the lifetimes of a transient alkaline pH milieu ($t_{lifetime,pH}$) until the pH ultimately drops again. Translated to the BRN and considering the start from an acidic pH regime, this implies that the urease reaction needs to be tuned to initially outrun the esterase reaction, while in long term the esterase reaction outweighs the urease, and is able to balance out the initial pH rise. Due to the pH-dependent activity curves, the urease features a beneficial, strong autocatalytic, self-reinforcing reaction (positive feedback), while the esterase shows a negative feedback when returning to the acidic regime.

Once the kinetic boundary conditions for the BRN ($v_{DA} >> v_{DD}$, $c_{DD} > c_{DA}$) are translated into controlled, transient, alkaline pH profiles, the latter can be coupled to pH-switchable self-assembling systems and materials to selectively control the timescales of the "ON" switching by a defined lag time and the "OFF" switching after a certain lifetime in an autonomous fashion without intervention from outside triggers. For analysis of the bio-pH-IFS, the transient pH

curves are quantified by their characteristic transitions in time (Scheme 4b). The timeline of the bio-pH-IFS starts with the "injection of the substrates", followed by a "lag time" after which the system is switched "ON" by a pH jump from the inactive, acidic to the active, alkaline state. When the pH returns to low pH, the system is switched "OFF" again. These "ON" and "OFF" signals are defined to the transition of pH 6, the later switching point of the DNA hydrogel (Figure SI 9). The "lifetime" is described by the time lapse between the "ON" (= lag time) and the "OFF" signal.

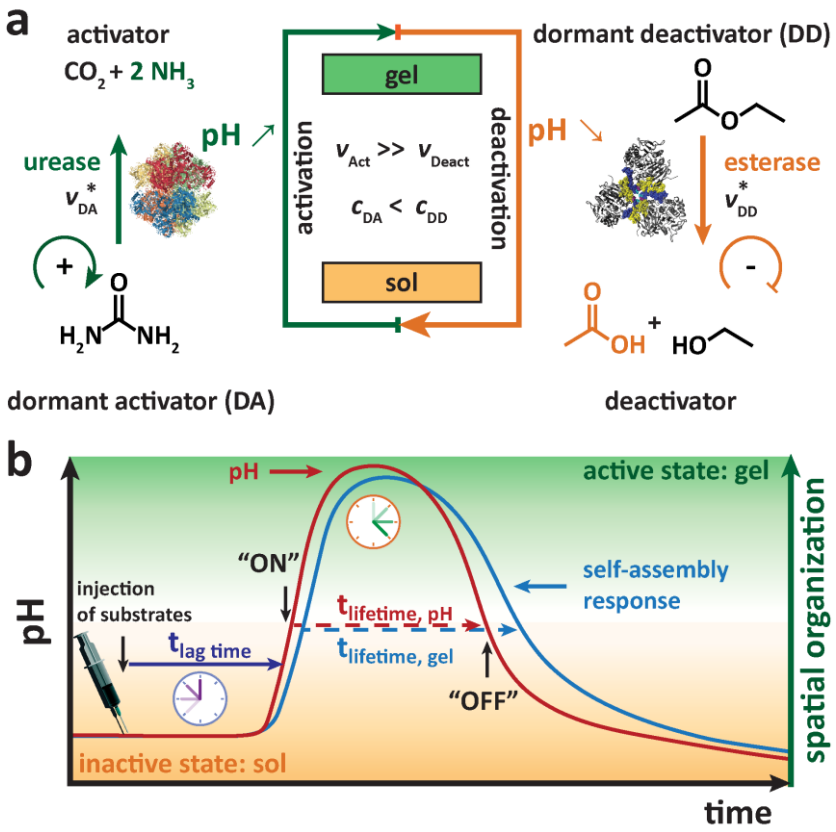

Scheme 4: Biocatalytic temporal control of a self-regulating transient pH-state by kinetic balancing of two antagonistic feedback-controlled enzymatic pH reactions. (a) BRN for internal pH modulation: The urease converts (v_{DA}) the dormant activator (DA, urea) to the active base amplified by autocatalytic positive feedback, while the antagonistic esterase transforms (v_{DD}) the dormant deactivator (DD, EA) to the active acid under negative feedback control (Figure SI8 for pH-dependent activity). (b) Schematic of the transient alkaline pH-profile (red) with an initial lag time as produced by the bio-pH-IFS in conjunction with the coupled self-assembly response (blue). The transient pH state is achieved by fulfilling the kinetic boundary condition $v_{DA} >> v_{DD}$, while having an ultimate excess of the DD. Initially, the system is static and then activated by simultaneous injection of the DA and the DD. Addition of an acidic buffer elongates the quasi-dormant period and implements an initial lag time to the system.

5.2 Experimental Section

Materials: All chemicals were purchased from Sigma-Aldrich unless otherwise stated: urease from *Canavalia ensiformis* (Jack bean, Type III, 15000-50000 units/g solid), esterase from porcine liver (≥ 15 units/g), bovine serum albumin (BSA, ≥ 95%), ethyl acetate (anhydrous, 99.8%), urea (ACS reagent), ethylenediaminetetraacetic acid disodium salt dihydrate (EDTA, CALBIOCHEM, biology grade), 2-morpholinoethanesulfonic acid (MES), sodium chloride (NaCl, 99%, ABCR), tris (hydroxymethyl)aminomethane hydrochloride (TRIS, Trizma Buffer substance pH 8.8 and pH 8.0), Trizma® base (≥99.8%), Trizma® hydrochloride (≥99.0%), 1.0 M hydrochloric acid solution (Fluka), 0.1 N hydrochloric acid (Merck), sodium hydroxide standard solution 0.999 N in H_2O (Fluka), 0.1 N sodium hydroxide (VWR), 4-nitrophenol (≥99%), 4-nitrophenyl acetate, citric acid monohydrate, trisodium citrate dihydrate (99.0%, Alfa Aesar), acetic acid, sodium acetate (99%), monosodium phosphate, sodium phosphate dibasic, ammonium persulfate (APS), N,N,N',N'- tetramethylethylenediamine (TEMED), acrylamide solution (40%), polyacrylamide.

Desalted oligonucleotides were supplied by Integrated DNA Technologies Inc. Sterile Milli-Q water with conductivity less than 0.055 mS/cm was used throughout all DNA experiments.

Table 1: Oligonucleotide sequences

ID	oligonucleotide sequence
1	5'-TC TAT TCG CAT GAG GAT CCA TTC ACC GTA CCC TAA CCC TAA CCC TAA CCC-3'
2	5'-TA CGG TGA ATG GAT CCT CAT GCG AAT AGA CCC TAA CCC TAA CCC TAA CCC-3'
3	5'-acrydite-TGT TAG TGT TAG TGT TAG-3'
4	5'-TGT TAG TGT TAG TGT TAG-3'

UV-Vis spectroscopy: UV-Vis spectra were collected on a Varian Cary 50 Bio UV/Visible spectrophotometer.

pH measurements: pH curves were recorded on a 12-channel pH-multimeter (EA Instruments LTD) and on a Titrando 905 titration unit in conjunction with a biotrode (Metrohm) for small volume measurements, respectively.

Rheometer: All rheological experiments were carried out on a Kinexus Pro rheometer (Malvern) using a 20 mm plate-plate geometry with a gap size of 0.25 mm (95 µL) and a DHR 3 rheometer (TA instruments) in conjunction with a 20 mm cone-plate (1°, 42 µL) geometry, respectively and at 23 °C in combination with a solvent trap, unless otherwise stated.

Programming of transient alkaline pH-profiles preceded by an initial lag time by a biocatalytic internal pH feedback system (bio-pH-IFS): The bio-pH-IFS system was prepared freshly on a daily basis in an aqueous solution with 0.5 gL^{-1} bovine serum albumin (BSA) and varying amounts of urease, esterase and an acetate buffer stock solution in accordance to the desired time-programmed pH profile. With regard to the subsequent coupling to the DNA hydrogel, the solution also contained 100 mM NaCl, 0.1 mM TRIS, 0.1 mM EDTA. The acetate buffer stock solution was prepared with a constant volume ratio of sodium acetate (1M) to acetic acid (1M), NaOAc/HOAc = 3.7 mL / 6.3 mL. The pH of the bio-pH-IFS solution, containing different amounts of the acetate buffer (0 – 40 mM) was precisely adjusted to pH 4.5 using $NaOH_{(aq)}$ and $HCl_{(aq)}$ (1 M) before activation of the system by simultaneous injection of calculated amounts of urea (from 5 M stock) and ethyl acetate. The substrate concentrations in the final bio-pH-IFS solution were kept constant throughout all experiments with 240 mM urea and 60 mM ethyl acetate. Each pH curve is the average data of at least three measurements.

Esterase activity assay in dependence of pH: The pH-dependent esterase activity was monitored in a colorimetric assay of the hydrolysis of 4-nitrophenyl acetate within the range of pH = 4 - 10 in buffered solutions. Hydrolysis of 4-nitrophenyl acetate results in the release of acetic acid and 4-nitrophenol. The kinetic UV-Vis assay was evaluated at the wavelength of 348 nm, which is the isosbestic point (pH-independent absorbance) of nitrophenol. For a constant pH throughout the measurements, the assay was performed in the presence of 100 mM buffer of respective pH (buffer composition, see Table 2). The assay was conducted at an enzyme concentration of 0.01 gL^{-1} esterase for four different substrate concentrations, 0.01 mM, 0.05 mM, 0.10 mM and 0.25 mM of 4-nitrophenyl acetate. V_{max} was determined from Lineweaver-Burk plots.

Table 2: Composition of the buffer substances utilized during the kinetic esterase activity assay.

All buffers were diluted to give a final concentration of Trizma HCl/base, Na_2HPO_4/NaH_2PO_4, citric acid/ trisodium citrate dihydrate = 0.1 M.

pH	Trizma base [gL^{-1}]	Trizma HCl [gL^{-1}]	0.5 M Na_2HPO_4 [mL]	0.5 M NaH_2PO_4 [mL]	0.5 M citric acid [mL]	0.5 M trisodium citrate dihydrate [mL]
9	8.78	1.22				
8			9.47	0.53		
7			6.1	3.9		
6			1.23	8.77		
5					3.5	6.5
4					5.9	4.1

Synthesis of poly(acrylamide-co-DNA): First, the acrydite-functionalized oligonucleotide (**3**) was dissolved in 10 mM TRIS buffer (pH 8) to give a 2 mM stock solution. Then, a monomer solution with 2 wt% acrylamide and 1 mM acrydite-functionalized oligonucleotide (**3**) was prepared by mixing the corresponding stock solutions with 10 mM TRIS buffer (pH 8) to a final reaction volume of 860 µL. In parallel, 25 µL TEMED and 50 mg APS were dissolved in 500 µL sterile Milli-Q water to obtain the catalyst/initiator solution. Nitrogen was bubbled through both solutions. The polymerization reaction was initiated by addition of 17.2 µL APS/TEMED solution to the monomer mixture. After 5 min of polymerization at room temperature, the reaction tube was transferred to the refrigerator, where polymerization was continued for 16 h at 4 °C. Finally, the copolymer was purified by spin filtration using 30 kDa Amicon Ultra Centrifugal Filters and redispersion in water until the filtrate was free of DNA. The ratio of copolymerized DNA was determined by UV-Vis spectroscopy (see Figure SI7) The purified copolymer was dried under a gentle flow of nitrogen gas. Lastly, the copolymer was redissolved in an aqueous solution containing 100 mM NaCl, 0.1 mM EDTA and 0.1 mM TRIS pH 8.8 to give a mass content of 2 wt% of copolymer in solution.

Determination of DNA content in poly(acrylamide-co-DNA) by UV-VIS spectroscopy: The molar ratio of acrylamide to oligonucleotide (**3**) repeating units in the copolymer was determined by UV-Vis. To this end, a calibration curve was constructed by analyzing absorption spectra of different aqueous solutions containing 1 µM oligonucleotide (**3**) and varying amounts of polyacrylamide corresponding to 10 µM, 20 µM, 40 µM, 75 µM, 100 µM,

200 µM, 300 µM, 400 µM, 500 µM, 600 µM of acrylamide (AAm) monomer units. Absorption was read at 200 nm for the polymerized acrylamide unit and at 260 nm for the oligonucleotide. The absorption ratio A200/A260 was plotted against the corresponding concentration ratio of acrylamide/oligonucleotide (**3**) and the calibration curve based on linear regression yields a molar ratio of 301/1 of acrylamide to oligonucleotide sequences for the synthesized copolymer.

Hybridization of double i-motif crosslinker: Stock solutions (1 mM) of the oligonucleotide sequences (**1**) and (**2**) of the crosslinker unit were initially prepared by dissolving each DNA strand separately in sterile Milli-Q water with 100 mM NaCl, 0.1 mM EDTA and 0.1 mM TRIS pH 8.8. The double i-motif crosslinker was then formed by annealing equimolar amounts of sequence (**1**) and (**2**) by a slow cooling program from 90 °C to 20 °C in about 2.5 hours. The final molar concentration of the hybridized double i-motif crosslinker was 0.5 mM which corresponds to a mass content of 1.5 wt% in solution.

Preparation of the hybrid DNA hydrogel: The hydrogel (1.8 wt%) was formed by mixing the solution of the copolymer with the solution of the double i-motif crosslinker while keeping a stoichiometric ratio of the complementary sequences (0.4 mM) in the copolymer and the i-motif overhang sequences of the duplex crosslinker (0.2 mM, the linker contains two i-motif overhangs). The pH of the hydrogel was adjusted either by 1 M TRIS to pH 8 or by 1 M MES to pH 5 for characterization of the gel and the sol state under static pH conditions, respectively.

Rheological characterization of the DNA hydrogel at different static pH conditions and in response to temperature: Mechanical properties of the DNA hydrogel (1.8 wt%) were characterized in the sol state at pH 5 and in the gel state at pH 8.5 after equilibration under static pH conditions at 20 °C, using a cone-plate geometry (40 mm, 1 °) and a sample volume of 350 µL (gap size 0.03 mm). Oscillatory amplitude sweep (1 Hz, 0.1 to 10 % strain) and oscillatory frequency sweep (1 % strain, 0.1 to 10 Hz) tests were performed beforehand to ensure characterization within the linear viscoelastic region. Accordingly, oscillatory amplitude sweep test were carried out at 1 Hz and oscillatory frequency sweep tests at 1 % strain. The thermal melting transition of the gel was analyzed at pH 8.5 with a temperature ramp cycling two times from 20 °C to 40 °C to 20 °C applying oscillatory amplitude sweep experiments at each temperature with requested strains: 0.10 %, 0.20 %, 0.29 %, 0.43 %, 0.63 %, 0.93 % to 1.00 % at 1 Hz frequency.

Internal pH-curve of bio-pH-IFS coupled to the DNA system: Time-resolved pH curves of the

bio-pH-IFS in presence of the DNA sequences with concentrations analogous to the DNA hydrogel were recorded using free oligonucleotide sequences of (**1**), (**2**) and (**4**) without the polymer matrix to preclude invalid, diffusion-limited pH measurements in the gel state. All samples were prepared from stock solutions with 100 mM NaCl, 0.1 mM EDTA and 0.1 mM TRIS. First, the enzymes urease and esterase in conjunction with BSA were freshly predissolved altogether in a 2x stock solution, whereas the oligonucleotides were added from 2 mM stocks, respectively. Each sample was then prepared from these stock solutions to give a total volume of 150 µL with final concentrations of DNA sequences corresponding to the DNA hydrogel (for a 1.8 wt% gel: 0.2 mM of (**1)** and (**2)**, 0.4 mM of (**4)**) and 0.6 gL^{-1} urease, 0.5 gL^{-1} esterase, 0.5 gL^{-1} BSA and varying amounts of acetate buffer. The lag time was programmed by variation of the acetate buffer concentration between 0 mM and 40 mM. After precise adjustment of the starting pH to 4.5 with $NaOH_{(aq)}$ and $HCl_{(aq)}$ (1M), the bio-pH-IFS system was activated by simultaneous injection of the substrates urea (60 mM, added from 2.5 M stock in water) and ethyl acetate (240 mM). Substrate concentrations refer to the initial sample volume of 150 µL.

Temporal programming of the DNA hydrogel by the bio-pH-IFS with control of the initial lag time: The bio-pH-IFS-driven DNA hydrogel was prepared from a 4 wt% copolymer solution, 3 wt% double i-motif crosslinker solution, 2.2x enzyme stock (containing 1.32 gL^{-1} urease, 1.1 gL^{-1} esterase and 1.1 gL^{-1} BSA), and 1 M acetate buffer. All stock solutions were prepared in 100 mM NaCl, 0.1 mM EDTA and 0.1 mM TRIS. The resulting mixture contained 1.8 wt% of DNA hydrogel (copolymer + i-motif linker) and a bio-pH-IFS of 0.6 gL^{-1} urease, 0.5 gL^{-1} esterase, 0.5 gL^{-1} BSA. Temporal programming of the lag time before gelation was achieved by variation of the acetate buffer concentration from 0 mM to 40 mM. The pH of the mixture was adjusted to 4.5 with $NaOH_{(aq)}$ and $HCl_{(aq)}$ (1M) just prior to activation of the system by simultaneous injection of urea (60 mM, from 2.5 M stock in water) and ethyl acetate (240 mM) as substrates to the reaction mixture.

Determination of the initial lag time prior to transient gelation by rheology: The time-programmed DNA hydrogel containing the bio-pH-IFS was prepared as described above. The activated system was immediately transferred to the rheometer and gelation was monitored by oscillatory time sweep experiments at 1 Hz and 1 % strain. The lag time prior to gelation was evaluated to the point where the storage modulus G′ reached half of its plateau value. Return to the sol state could not be recorded due the open atmosphere of the rheometer set-up, with

uncontrollable release of volatiles (NH_3, CO_2, EA).

Tube inversion test with transient entrapment of a magnetic bead for lifetime determination of the transient gelation by video analysis: The time-programed DNA hydrogel containing the bio-pH-IFS was prepared as described above. Additionally, a small magnetic bead was added as a probe to monitor gelation and the plastic vial was immediately closed afterwards. Gelation of the sample was tested by bead actuation using an external magnet (NdFeB, from supermagnete, Germany, model type: S-20-02-N) in 5 min intervals. When the magnetic bead did not move any more (= initial lag time), the tube was inverted with the entrapped bead. The bead stays locked in place as long as the gel is solid and only begins to move when the gel disintegrates again. The lifetime of the gel was determined by video analysis to the point when the bead fell to half distance of the DNA solution volume. Due to capillary forces and the small volume, the liquid DNA solution does not run down the plastic tube.

5.3 Results and Discussion

Figure 25 demonstrates details on the temporal programming of the transient alkaline pH profiles. After initial screening experiments, we chose an enzyme ratio of urease/esterase = 3/1 (w/w), which satisfies the kinetic requirement of faster base than acid production ($v_{DA} >> v_{DD}$). Beneficially, urease exhibits naturally a much higher activity than esterase, which facilitates installation of the kinetic boundary condition. The starting pH is adjusted to pH 4.5 in 10 mM acetate buffer with both enzymes present and then activated by simultaneous addition of both fuel substrates, urea (DA) and EA (DD). The substrate concentrations are set to 60 mM urea and 240 mM EA for all experiments. The excess of the DD (EA) ensures ultimate deactivation to the acidic "OFF"-state. At this low starting pH, both enzymes are almost inactive (see Figure SI 8) keeping the complete system initially in a quasi-dormant mode with very low turnover. However, due to the bell-shaped pH-activity profile of urease with a maximum turnover rate at around pH 7,[27] the urea/urease reaction self-accelerates more strongly upon base production, and a steep pH jump from pH 4.5 to ca. pH 8.5 is achieved within minutes by positive feedback amplification. The upper alkaline pH of the system is limited to ca. pH 9 due to formation of an ammonium buffer. Once the DA (urea) is sufficiently consumed, the esterase becomes dominant, being itself highly active at this alkaline pH, and regulates the return to the acidic regime by excess formation of acetic acid from the DD. The pH decay takes longer compared to the pH increase and slows down with time, visible by a reduced slope in the transient pH

profiles after around pH 6.5. This is due to the fact that the esterase leaves its high activity window owing to its self-deactivating acid production (negative feedback). Finally, the pH levels off at around pH 4.75 in the buffer region of the acetate.

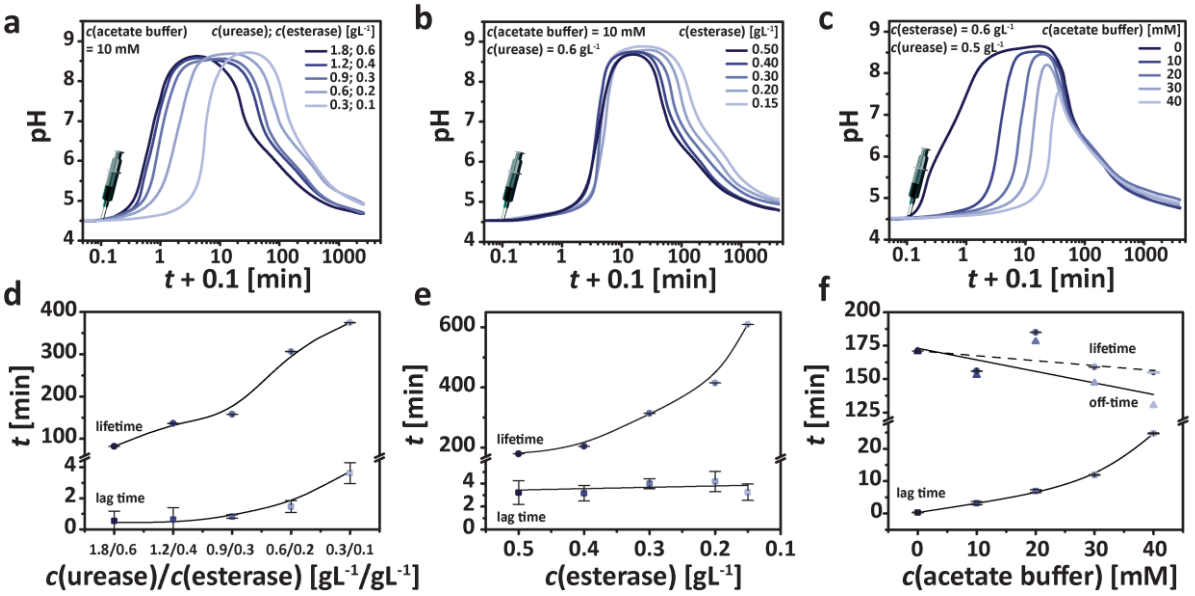

Figure 25: Temporal programming of the lag time and the lifetime of transient alkaline pH-states under biocatalytic control. (a) Symmetric decrease of the enzyme concentrations at a constant ratio of urease/esterase = 3/1 (w/w) results in a delayed onset and longer lifetimes of the transient alkaline state. (b) The esterase concentration controls the lifetime of the transient pH-state at *c*(urease) = 0.6 gL^{-1} = const. (c) The concentration of acetate buffer regulates the initial lag time; *c*(urease) = 0.6 gL^{-1}, *c*(esterase) = 0.5 gL^{-1}. (d-f) Corresponding lag times and lifetimes of the pH curves analyzed with respect to pH 6. The "OFF"-time is shown in (f) to demonstrate orthogonal programming of the "ON" and "OFF" timescales. Experimental conditions: 60 mM urea, 240 mM EA, 10 mM sodium acetate buffer, 0.5 gL^{-1} BSA, and $pH_{initial}$ 4.5. The solutions contain 0.1 mM TRIS, 0.1 mM EDTA, 100 mM NaCl with regard to later coupling to the DNA hydrogel.

To demonstrate the elegant biocatalytic control of the bio-pH-IFS, we showcase two characteristic ways to orchestrate the time signature of the temporal pH profile by changing only the concentrations of the two enzymes in the BRN. First, a symmetric reduction of the overall enzyme concentrations at a constant *c*(urease)/*c*(esterase) ratio simultaneously decreases the turnover numbers of both biocatalytic reactions. These slower kinetics shift the onset of the pH increase to slightly higher timescales, and extend the lifetime of the alkaline pH state substantially (Figure 25 a, d). For instance, the time of the "ON" (lag time) and the "OFF" signal (lag time + lifetime) are less than 1 min and 2 h, respectively, for the highest enzyme

pair concentration *c*(urease)/*c*(esterase) = 1.8 gL^{-1}/0.6 gL^{-1}. This extends to 5 min and 6 h for the lowest concentration *c*(urease)/*c*(esterase) = 0.3 gL^{-1}/0.1 gL^{-1}. Second, an increase of the esterase concentration from 0.15 gL^{-1} to 0.5 gL^{-1} at a constant c(urease) = 0.6 gL^{-1} (otherwise unchanged system parameters) speeds up the formation of the deactivator and gradually reduces the lifetime from 10 to 3 hours without altering the prior lag time (Figure 25 b, e). Consequently, the bio-pH-IFS permits individual programming of the "ON" and the "OFF" signal.

The decisive way to increase control over the lag time is as follows. The lag time of the system is mainly determined by the activity state of the enzymes, in particular, of the autocatalytic urease reaction (pH-activity profile of urease and esterase in Figure SI 8). A simple, yet efficient way to keep both enzymes in their low activity state (pH < 4.5) is to delay the pH increase by providing an acidic buffer. The buffer scavenges the formed NH_3 (dominant reaction; autocatalytic urease) and maintains the system in a quasi-dormant state until the buffer capacity is used up. Subsequently, the urease reaction enters its self-accelerating state and switches the system "ON" to alkaline pH. Temporal programmability of the initial lag time for an overall enzyme concentration of *c*(urease)/*c*(esterase) = 0.6 gL^{-1}/0.5 gL^{-1} as function of an acetate buffer concentration is shown in Figure 25 c, f. In absence of any buffer, the pH increases immediately in less than 30 s to pH 6. However, an increase of the acetate buffer to 40 mM elongates the lag time up to 25 min. The pH returns to the "OFF"-state after ca. 2.6 h for all systems independent of the lag time, implying slightly shortened lifetimes by the period of the respective lag time (Figure 25 f).

After having demonstrated the crucial capabilities of the bio-pH-IFS for temporal precision programming of autonomous pH-cycles, we will showcase its use to program the start and end point of the transient gelation of a DNA hydrogel in a closed system. We chose the i-motif, a pH-dependent DNA secondary structure, as pH-switchable crosslinking unit in polymer-based DNA hybrid hydrogels. The i-motif forms at slightly acidic pH from a cytosine-rich sequence, that folds upon partial protonation of the cytosine bases into a compact tetraplex due to intercalation of hemi-protonated cytosine^{+}-H-cytosine base pairs. i-motif-based DNA hydrogels are in principal known and have shown great promise for shape-memory materials.[22, 23, 28-31] However, such previous i-motif-based DNA hydrogels were designed to typically gel at acidic pH *via* intermolecularly folded i-motif structures. This is not applicable for our

conditions, and, therefore, we conceived a new type of a pH-sensitivee DNA hybrid hydrogel able to undergo gelation at alkaline pH.

Our i-motif DNA hybrid hydrogel is assembled from two components: (i) a DNA-containing polyacrylamide (PAAm) copolymer and (ii) separate mobile DNA double i-motif duplex crosslinkers. The i-motif crosslinkers are formed from two oligonucleotides, **1** and **2,** that partially hybridize into a duplex (blue) with a single-stranded 5′-end overhang at each side featuring the i-motif sequence (green, Figure 26 a). The pH-sensitive DNA i-motif switch is the central crosslinking element and is provided by these i-motif overhangs and their complementary sequence partners (red, **3),** which are copolymerized into the PAAm chains. The PAAm copolymer is synthesized by free radical copolymerization of acrylamide with the acrydite-functionalized oligonucleotide **3** (red, Figure 26 a). The molar incorporation efficiency of **3** amounts to 1/300 per acrylamide unit as determined by UV-Vis spectroscopy (Figure SI 7). On the hydrogel level, the i-motif duplex crosslinkers self-protect at low pH due to formation of the folded (unreactive) i-motif tetraplex, leading to a liquid sol state (Figure 26 a, bottom). Above the pH switching point of the i-motif (ca. pH 6, see Figure SI 9), the tetraplex ends of the DNA duplex linker unfold, and induce crosslinking to the gel state by hybridization with the copolymerized strand **3** (Figure 26 a, top). Thus, the i-motif overhang of the mobileDNA duplex linker functions as pH-dependent sticky end and imposes the pH-dependent gelation behavior on the hybrid DNA hydrogel. All of the following gels are prepared with a stoichiometric ratio between the copolymerized complementary strands and the i-motif sequences at a total mass content of 1.8 wt%.

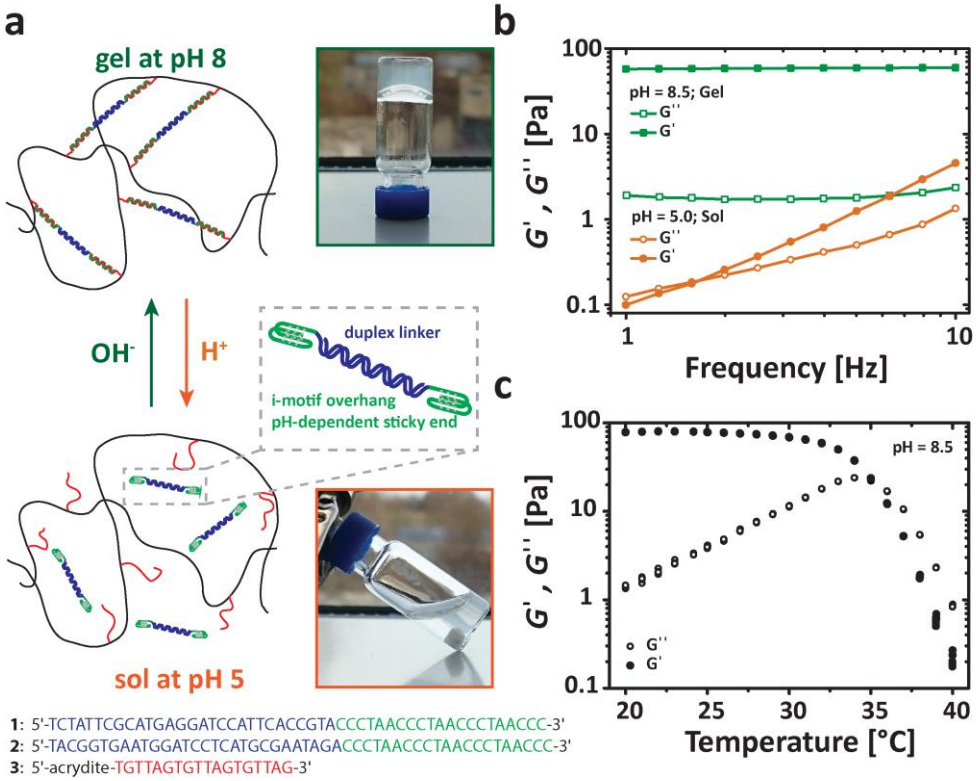

Figure 26: Rheological characterization illustrating the pH-responsiveness of the DNA hybrid hydrogel based on the pH-sensitive i-motif switch crosslink. (a) Illustration of the pH-induced transition between sol (bottom, pH 5) and gel (top, pH 8) below the melting temperature of the i-motif switch along with the corresponding photographs. The double i-motif duplex crosslinkers (inset shows close-up: sequences 1 and 2 are color-coded blue for the self-complementary duplex and green for the pH-sensitive i-motif overhang) allow crosslinking of the gel by hybridization with the copolymerized oligonucleotides (3, red) in the polyacrylamide matrix only at alkaline pH when the i-motif overhang (green) is unfolded. (b) Frequency sweep tests of the DNA hydrogel at a constant strain of 1 % at pH 5 and pH 8.5 show the characteristic viscoelastic properties (storage modulus G′, loss modulus G″) of the sol (orange) and the gel state (green) at 20 °C. (c) Temperature-dependent amplitude sweep tests at 1 Hz for various strains between 0.10 % and 1.00 % at pH 8.5. The temperature-induced gel/sol transition can be identified by a clear crossover at around 35 °C, which is induced by the melting of the i-motif switch crosslink (i.e. dehybridization).

The responsiveness of the DNA hydrogel is confirmed by rheology within the linear viscoelastic region (Figure 26). Frequency sweep experiments under acidic and alkaline conditions clearly distinguish the sol and gel state (Figure 26 b). For the sol state at pH 5, a frequency-dependent crossover from the storage modulus G' over the loss modulus G'' is observed, which is typical of polymer solutions. By contrast, the gel state at pH 8.5 displays

dominant elastic properties throughout the whole frequency spectrum with a storage modulus G' constantly higher than the loss modulus G''. Furthermore, temperature-dependent measurements at pH 8.5 reveal a clear gel/sol transition with a distinct crossover of G' and G'' at around 35 °C. This correlates to the melting temperature of the i-motif/complementary strand duplex[32] and confirms that the gel state is indeed formed through duplex hybridization (Figure 26 c).

In the next step, we couple the bio-pH-IFS to the pH-sensitive DNA hydrogel to address autonomously controlled hydrogels with programmable lag times and lifetimes. Since the introduction of the lag time is the key advance of this antagonistic DA and DD approach, we focus on the programmability of the initial lag time to delay purposefully the starting point ("ON" signal) of the transient gelation of our DNA hydrogel, while maintaining similar lifetimes. Therefore, enzyme and substrate concentrations remain unchanged during the following experiments, and only the acetate buffer concentration is varied as a control handle for tuning the length of the initial lag time (see Figure 25 c, f).

We assemble the copolymer and the i-motif DNA duplex linkers together with both enzymes of the bio-pH-IFS (0.5 gL^{-1} urease and 0.6 gL^{-1} esterase) in a buffer system (100 mM NaCl, 0.1 mM EDTA, 0.1 mM TRIS, 0.5 gL^{-1} BSA) at pH 4.5. The varying parameter will be the concentration of the acetate buffer. The system is subsequently initiated by simultaneous addition of both substrates, urea (60 mM) and EA (240 mM), which drive the BRN and thereby the DNA hydrogel. The snapshot series in Figure 27a depicts a typical experiment at 20 mM acetate buffer. Therein, the actuation of an entrapped magnetic bead serves as an optical control for the sol/gel transition to probe the lag time, while the tube inversion test with concomitant falling of the entrapped bead serves as the lifetime indicator of the gel/sol transition. Initially, the magnetic bead is mobile in the solution and can be easily lifted by an external magnet. However, after ca. 20 min the bead is trapped in the gel network at the bottom of the tube, referred to as $t_{\text{lag time, video}}$ later on. After inversion of the tube the bead stays locked in position until ca. 17.50 h, whereafter it continuously falls down due to weakening of the gel strength and complete transition to the sol state. The gel/sol transition is evaluated for when the bead reaches half of the gel height (= "OFF"-state at 17.75 h, Figure 27) Subtraction of the lag time (20 min) yields a lifetime of ca. 17.4 h, $t_{\text{lifetime, video}}$. Due to the small volume (150 µL), capillary forces and interface pinning prevent the liquid polymer solution from running down to the bottom of the tube. However, the magnetic bead is completely mobile again.

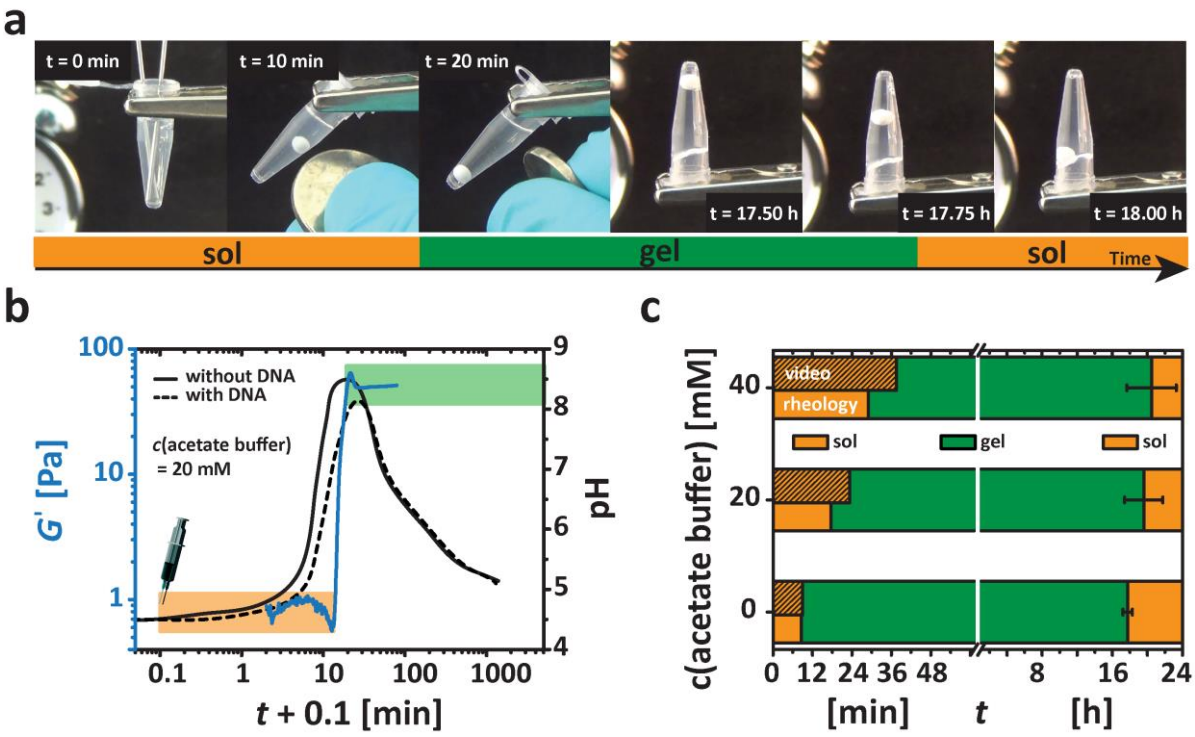

Figure 27: Temporal programming of the transient life cycle of autonomous DNA hydrogels with a tunable lag time controlled by the amount of the acetate buffer. (a) Snapshot series of a system with 20 mM acetate buffer. The DNA-polymer solution gels within ca. 20 min (= lag time) after injection of the substrates. The gel lifetime is ca. 17.4 h as determined with the falling ball method at half maximum height. The system returns to the fully liquid sol state after 18 h. (b) Rheological determination of the lag time by monitoring the development of G′ for a system with 20 mM acetate buffer. The pH curves of the pristine bio-pH-IFS (black line) and in presence of equivalent amounts of DNA sequences (dashed line) are shown for comparison. (c) Sol-gel-sol plots illustrate programmable lag times as a function of the acetate buffer concentration with similar lifetimes of the gel state (green). The lag time was evaluated both from rheology (left orange bars) at 50% maximum of final G′ and from videos of the entrapped magnetic bead (left shaded orange bars). All solutions contain 1.8 wt% of the DNA hydrogel components, 0.5 gL^{-1} urease, 0.6 gL^{-1} esterase, 0.5 gL^{-1} BSA, 100 mM NaCl, 0.1 mM EDTA, 0.1 mM TRIS buffer, and were adjusted to pH = 4.5 before being activated by 60 mM urea and 240 mM EA (23 °C).

The timescales and the internal control mechanism for the autonomously driven transient gelation can be rationalized by looking at the corresponding pH curves generated by the bio-pH-IFS. The pristine bio-pH-IFS with 20 mM acetate buffer produces an initial lag time of around

5 min (Figure 27 b, solid black line) before reaching pH 6, which is the switching point of the i-motif. In presence of the DNA sequences, this lag time elongates to 8 min due to protonation of the nucleotides serving as a load in the integrated system (Figure 27 b, dashed curve). The macroscopic DNA hydrogel state (sol/gel transition) responds to this dynamic pH change with a more distinct delay and can be followed precisely via the time-dependent development of the storage modulus, which jumps from initially ca. 1 Pa (sol) to ca. 60 Pa (gel) after 20 min ($t_{\text{lag time, rheo}}$; Figure 27 b, blue curve). Herein, we define the lag time to the point where G' reaches half of its plateau value. Unfortunately, rheology only offers to precisely determine the lag times, because prolonged experiments to measure full lifetime cycles are not feasible due to the small volumes and multiple and partly volatile components (CO_2, NH_3, EA). For reproducible lifetime cycles it is important to work in fully closed systems. Therefore, all lifetimes are evaluated from video sequences of the tube inversion tests. Notably, the gel lifetimes clearly extend beyond the "OFF" signal of the pH curves as a result of kinetic entrapment, by counter ion and crowding effects. However, this does not affect reproducibility of the obtained lifetimes. Figure 27 c quantifies the desired programmability of the initial lag time as a function of the acetate buffer concentration by time-resolved sol-gel-sol plots. The unbuffered system Figure 27 c, bottom) shows only a very short lag time of ca. 9 min compared to not even 1 min in the pristine pH feedback system (Figure 25). The delay stems from the intrinsic buffer capacity of the DNA nucleotides, and the time-dependent gelation process. Increasing the buffer concentration to 40 mM delays the point of gelation (Figure 27 c, left orange bar) further to ca. 30 min, because the enzymes are kept longer in their low activity state at acidic pH by the increased buffer capacity. Buffer concentrations higher than 40 mM are detrimental to gelation due to the decreasing pH jump height, which is insufficient for triggering the i-motif switch crosslink. The lag times derived from the actuation of the bead (Figure 27 c, $t_{\text{lag time, video}}$, shaded orange bar) are slightly larger than the values from rheology ($t_{\text{lag time, rheo}}$, left orange bar), but follow the same linear trend. Importantly, the lifetimes of the gel (green bar) are hardly affected by the buffer concentration. Only a slight increase from around 17 to 19 hours (ca. 10 %) can be detected. This is an important feature as it demonstrates the ability to orthogonally program both the "ON" and the "OFF" switching of the gel state (see also Figure 26).

5.4 Conclusion

In summary, we demonstrated the first example of a pH-responsive DNA hydrogel with a fully programmable autonomous life cycle empowered by an antagonistic enzyme pair in a BRN.

The BRN enables precise and selective internal temporal control over the initial lag time and the lifetime of the temporary gel state. It uses two counteracting pH-modulating enzymes to install non-linear, feedback-controlled transient alkaline pH profiles (bio-pH-IFS). The enzymes control the formation rates of base and acid in a time-controlled fashion, and allow elegant control via their concentrations and added buffers. The buffer capacity is the main parameter to control the initial lag time by keeping both enzymes in a low activity state and by scavenging pH modulating products, whereas variations in the enzyme concentrations are decisive in changing the lifetime.

Upon coupling the DNA hydrogel with the bio-pH-IFS, the material state develops on a programmable pathway after injection of the fuel substrates in full autonomy. Our time-programmed hydrogel system promises good biocompatibility and facile incorporation of other functional nucleic acids and bioactive compounds. Taken together, the programmable lag time with the temporary gelation time render this transient DNA hydrogel interesting as injectable biomaterial for time-controlled release, as temporary sealant or adhesive in biomedical applications. Reversible shape memory could broaden its functionality further. Additionally, the bio-pH-IFS offers opportunities beyond driving autonomous hydrogels. The programmable lag time may allow remote reaction control and is particularly attractive for studying self-assembly phenomena by in-situ methods in closed analytical systems.

5.5 Supporting Information

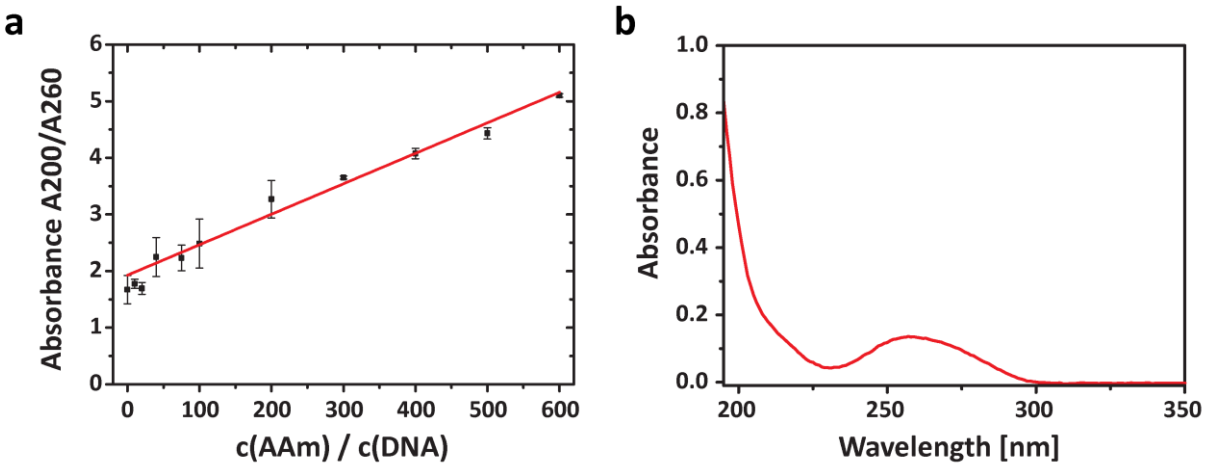

Figure SI 7: Determination of the DNA content in poly(acrylamide-co-DNA) by UV-Vis

spectroscopy. (a) Calibration line given by the ratio of absorbance read at 200 nm and 260 nm representative for the polyacrylamide and oligonucleotide repeating units in dependence of different concentration ratios. (b) UV-Vis spectrum of the synthesized copolymer.

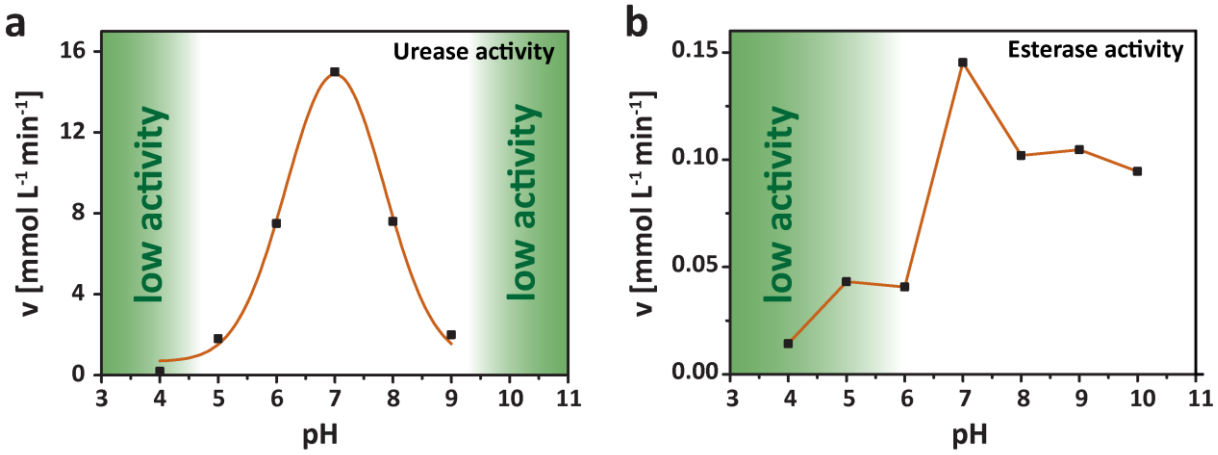

Figure SI 8: pH-dependent enzyme activities: (a) 0.1 gL^{-1} urease (adapted from Ref[27]) and (b) 0.01 gL^{-1} esterase.

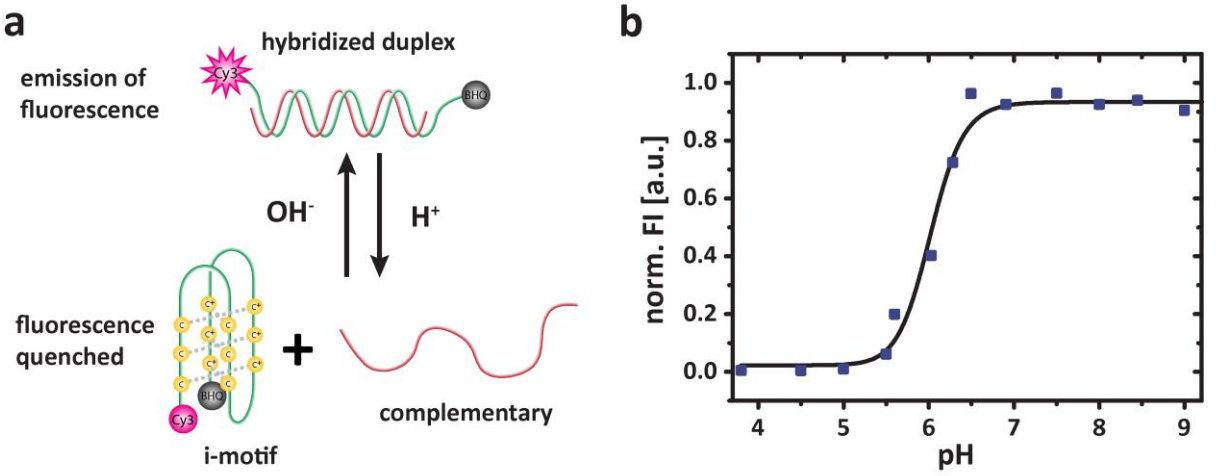

Figure SI 9: i-motif switch transition as determined by pH-dependent fluorescence spectroscopy (adapted from Ref[33]): (a) Schematic illustration of the two conformational states of the i-motif switch in dependence of pH. The i-motif sequence is labeled with the pH-insensitive Cy3 fluorophore at the 5′-end and the Black Hole Quencher 2 at the 3′-end. At low pH, fluorescence emission is completely

quenched due to the close proximity of the fluorophore/quencher pair in the folded i-motif tetraplex. Upon pH increase the i-motif tetraplex unfolds and hybridizes with the complementary strand, which leads to the spatial separation of the fluorophore/quencher pair and fluorescence emission. (b) The i-motif switch shows a transition midpoint at ca. pH 6, c(i-motif switch) = 0.5 μM, $\lambda_{exc.}$ = 520 nm, $\lambda_{em.}$ = 564 nm.

5.6 References

1. Bray, D., *Nature* **1995,** *376*, 307-312.
2. Kholodenko, B. N., *Nat. Rev. Mol. Cell Biol.* **2006,** *7*, 165-176.
3. Lim, W. A.; Lee, C. M., Tang, C., *Mol. Cell* **2013,** *49*, 202-212.
4. van Roekel, H. W.; Rosier, B. J.; Meijer, L. H.; Hilbers, P. A.; Markvoort, A. J.; Huck, W. T., de Greef, T. F., *Chem. Soc. Rev.* **2015,** *44*, 7465-7483.
5. Heinen, L., Walther, A., *Soft Matter* **2015,** *11*, 7857-7866.
6. Merindol, R., Walther, A., *Chem. Soc. Rev.* **2017**.
7. Hirst, A. R.; Roy, S.; Arora, M.; Das, A. K.; Hodson, N.; Murray, P.; Marshall, S.; Javid, N.; Sefcik, J.; Boekhoven, J.; van Esch, J. H.; Santabarbara, S.; Hunt, N. T., Ulijn, R. V., *Nat. Chem.* **2010,** *2*, 1089-1094.
8. Amir, L.; Tam, T. K.; Pita, M.; Meijler, M. M.; Alfonta, L., Katz, E., *J. Am. Chem. Soc.* **2009,** *131*, 826-832.
9. Huang, Y.; Ran, X.; Lin, Y.; Ren, J., Qu, X., *Anal. Chim. Acta* **2015,** *870*, 92-98.
10. Ikeda, M.; Tanida, T.; Yoshii, T.; Kurotani, K.; Onogi, S.; Urayama, K., Hamachi, I., *Nat. Chem.* **2014,** *6*, 511-518.
11. Semenov, S. N.; Wong, A. S.; van der Made, R. M.; Postma, S. G.; Groen, J.; van Roekel, H. W.; de Greef, T. F., Huck, W. T., *Nat. Chem.* **2015,** *7*, 160-165.
12. Debnath, S.; Roy, S., Ulijn, R. V., *J. Am. Chem. Soc.* **2013,** *135*, 16789-16792.
13. Pappas, C. G.; Sasselli, I. R., Ulijn, R. V., *Angew. Chem. Int. Ed.* **2015,** *54*, 8119-8123.
14. Postma, S. G.; Vialshin, I. N.; Gerritsen, C. Y.; Bao, M., Huck, W. T., *Angew. Chem. Int. Ed.* **2017,** *56*, 1794-1798.
15. Heuser, T.; Steppert, A. K.; Lopez, C. M.; Zhu, B., Walther, A., *Nano Lett.* **2015,** *15*, 2213-2219.
16. Heuser, T.; Weyandt, E., Walther, A., *Angew. Chem. Int. Ed.* **2015,** *54*, 13258-13262.
17. Heuser, T.; Merindol, R.; Loescher, S.; Klaus, A., Walther, A., *Adv. Mater.* **2017**.
18. Walther, A., Heinen, L., *Chem. Sci.* **2017**.
19. Jee, E.; Bansagi, T., Jr.; Taylor, A. F., Pojman, J. A., *Angew. Chem. Int. Ed.* **2016,** *55*, 2127-2131.
20. Li, J.; Mo, L.; Lu, C. H.; Fu, T.; Yang, H. H., Tan, W., *Chem. Soc. Rev.* **2016,** *45*, 1410-1431.
21. Liu, J., *Soft Matter* **2011,** *7*, 6757.
22. Cheng, E.; Xing, Y.; Chen, P.; Yang, Y.; Sun, Y.; Zhou, D.; Xu, L.; Fan, Q., Liu, D., *Angew. Chem. Int. Ed.* **2009,** *48*, 7660-7663.
23. Guo, W.; Lu, C. H.; Orbach, R.; Wang, F.; Qi, X. J.; Cecconello, A.; Seliktar, D., Willner, I., *Adv. Mater.* **2015,** *27*, 73-78.
24. Lilienthal, S.; Shpilt, Z.; Wang, F.; Orbach, R., Willner, I., *ACS Appl. Mater. Interfaces* **2015,** *7*, 8923-8931.
25. Shin, S. W.; Park, K. S.; Jang, M. S.; Song, W. C.; Kim, J.; Cho, S. W.; Lee, J. Y.; Cho, J. H.; Jung, S., Um, S. H., *Langmuir* **2015,** *31*, 912-916.

26. Zhang, L.; Lei, J.; Liu, L.; Li, C., Ju, H., *Anal. Chem.* **2013,** *85*, 11077-11082.
27. Fidaleo, M., Lavecchia, R., *Chem. Biochem. Eng. Q.* **2003,** *17*, 311-318.
28. Zhou, X.; Li, C.; Shao, Y.; Chen, C.; Yang, Z., Liu, D., *Chem. Commun.* **2016,** *52*, 10668-10671.
29. Guo, W.; Lu, C. H.; Qi, X. J.; Orbach, R.; Fadeev, M.; Yang, H. H., Willner, I., *Angew. Chem. Int. Ed.* **2014,** *53*, 10134-10138.
30. Hu, Y.; Kahn, J. S.; Guo, W.; Huang, F.; Fadeev, M.; Harries, D., Willner, I., *J. Am. Chem. Soc.* **2016,** *138*, 16112-16119.
31. Lu, C. H.; Guo, W.; Hu, Y.; Qi, X. J., Willner, I., *J. Am. Chem. Soc.* **2015,** *137*, 15723-15731.
32. Liu, D., Balasubramanian, S., *Angew. Chem. Int. Ed.* **2003,** *42*, 5734-5736.
33. Heinen, L., Walther, A., *Chem. Sci.* **2017**.

6 LIST OF PUBLICATIONS

Heinen, L., Heuser, T., Walther, A., Antagonistic Enzymes in a Biocatalytic pH Feedback System Program Autonomous DNA Hydrogel Life Cycles, *Submitted*

Heuser, T., Merindol, R., Löscher, S., Klaus, A., Walther, A., Photonic Devices Out of Equilibrium: Transient Memory, Signal Propagation, and Sensing, *Advanced Materials*, **2017**, DOI: 10.1002/adma.201606842

Tigges, T., Heuser, T., Tiwari, R., Walther, A., 3D DNA Origami Cuboids as Monodisperse Patchy Nanoparticles for Switchable Hierarchical Self-Assembly, *Nano Letters*, **2016**, 16, 7870-7874

Han, K., Tiwari, R., Heuser, T., Walther, A., Simple Platform Method for the Synthesis of Densely Functionalized Microgels by Modification of Active Ester Latex Particles, *Macromolecular Rapid Communication*, **2016**, DOI: 10.1002/marc.201600213

Tiwari, R., Heuser, T., Weyandt, E., Wang, B., Walther, A., Polyacid microgels with adaptive hydrophobic pockets and ampholytic character: synthesis, solution properties and insights into internal nanostructure by *cryogenic*-TEM, *Soft Matter*, **2015**, 11, 8342-8353

Heuser, T., Weyandt, E., Walther, A., Biocatalytic Feedback-Driven Temporal Programming of Self-Regulating Peptide Hydrogels, *Angewandte Chemie Internationale Edition*, **2015**, 54, 13258-13262

Heuser, T., Steppert, A.-K., Molano Lopez, C., Zhu, B., Walther, A., Generic Concept to Program the Time Domain of Self-Assemblies with a Self-Regulation Mechanism, *Nano Letters*, **2015**, 15, 2213-2219

7 ACKNOWLEDGEMENT

Mein größter Dank gilt Prof. Andreas Walther für seine herausragende Betreuung im Verlauf meiner Promotion und Unterstützung in allen wissenschaftlichen Bereichen. Ich kann auf eine sehr erfolgreiche Zusammenarbeit zurückblicken und danke ihm besonders für die vielen Möglichkeiten, die er mir in den vergangenen Jahren gewährt hat. Meine Arbeit auf internationalen Konferenzen vorzustellen, sowie Forschungskooperationen mit verschiedenen internationalen Partnern und der damit verbundene Aufenthalt in England, haben mich sowohl persönlich als auch fachlich sehr bereichert. Des Weiteren danke ich Prof. Martin Möller, für die umfangreichen wissenschaftlichen Möglichkeiten und die inspirierende Atmosphäre, die er am DWI geschaffen hat.

Außerdem möchte ich mich bei allen Kollegen meiner Arbeitsgruppe bedanken, die mich über die Jahre begleitet haben und die Zeit am DWI zu einer besonderen Erinnerung haben werden lassen. Großer Dank gebührt allen Kollegen, die ihre Zeit und Arbeit in gemeinsame Projekte investiert haben und so an der Realisation meiner Publikationen mitgewirkt haben: Ann-Kathrin Steppert, Baolei Zhu, Catalina Molano Lopez, Elisabeth Weyandt, Dr. Rémi Merindol, Aileen Klaus, Sebastian Löscher, Alexander Steinschulte und Laura Heinen. Besonderer Dank gilt Laura Heinen, Dr. Rémi Merindol, Dr. Tobias Rudolph und Thomas Tigges für die vielen wissenschaftlichen Diskussionen und ihre inspirierende Kooperation. Weiterer Dank gilt Thomas Tigges für seine fachliche als auch persönliche Unterstützung während meines gesamten Studiums.

Weiterer Dank gilt Dr. Walter Tillmann für die Durchführung der Infrarotspektroskopie, Rainer Haas für die Durchführung der Gel-Permeations-Chromatographie sowie den Studenten deren Ergebnisse im Rahmen meiner Betreuung ihrer Master- und Bachelorarbeiten sowie Forschungspraktika meine Doktorarbeit bereichert haben: Ann-Kathrin Steppert, Elisabeth Weyandt, Julia Wohland, Aileen Klaus und Catalina Molano Lopez.

Mein herzlichster Dank gebührt meiner Familie, die mich auf meinem Weg durch das Studium und die Promotion mit fortwährender Unterstützung begleitet hat.